IDENTIFICATION OF FLUTTER DERIVATIVES OF TRUSS BRIDGE DECK FROM GUST RESPONSE

トラス橋桁のガスト応答からの非定常空気力係数の同定

HOANG TRONG LAM

Department of Civil Engineering
Yokohama National University
Yokohama, Japan

March 2017

IDENTIFICATION OF FLUTTER DERIVATIVES OF TRUSS BRIDGE DECK FROM GUST RESPONSE

A Dissertation

Submitted to the Graduate School
of the Yokohama National University
In Partial Fulfillment of the Requirements
for the Degree of

Doctor of Philosophy

By
HOANG TRONG LAM

Academic advisors:
Prof. Dr. Hiroshi KATSUCHI
Prof. Dr. Hitoshi YAMADA
Assoc. Prof. Dr. Mayuko NISHIO

Department of Civil Engineering
Yokohama National University
Yokohama, Japan

March 2017

IDENTIFICATION OF FLUTTER DERIVATIVES OF TRUSS BRIDGE DECK FROM GUST RESPONSE

Abstract

Long-span cable supported bridges are highly susceptible to wind excitation and the aerodynamic instability such as flutter phenomenon play an important role in the design of these bridges. This phenomenon is well represented in term of flutter derivatives that are function of the reduced frequency and body shape and can be identified from section model test by using system identification method.

System identification techniques which have been applied to identify the flutter derivatives can be classified into two broad groups. A deterministic system identification technique, that is applied for only free decaying vibration signal or impulse response. Therefore, in this system the buffeting force and their responses are considered as external noise, so this causes more difficulties at high wind velocity such as noise increase due to turbulence. The other is a stochastic system identification technique that is not only applied for free decaying signal but also buffeting response. In this system identification technique the deterministic knowledge of the input is replaced by the assumption that the input is a realization of a stochastic process.

The wind in the atmospheric boundary layer is always turbulence. Therefore any research of wind-induced vibration problems must consider this issue. Not many researchers have focused clearly on the effects of turbulence on aero-elastic forces, especially at high turbulence intensity.

This study is to clarify the effects of oncoming turbulence on the self-excited force of a suspended long span bridge deck. In the study reported herein, the more challenging is the application of a system identification method to identify flutter derivatives from gust responses for the section model. The gust response is obtained by an experimental wind tunnel test for a trussed deck section. The output only time domain analysis stochastic system identifications: covariance stochastic system (SSI_cov) and data driven stochastic system (SSI_data) methods are proposed to extract simultaneously all flutter derivatives (FDs) from two degrees of freedom system. The results are also compared with those from smooth flow as well as free decay response.

Both covariance stochastic system and data driven stochastic system methods show

a good identification results even under turbulent flows because a feature of those methods treat buffeting force and response as inputs instead of noises. The SSI_data method is appreciably faster than SSI_cov method. An identification of flutter derivatives from buffeting responses is plausible. The advantage of this technique is easier to obtain buffeting response under turbulent flows. This is less time consuming than free decay test. Especially at high wind velocity it can avoided that the vertical free decay data is too short causing less accuracy.

Turbulent flows significantly affect dynamic responses and flutter derivatives of the truss bridge deck section. Buffeting raises the response amplitude level progressively in proportion to the reduced wind speed and turbulent intensity. Specifically, turbulence induces buffeting response but increase flutter critical velocity.

LIST OF TABLE

LIST OF FIGURES

NOMENCLATURE

V_r	=	reduced wind velocity
U	=	mean wind velocity
f	=	frequency
B	=	deck width
D	=	deck height
A_i^*	=	torsional flutter derivatives
H_i^*	=	vertical flutter derivatives
I_u	=	horizontal turbulent component
I_w	=	vertical turbulent component
m	=	mass
I	=	mass moment of inertia
h	=	vertical displacement
L_{se}	=	self-excited lift force
M_{se}	=	self-excited moment
L_b	=	buffeting lift force
M_b	=	buffeting moment
C	=	system damping matrix
C_h	=	mechanical damping of vertical mode
C_α	=	mechanical damping of torsional mode
M	=	mass matrix
C^e	=	effective damping matrix (gross damping matrix)
K^e	=	effective stiffness matrix (gross stiffness matrix)
L_{hR}, $L_{\alpha R}$		flutter derivatives
K	=	reduced frequency, $B\omega/U$
k	=	reduced frequency, $b\omega/U$
b	=	half model width
K_h	=	reduced frequency, $B\omega_h/U$
K_α	=	reduced frequency, $b\omega_a/U$
A	=	state matrix
x	=	state vector
E	=	Expectation
T	=	Toeplitz matrix
H	=	Hankel matrix

Y_p = past output

Y_f = future output

P = projection matrix

O = observation matrix

Dc = transmission

w_k = process noise

v_k = measurement noise

QR = QR factorization

K_k = Kalman gain

I_i = turbulence intensity

L_i^x = turbulence integral length scale

R_{xx} = autocorrelation

S_u = power spectrum density function

σ = standard deviation

ω_h = circular frequency of heaving mode

ω_α = circular frequency of peaching mode

f_h = frequency of heaving mode

f_α = frequency of peaching mode

δ = logarithmic decrement

ρ = air density

α = torsional displacement

ε = frequency ratio

ξ = damping ratio

ξ_h = vertical damping ratio

ξ_α = torsional damping ratio

ω = natural circular frequency

δ = logarithmic decrement of damping

$\hat{X}$ = Kalman filter state sequence

$k_a^{'}, k_a^{''}, k_b^{'}, k_b^{''}$ *and* $m_a^{'}, m_a^{''}, m_b^{'}, m_b^{''}$ "Küssner coefficients"

Φ = mode shape

Ψ = eigenvector; Σ = covariance matrix

ACKNOWLEDGEMENTS

I am sincerely grateful to my advisors, Professor Hiroshi Katsuchi, Professor Hitoshi Yamada and Associate Professor Nishio Mayuko of Yokohama National University, for their guidance during the course of this study. I thank Professor Hiroshi Katsuchi for his support and encouragement, for opening opportunities for me in research topic in addition to my dissertation research, for his hospitality and kindness to me.

I also thank my committee members Professor Hitoshi Yamada, Professor Hiroshi Katsuchi, Associate Professor Nishio Mayuko, Professor Tsubaki Tatsuya and Associate Professor Dionysius Siringoringo for their time, arranging schedules, for their kind and constructive comments on this dissertation.

I would like to express my sincere thanks to Ministry of Education of Viet Nam which have supported all the financial during PhD course. Special I would like to express my grateful to my colleagues, and Department of Bridge and Road of Da Nang University of Science and Technology.

I also thank the faculty and staff of the Civil Engineering Department, Yokohama National University, for their assistance and kind help in many aspects.

Last but not least, I would like to thank my family: my wife, my little son and my parents who always give me encouragement for finishing thesis.

TABLE OF CONTENT

CHAPTER 1

INTRODUCTION

1.1 Bridge aerodynamic and turbulence effect

The design of long span bridges, either suspension or cable stayed bridges must be withstood the forces induced by the wind effect. In addition, such bridges are highly susceptible to wind excitation because of their inherent flexibility, low structural damping and light in weigh. Wind loads play an importance role in the design of these structures. The action of wind loads are broadly divided into two groups, aerostatic and aerodynamic loads (figure 1.1).

The effects of aerostatic such as deflection and stress are caused by wind load (primary effect of wind). It shall be considered for all structures and instability for flexible structures (long span bridge). Estimate of wind load effect on a structure is the most important aspect in the wind actions. Considering wind load is enough for most ordinary structures. Wind load does not decide the structure in most cases, but is needed to secure the horizontal stiffness of the structure.

The aerodynamic force can be divided into two main groups: limited-amplitude response (limited vibration) and divergent-amplitude response vibrations (self-excited vibration). First category responses occur for not only large structure (flexible) but also secondary

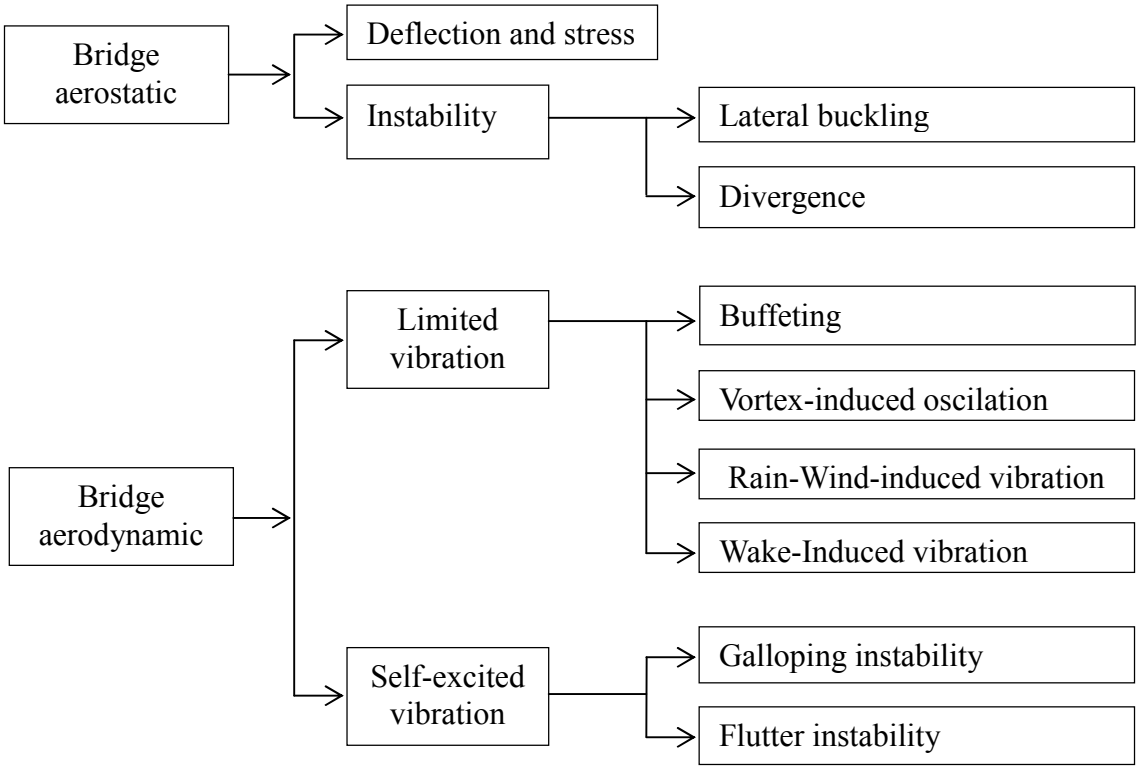

Figure 1.1 Classification of wind action on bridge

members. This part comprises: the buffeting force; vortex-induced oscillation; rain-wind-induced vibration of stay; wake-induced vibration occurs with parallel-aligned decks.

Whereas second category responses occur for only large structure (flexible) and consist of flutter and galloping.

Based on relationship between amplitude of response and non-dimensional reduced wind velocity (V_r=U/fB; where U: mean wind velocity, f: frequency, B: deck width), it can be classified that the vortex-induced vibration usually occur at low wind velocity range, the buffeting phenomenon is significant at medium velocity range up to high wind velocity, meanwhile, the flutter phenomenon occur at high wind velocity range (figure 1.2).

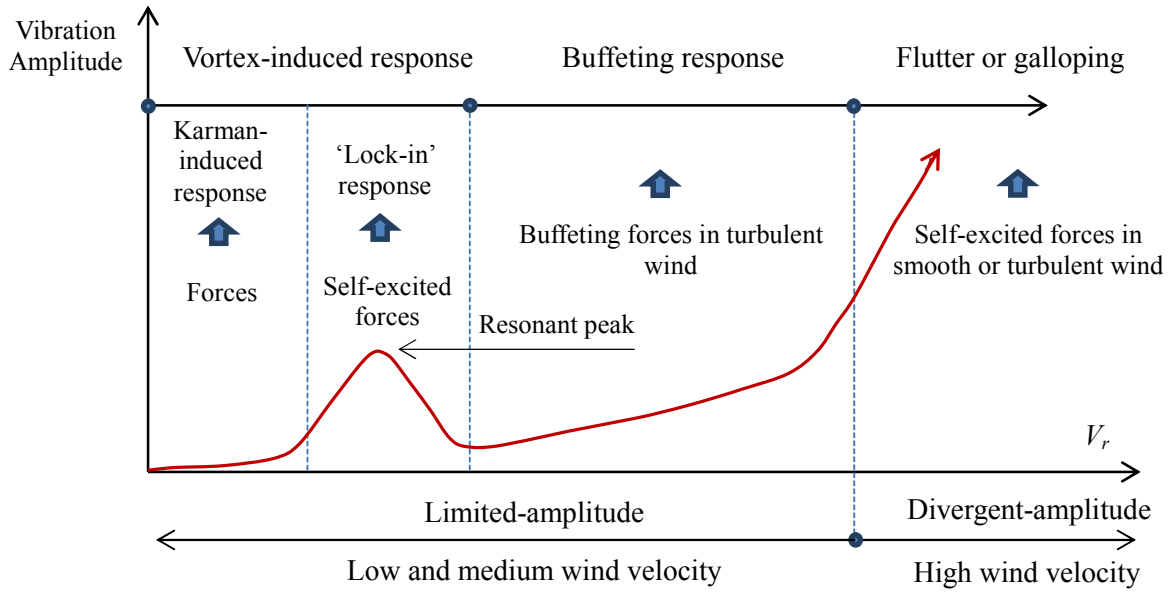

Figure 1.2 Response amplitude versus reduced wind velocity

The above-mention of bridge aerodynamics will be summarized hereafter:

The vortex-induced vibrations are limited-amplitude response produced by either the Karman vortex shedding or another results from vortex shedding on the surface and wake of structure. The vortex-induced vibration has not caused fatal disaster so far, but a fatigue problem sometimes. Vortex excitation produced downstream of an object excite the resonance of the object when they coincide with the latter's natural periodic. When the frequency of oscillation is equal to the frequency of vortex shedding, this is commonly known 'lock-in' phenomenon. In this region the largest amplitude oscillations occur. Vortex-induced vibration will be checked for bridge design through wind tunnel experiment and theoretical analysis.

The buffeting phenomenon: the breathing of natural wind forces the structure into vibration in

the vertical or in the direction of wind axis. Buffeting response itself will be a problem for only flexible structures or long-span bridges. Buffeting is a random response of structure due to the effect of turbulence on the oncoming wind flow or due to signature or self-induced turbulence. Buffeting response does not generally lead to catastrophic failures but is important for serviceability considerations such as fatigue limit state. Gust response problem can be solved via experimental and analytical investigation in frequency domain or time domain methods.

Rain-wind-induced vibrations of cables are excited by two different factors, that is an axial flow in the near wake and "formation of upper rivulet" and it was classified that each factor could excited a cable independently (Matsumoto *et al.* 1992).

Wake-induced vibrations appear when an elastic bluff body is immersed in the wake developed from an upstream body it will dynamically respond with *wake-induced vibrations.*

Galloping is an instability typical of slender structures having special cross-section or the effective of some ice-coated power line cable. Under certain conditions these structure can vibrate with large-amplitude in the direction normal of wind flow.

Flutter phenomenon is the results from an interaction between the elastic behavior of a body and the changing in the aerodynamic pressure and vice versa, these pressures force can be called "motion-induced" or "self-excited" force. The changes self-excited force via flutter derivative by turbulence in oncoming flow will be focus and the extraction of flutter derivative by using system identification method from gust responses is the main focus.

1.2 Flutter instability

Flutter is a divergent amplitude self-excited vibration generated by the aerodynamic wind-structure interaction and a total negative damping mechanism (the energy of motion derived from the aerodynamic exceeds the energy dissipated by the system though structural mechanical damping). There are two typical types of bridge flutter those are Torsional flutter (as the so call Stall flutter) that the fundamental torsional mode dominantly involves to the flutter instability and Couple flutter (as the so-called classical flutter) that the fundamental torsional mode couples with symmetric or asymmetric heaving mode. Various researchers show that the torsional flutter seem to dominant almost cases of bluff bridge section such as low slenderness ratio (B/D) rectangular section, stiffened truss section with open grating or solid slab, H-shape section, whereas high slenderness ratio rectangular and streamlined boxed bridge sections are favorable for coupled flutter.

Figure 1.3 shows the flutter phenomena of torsional flutter and coupled flutter cases. Torsional fundamental mode is defined as substantially torsional vibration around central point of cross-

section. In this mode, the derivation of phase between torsional (noses-up positive) and heaving response (downward positive) at mid-chord point, is 0^0 or 180^0 and correspond to torsional twist center is upstream point or downward point from the mid-chord point. These fundamental modes are expressed by T_0 and T_{180} (Figure 1.3a & 1.3b). On the other hand, heaving fundamental mode is defined as prominent heaving response induced by lift generated by slight pitching angle in quasi-steady sense with -90^0 or 90^0 as phase lag of heaving to torsional displacements. These two fundamental modes correspond to $dC_L/d\alpha>0$ or $dC_L/d\alpha<0$ and are expressed by H_{-90} or H_{90} (figure 1.3c & 1.3d), respectively (Matsumoto *et al.* 2008).

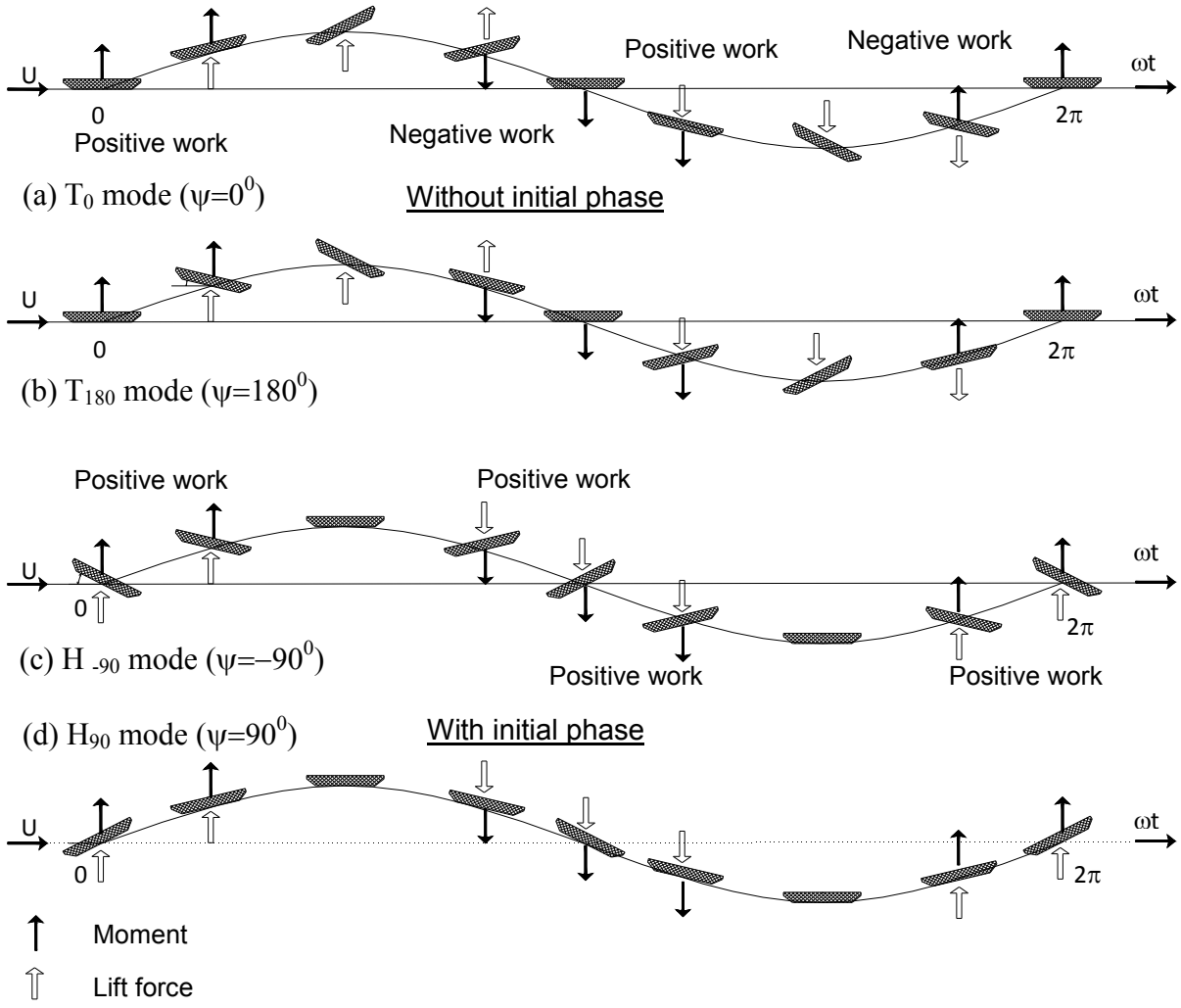

Figure 1.3 Form of torsional and heaving 2DOF coupled flutter

Base on series of experiments on various fundamental sections and based on flow-structure interaction phenomena that Matsumoto *et al.* (1996, 2001) classified the mechanism of flutter instability into these branches: Low-speed torsional flutter, high-speed torsional flutter, heaving-

branch coupled flutter, torsional-branch coupled flutter and coupled flutter, heaving-torsional coupled flutter.

Flutter problems can be divided into three groups those are analytical, experimental and simulation methods (figure 1.4). Analytical methods of flutter were motivated by airfoil and thin-plate section. Selberg (1961) developed Bleich's (1951) formula and apply for various types of bridge section, moreover, Kloppel (1967) expressed by empirical diagrams. Theodorsen (1935) introduced the complex function is known as Theodorssen's circulation functions to model self-excited force, however Theodorsen's self-controlled flutter forces are limitedly applied only for airfoil and thin-plate structures.

Most of bridge can be classified as bluff bodies which is a highly complex unsteady flow structure involves separated regions where large suction pressure generated, shear layer which may or may not reattach and vortex shed from the leading and trailing edges. This flow scenario is more complicated and a thin-airfoil model and it accompany formulations are inadequate for this scenario. Scanlan & Tomko (1971) developed experimental approach to build the real forms of self-excited forces by so-called flutter derivatives for 2DOF flutter problems and it is the most widely-used formulations for modern bridge flutter analysis with variety of bridge cross-section.

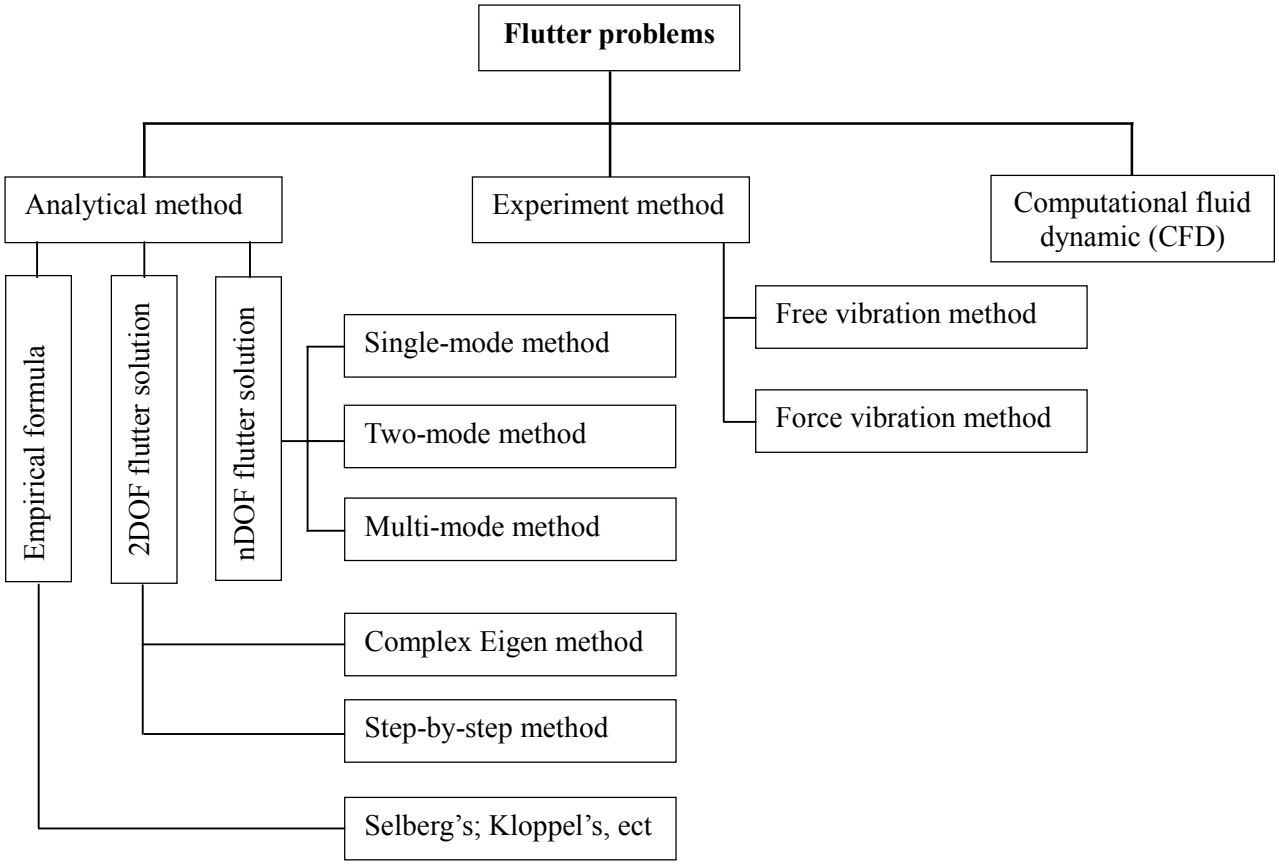

Figure 1.4 Analysis of flutter instability problems

Base on 2DOF flutter problems, Matsumoto (1995) introduced the step-by-step method which the flutter frequency in the heaving branch and torsional branch are converged by iterative calculation. On the other hand, in the complex eigenvalue method the flutter characteristics are solved base on an eigen-value problem.

For nDOF systems flutter problem, there are two methods: finite differential method in linear-time approximation and finite element method in modal space. Scanlan (1990) introduced single-mode and two mode-flutter analysis. Various recent researchers studied on multimode coupled flutter (Jain *et al.* (1996), Katsuchi *et al*. (1999), Chen *et al*. (2001)) and the results was in good agreement with the measurement and exhibited a significant coupling among modes.

The computational fluid dynamics (CFD) technique has developed very fast and many researchers studied on this field, first verified wind tunnel results and makes clearly mechanism of aerodynamic phenomena. So far CFD may become useful and might replace wind tunnel, however simulation still exist many limitation to apply for complex section and dynamic model.

The experimental method conducted on sectional model test in wind tunnel with free vibration test for very DOF (single DOF, 2DOF and 3DOF). The aeroelastic coefficient (flutter derivatives) will be obtained by system identification method.

1.3 Motivation and objectives of study

The motivation for this study is based on inconsistences in past studies, unclearly the turbulence effect on self-excited forces (or flutter derivative) and shortcoming of current free vibration method for extracting flutter derivatives (FDs) by section model test in wind tunnel. This section highlights briefly some inconsistencies in past experimental results and then comment upon these results and final propose the objectives of this study.

Designing for long-span bridges often used section-model test to identified stable section geometric from selected bridge deck section and aero-elastic model test for finalize the design.

Base on section models, the flutter derivatives will be obtained under smooth flow. Not many researchers have focused clearly on the effects of turbulence on aero-elastic forces. Scanlan & Lin (1978) are the pioneers who used a trussed deck section model and then concluded that flutter derivatives has an insignificant difference in smooth and turbulent flows (figure 1.5). However, Huston (1986) conducted a test on a model of the Golden Gate Bridge deck section and the results shown a significant discrepancy in flutter derivatives between smooth and turbulence flow as demonstrated in figure 1.6 (Haan & Kareem 2007). The torsional damping term A_2^* plays an important role on torsinal flutter instability, since its positive/negative value corresponds to the aerodynamic instability/stability of torsinal fluter.

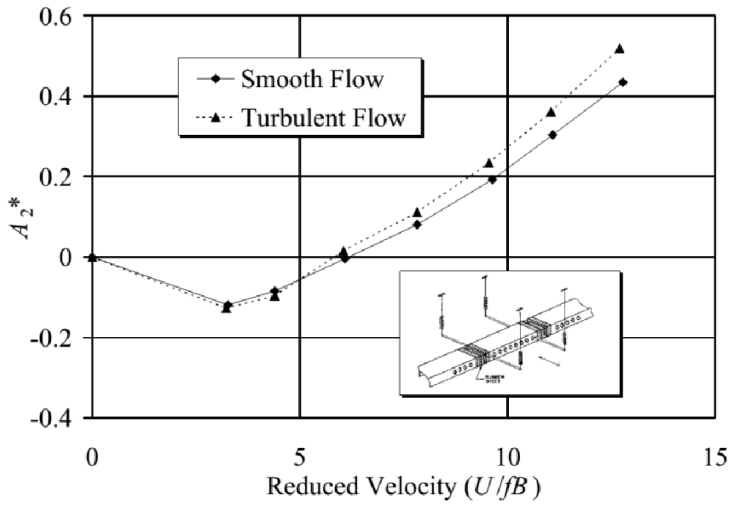

Figure 1.5 Flutter derivative (A_2^*) from the simulated trussed deck section model of Scanlan & Lin (1978)

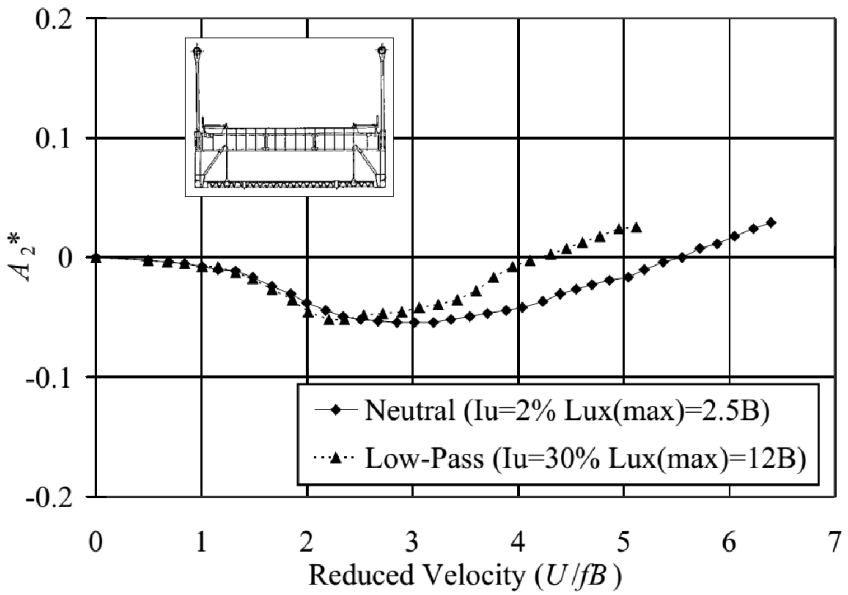

Figure 1.6 Flutter derivative A_2^* of the Golden Gate bridge deck section in flows generated by the neutral and low-pass mode of Huston's (1986)

Sarkar *et al.* (1994) conducted a single section model test under both smooth and turbulence flows and applied robust system-identification method Modified Ibrahim Time Domain (MITD) (Sarkar 1992). The bridge model was the Tsurumi Fairway Bridge with the cross section of the bridge is a trapezoidal, streamlined steel box girder. Their study shown two valuable conclusions 1) The turbulence flow does not appreciably affect the self-excited forces via the flutter derivatives (figures 1.7&1.8), 2) The MITD method is based on the assumption that there is no external

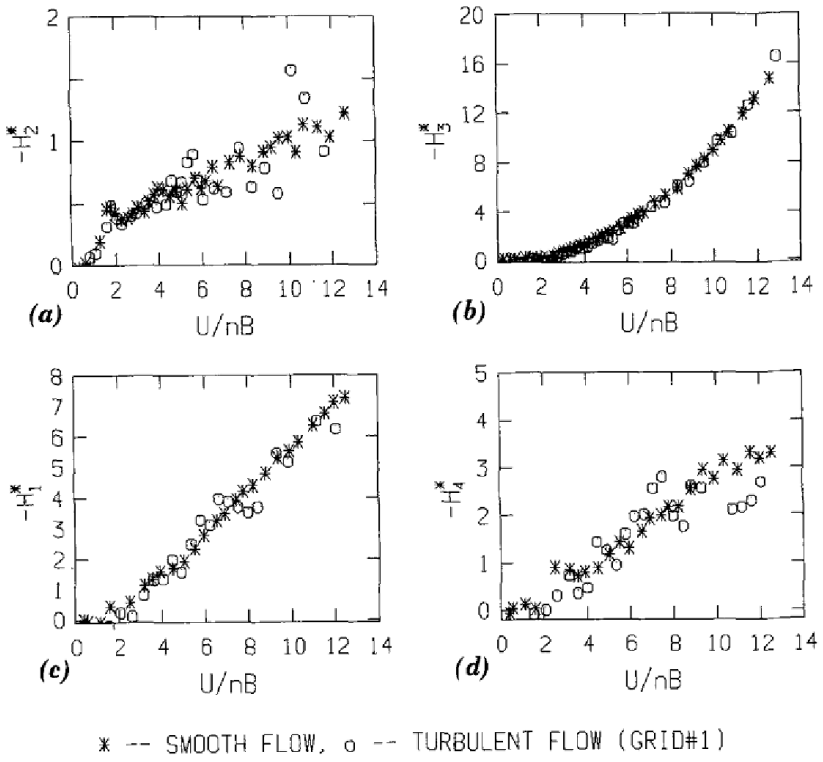

Figure 1.7 Effect of turbulence (a) H^*_2, (b) H^*_3, (c) H^*_1, (d) H^*_4 of Sarkar (1994)

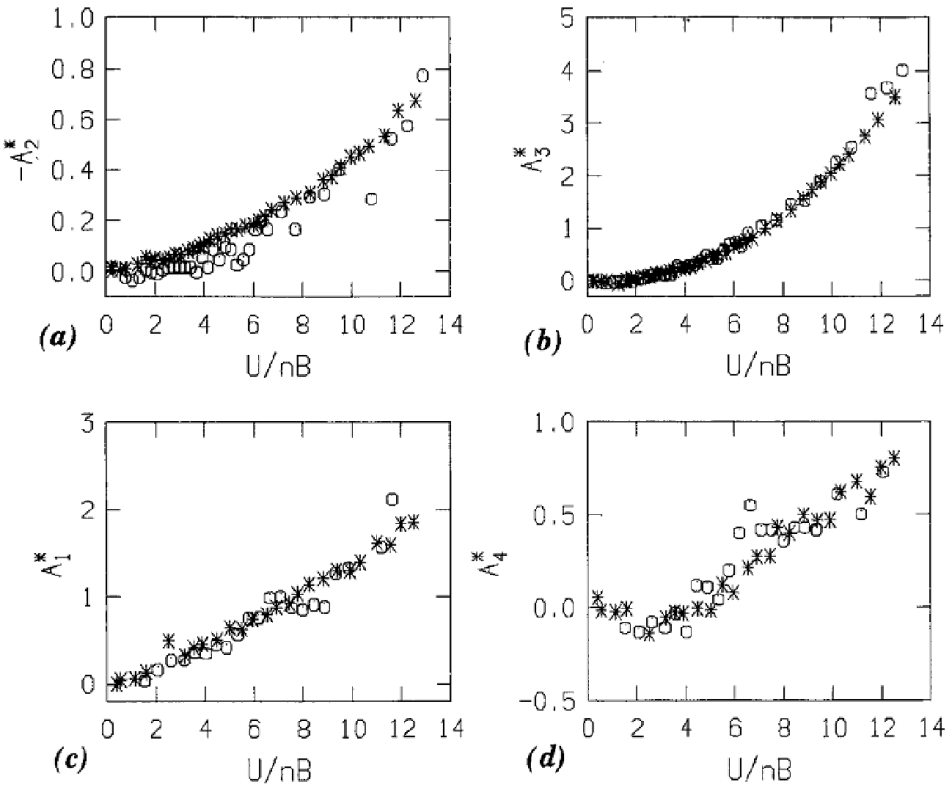

Figure 1.8 Effect of turbulence (a) A^*_2, (b) A^*_3, (c) A^*_1, (d) A^*_4 of Sarkar (1994)

excitation of the system. For a section model immerse in turbulent-flow, where the buffeting forces and these response are regarded as external force, and hence theoretical condition free vibration is violated. The MITD method treats the resulting forced response as though additional noise is present in the signals. This made the identification flutter derivatives more difficult and most likely reduced the accuracy. Note that the influence of turbulence on FDs is still debatable and will depend on the section.

For study on FDs, the free vibration technique of sectional model is often used and system identifications (SID) technique to extract FDs is widely applied. Various SID techniques were developed by many authors: the Extended Kalman Filter method (Yamada *et al.* (1992)).
Modified Ibrahim Time Domain method (Sarkar *et al.* (1992)), Unifying Least-squares method (Gu *et al.* (2000)) and Iterative Least-Squares method (Gan Chowdhury *et al.* (2003)). These systems are namely deterministic system identification techniques, which are only applied for free decaying vibration signal or impulse response. Therefore, in these systems the buffeting force and their responses are considered as external noise, so this causes more difficulties at high wind velocity such as noise increase due to turbulence.
Jakobsen *et al.* (1995) and Nikitas *et al.* (2011) extracted FDs from simulated buffeting response and from ambient vibration data from full-scale monitoring data using a covariance block Hankel matrix method (CBHM). Eigen realization algorithm (ERA) (Juang & Papa (1985)) method with preprocess output covariance was used by Zhang *et al.* (2004) to identify the FDs. These methods are namely stochastic system identification techniques (SSI), which are not only applied for free decaying signal but also buffeting response. In these SSI the deterministic knowledge of the input is replaced by the assumption that the input is a realization of a stochastic process. An advantage of those methods treats buffeting force and response as inputs instead of noises.

Kirkegaard *et al.* (1997) compared three state space systems: stochastic subspace identification (SSI), stochastic realization estimator matrix block Hankel (MBH) and prediction error method (PEM). The results show that the SSI method gives good results in terms of estimated modal parameters and mode shapes. The MBH is seen to give poor estimates of the damping ratios and the mode shapes compared with the other two techniques. In addition, the SSI is approximately ten times faster than the PEM.

On the other hand, there is a shortcoming involved in the free vibration method. At high wind velocity the extraction of FDs may not be obtained accurately because the aerodynamic damping of vertical mode is too high and vertical free-vibration data is too short for analysis.

From these considerations, the idea for applying SSI method to estimate FDs from gust responses of a truss bridge deck section is brought.

Objectives of studies in this dissertation are as follow:

Firstly, gust response is obtained by an experimental wind tunnel test for a trussed deck section with different turbulence properties.

Secondly, the output only time domain analysis stochastic system identification (SSI) method is including covariance-driven stochastic system identification (SSI_cov) and data-driven stochastic system identification (SSI_data) those is proposed to extract simultaneously all FDs from two degrees of freedom system.

Finally, the results obtained from two systems will be compared. Clarify the turbulence effect on dynamic response and self-excited force via flutter derivatives. The flutter derivatives extracted by gust responses which obtained from wind tunnel test. The results are also compared with conventional method that is free vibration method.

1.4 Structure and outline of study

The aim of the study is to clarify the effects of oncoming turbulence on the self-excited force of a suspended long span bridge deck by using a section model. The more challenging is the application of a stochastic system identification method to identify FDs from gust responses for the section model. The gust response is obtained by an experimental wind tunnel test for a trussed deck section. The stochastic system identification is proposed to extract simultaneously all FDs from two degrees of freedom system. The results are also compared with those from smooth flow and free decay response.

The dissertation is classified by the 6 chapters including the first chapter introduction and the final conclusion. The main content of each chapters are briefly presented as follows:

In chapter 2, summarizes the approach taken in the current work to address the motivating issues raised in this chapter. This summary includes some discussion of the literature on the effects of turbulence on self-excited force and system identification method. Final part of chapter presents the problematic in formulation of self-excited forces and applied Scanlan's method for 2DOF with two different frequencies.

In chapter 3, presents the stochastic system identification (SSI_cov and SSI_data) theory will be presented and application of stochastic system identification method to extract flutter derivatives. Final part will be presented method for elimination of noise effect.

In chapter 4, outlines the experimental equipment used to generate gust response including the turbulence generation techniques, turbulence measurement, model configuration and model vibration measurement method. The turbulence properties and the effects of turbulence on model

dynamic will be also presented.

In chapter 5, presents the application of stochastic system identification method for extracting flutter derivatives by gust response from wind tunnel data and white noise and colored noise simulation data are going to be presented. The results will be discussed and compared.

In chapter 6, summarizes the major conclusions of the work and proposes research goals for future study.

CHAPTER 2

APPROACH AND BACKGROUND

The current approach addresses the issues aforementioned in chapter 1 with wind tunnel equipped with section-model, oscillating in a series of smooth turbulence flows. In addition, the extraction flutter derivatives by gust responses can be analyzed by ambient vibration technique of full-scale bridges. This chapter describes the approach taken in this dissertation and then summarizes existing literature on system identification to extract flutter derivatives and background of self-excited forces.

2.1 Current approach

The wind in the atmospheric boundary layer is always turbulence. Therefore any study of wind-induced vibration problems must consider this issue. Not many researchers have focused clearly on the effects of turbulence on self-excited forces, especially at high turbulence intensity. Generally, bridge aerodynamic problems in practically all cases are nonlinear; however, to treat the problem simply linear analytical approaches are often used. There are two main reasons (Simiu and Scanlan 1996). Firstly, the structure is usually analyzed as a linear elastic one and its action dominates the form of the response. Secondly, it is the incipient or starting condition, which may be treated as having only small amplitude that separates the stable and unstable regimes. For linear fluid-structure interaction problems, the buffeting forces can be ignored when studying on motion stability. The present of turbulence in the flow is equivalent to more noisy input signal. The flutter derivatives depend on a kind of cross-section and reduced frequency. A major analysis tool in previous study is a wind tunnel test by section-model.

The experimental methods use for identifying flutter derivatives can be groups under two categories: force method (Han 2000; Sarkar et al. 2009) which known as the most accurate method for the deification of flutter derivatives, but because of its requirement for more complex apparatus, therefore research and wind tunnel test of this method are not popular. The implementation of this method is that the bridge deck section is driven by a sinusoidal motion with constant amplitude and frequency of either vertically or rotationally. A balance system is used to measure and analyze the aerodynamic forces acting on the section model then the flutter derivatives can be identified from these forces. Force method is not necessary to couple the degree of freedoms of the motion. The vertical flutter derivatives H_1^*, H_4^*, A_1^*, A_4^* are obtained from the aerodynamic forces generated by the force of vertical vibration, and the torsional flutter

derivatives H_2^*, H_3^*, A_2^*, A_3^* are obtained from the aerodynamic forced generated by the force of rotational vibration.

By the free vibration test, the bridge deck section model is attached to a rigid test frame at each corner suspended with the help of helical springs. Then the system is given an initial displacement in the corresponding degrees of freedom. The vertical and torsional displacements can be recorded from measurement. The aero-elastic parameter such as the frequency and damping of vibration signals are identified by system identification methods. This method is simple and does not require a complex device. The disadvantage of the free vibration method compared with the forced vibration method is that the flutter derivatives cannot be obtained directly.

SID can be classified in two main groups as namely: deterministic system identification techniques: Extended Kalman Filter method (Yamada *et al.* (1992)), Modified Ibrahim Time Domain method (Sarkar *et al.* (1992)), Unifying Least-squares method (Gu *et al.* (2000)) and Iterative Least-Squares method (Gan Chowdhury *et al.* (2003)). These systems which are only applied for free decaying vibration signal or impulse response. Therefore, in these systems the buffeting force and their responses are considered as external noise, so this causes more difficulties at high wind velocity such as noise increase due to turbulence. Second group is stochastic system identification techniques such as covariance block Hankel matrix method (CBHM) (Jakobsen *et al.* (1995)), natural excitation technique (NExT) in combination with eigensystem realization algorithm (ERA) (Juang & Papa (1985)) NExT-ERA (Zhang *et al.* (2004)), and stochastic subspace identification (SSI) (Peeter (1999)). These methods, which are not only applied for free decaying signal but also buffeting response. In these systems the deterministic knowledge of the input is replaced by the assumption that the input is a realization of a stochastic process. An advantage of those methods treats buffeting force and response as inputs instead of noises.

2.2 Literature reviews on system identification and extract flutter derivatives from gust response

The flutter derivatives of bridge decks are essential parameter necessary to estimate the flutter stability of long-span bridges, which can be identified through experimental method. There are two kinds of techniques to obtain the parameters with section model of bridge deck: the forced vibration test and free vibration technique by using system identification method.

Scanlan *et al.* (1971) proposed a method to extract the flutter derivatives of bridge deck with free vibration decay, but Scanlan's method requires three steps of test. Separated torsional and vertical bending motions have to be constrained modes corresponding, respectively to obtain

uncoupled derivatives (direct derivatives). Then, the coupled terms are obtained from couple vibration where the vertical and torsional motions of the model must have same frequency at each wind velocity. The main problem in this technique is a proper excitation of the couple motion and a length of time history records with increase in wind speed due to aerodynamic damping. In addition, large initial amplitude often includes nonlinear damping force effect.

Yamada *et al.* (1992) developed a technique of simultaneous identified all eight flutter derivatives from coupled vibration by using the Extended Kalman filter method. In this study, wind tunnel test conducted at high reduced wind speed near flutter onset where aerodynamic vibration tends to have coupled. When the wind velocity is closely or above the flutter critical wind velocity the coupled vibration was excited during free vibration, and the system identification seem to be worked well. However at low wind speed range, the uncoupled vibration is dominant the system identification does not give a good results.

Iwamoto and Fujino (1995) used a similar method with Yamada (1992) to extract all eight flutter derivatives from free vibration technique. This study proposed the method to solve two problems that are 1) How to reduce the number of flutter derivatives in a two degree-of-freedom system. The free vibrations of one DOF systems contain four parameters: modal frequencies, modal damping, amplitude ratio and phase lag. Therefore, it is impossible to extract all eight flutter derivatives from one mode vibration because lack of condition. This study proposed method to reduce the number of flutter derivatives to eight in 2 DOF system heaving and torsional mode. 2) The drawback of free vibration technique is that at high wind velocity because the aerodynamic damping of the vertical-dominant mode is too high to obtain vibration data which are long enough for the identification. The accurately of identification is reduced. In order to solve this problem wind tunnel test are conducted with section models which is increased of mass and inertial moment at high wind velocity.

Sarkar *et al.* (1994) conducted a single section model test under both smooth and turbulence flows (turbulence intensity around 2.44% to 3.42%) and applied system-identification method Modified Ibrahim Time Domain (MITD) (Sarkar 1992). This method was found to be easy applied to the free decaying time history data. The bridge model using in this study was the streamlined steel box girder. This study shown two significant conclusions: 1) The flutter derivatives obtained from turbulent flow fluctuate those value under smooth flow. The turbulence flow seems to be insignificant affect the self-excited forces through the flutter derivatives, 2) The MITD method is a deterministic system which is applied to free vibration technique there is no external excitation of the system. Under turbulent flow case, where the buffeting forces and their response are same external excitation, the MITD method consider the resulting forced response as

additional noise is present in the signals. This made the identification flutter derivatives process more difficult and reduced the accuracy. The presence of turbulence in flow this is equivalent to add a noise into a signal and signal become more noisy input to the system identification method. The MITD method treats a free response rather than force vibration. This reason made the extraction process more complicated and reduced the accuracy of the identified flutter derivative.

Jakobsen *et al.* (1995) presents a method based on application of a Covariance Block Hankel Matrix (CBHM) method for the identification flutter derivatives by using ambient vibration. The flutter derivatives extracted for the streamlined bridge cross section show that the method is efficient in returning reliable estimate.

Boonyapinyo *et al*. (2010) applied a stochastic subspace identification technique to extract FDs of a thin bridge deck from wind tunnel test in both smooth and turbulent flows. The conclusion of this paper is that the proposed system can be used to estimate flutter derivatives from buffeting responses with reliable results and an advantage of the stochastic system considers the buffeting force and response as input instead of noise. Therefore, the ratio of signal to noise is not affected by wind speed and the flutter derivatives at high wind speeds are readily available.

Jones *et al.* (1995) presents an overview of a Kalman filter method for assessing dynamic characteristics of bridges under wind excitation on full-scale model (ambient vibration). The identification routine was found to be reliable when tested using simulated data. Nikitas *et al.* (2011) extracted FDs from ambient vibration data from full-scale monitoring data using a covariance block Hankel matrix method (Jakobsen *et al.* (1995)). The advantage of extract flutter derivatives from ambient vibration is that the responses reflect real structure response such as natural coupling between the vertical and torsional mode and atmospheric effect. The limitation of this method is related to angle of attack, skew angle as well as uncertainties in the modal masses distortion from traffic effect, etc.

2.3 Formulation of self-excited force

Consider a section of a bridge deck (figure 2.1) subjected to the action of a smooth oncoming flow. The system is assumed to have two degrees of freedom (DOF): bending displacement and twist (torsional displacement) denote by h and α, respectively. A unit of the system has mass m, mass moment of inertia I.

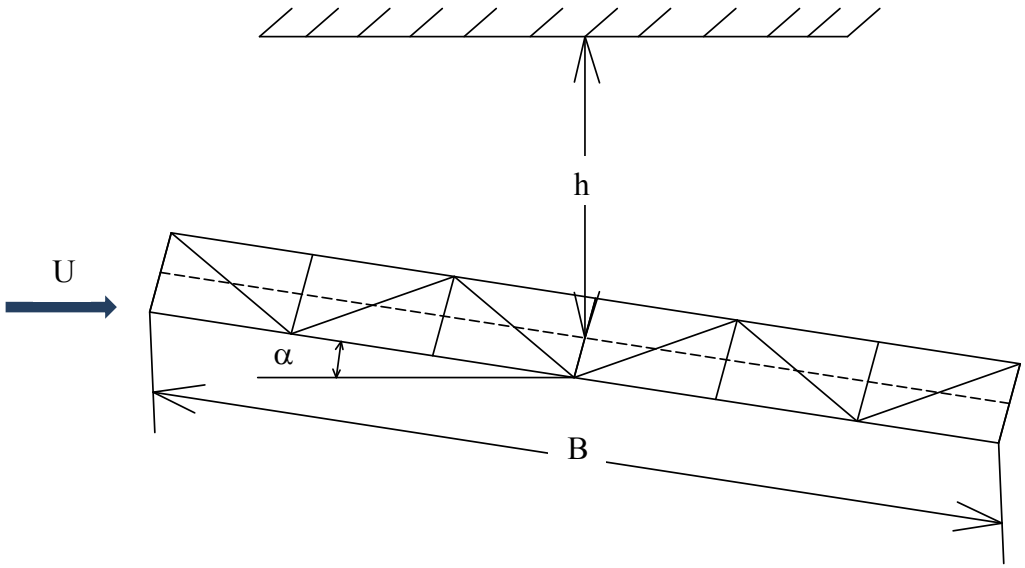

Figure 2.1 Bluff body shape

The equation of motion can be written as:

$$\begin{aligned} m[\ddot{h}+2\xi_h\omega_h\dot{h}+\omega_h^2 h] &= L_{se} \\ I[\ddot{\alpha}+2\xi_\alpha\omega_\alpha\dot{\alpha}+\omega_\alpha^2\alpha] &= M_{se} \end{aligned} \tag{2.1}$$

where m and I are mass and mass moment of inertial per unit length, respectively; $\omega_h=2\pi f_h$ and $\omega_a=2\pi f_a$ are circular frequencies of heaving and pitching mode (in still air), respectively; ξ_h and ξ_a are heaving and torsional damping ratio to critical, respectively; L_{se} and M_{se} are the aerodynamic self-excited lift and moment, respectively.

For small oscillations the self-excited lift and moment on a bluff body may be calculated as linear in the structural displacement, rotation and their first two derivatives, and that it is possible to measure the aerodynamic coefficients by wind tunnel test. There are various forms for the linear expressions for self-excited forces.

Scanlan and Tomko (1971) introduced the real form of the self-excited aerodynamic lift force L_{se} and moment M_{se} which act on a bridge deck oscillating sinusoidal are written as

$$\begin{aligned} L_{se} &= \frac{1}{2}\rho U^2 B\left[KH_1^*(K)\frac{\dot{h}}{U}+KH_2^*(K)\frac{B\dot{\alpha}}{U}+K^2H_3^*(K)\alpha+K^2H_4^*(K)\frac{h}{B}\right] \\ M_{se} &= \frac{1}{2}\rho U^2 B^2\left[KA_1^*(K)\frac{\dot{h}}{U}+KA_2^*(K)\frac{B\dot{\alpha}}{U}+K^2A_3^*(K)\alpha+K^2A_4^*(K)\frac{h}{B}\right] \end{aligned} \tag{2.2}$$

Where ρ is the air density; the reduced frequency is defined as $K=B\omega/U=B(2\pi f)/U$; B is deck width; U is the uniform approach velocity of the wind, and ω is the circular frequency of oscillation (f is the frequency of oscillation). H^*_i and A^*_i (i =1,2,3,4) are non-dimensional

function of K namely as flutter derivatives. The quantities α, $\dot{h}/U$, and $B\dot{\alpha}/U$ are effective of angle of attack and therefore also dimensionless.

In France, the self-excited force written in the form as:

$$\begin{aligned} L_{se} &= -\pi\rho U^2 b\left(k_a^{'}\frac{h}{b}+k_a^{''}\frac{\dot{h}}{b\omega}+k_b^{'}\alpha+k_b^{''}\frac{\dot{\alpha}}{\omega}\right) \\ M_{se} &= -\pi\rho U^2 b^2\left(m_a^{'}\frac{h}{b}+m_a^{''}\frac{\dot{h}}{b\omega}+m_b^{'}\alpha+m_b^{''}\frac{\dot{\alpha}}{\omega}\right) \end{aligned} \tag{2.3}$$

where the notation $k_a^{'}, k_a^{''}, k_b^{'}, k_b^{''}$ *and* $m_a^{'}, m_a^{''}, m_b^{'}, m_b^{''}$ are called the " Küssner coefficients"; b is haft chord.

Yamada et al. (1992) used formulation in the complex form as:

$$\begin{aligned} L_{se} &= -\pi\rho B^2\left[\left(L_{hR}+iL_{hI}\right)\ddot{h}+\left(L_{\alpha R}+iL_{\alpha I}\right)\ddot{\alpha}\right] \\ M_{se} &= -\pi\rho B^4\left[\left(M_{hR}+iM_{hI}\right)\ddot{h}+\left(M_{\alpha R}+iM_{\alpha I}\right)\ddot{\alpha}\right] \end{aligned} \tag{2.4}$$

where L_{hR}, $L_{\alpha R}$... are the flutter derivative

The flutter derivatives in Eqs.(2.2&2.3&2.4) to make compare with the Theodosen's coefficient as flow:

$$\begin{aligned} K^2H_1^* &= 2\pi K^2 L_{hI} = -2\pi k_a^{''} = 2\pi KF \\ K^2H_2^* &= 2\pi K^2 M_{hI} = -\pi k_b^{''} = \frac{-\pi K}{2}\left[1+\frac{4G}{K}+F\right] \\ K^2H_3^* &= 2\pi K^2 M_{hR} = -\pi k_b^{'} = -\pi\left[2F-\frac{GK}{2}\right] \\ K^2H_4^* &= 2\pi K^2 L_{hR} = -2\pi k_a^{'} = \frac{\pi}{2}K^2\left[1+\frac{4G}{K}\right] \\ K^2A_1^* &= 2\pi K^2 M_{hI} = -\pi m_a^{''} = \frac{\pi KF}{2} \\ K^2A_2^* &= 2\pi K^2 M_{\alpha I} = -\frac{\pi}{2}m_b^{''} = -\frac{\pi}{2}\left[\frac{K}{4}-G+\frac{\mathrm{KF}}{4}\right] \\ K^2A_3^* &= 2\pi K^2 M_{\alpha R} = -\frac{\pi}{2}m_b^{'} = -\frac{\pi}{2}\left[\frac{K^2}{32}+\mathrm{F}-\frac{KG}{4}\right] \\ K^2A_4^* &= 2\pi K^2 M_{hR} = -\pi m_a^{'} = -\frac{\pi}{2}\left[KG\right] \end{aligned} \tag{2.5}$$

Where F(k) and G(k) are the real and imaginary parts of Theodorsen's circulation function; $k=b\omega/U$ is reduced frequency; b is the haft-chord

2.4 Problematic in formulation of self-excited force

The aerodynamic lift force and moment in this study follow by Tomko and Scanlan (1971) is expressed by

$$\begin{aligned} L_{se} &= \frac{1}{2}\rho U^2 B\left[KH_1^*(K)\frac{\dot{h}}{U} + KH_2^*(K)\frac{B\dot{\alpha}}{U} + K^2H_3^*(K)\alpha + K^2H_4^*(K)\frac{h}{B}\right] \\ M_{se} &= \frac{1}{2}\rho U^2 B^2\left[KA_1^*(K)\frac{\dot{h}}{U} + KA_2^*(K)\frac{B\dot{\alpha}}{U} + K^2A_3^*(K)\alpha + K^2A_4^*(K)\frac{h}{B}\right] \end{aligned} \tag{2.6}$$

where h and α are the vertical and torsional displacement, respectively. H^*_i and A^*_i *(i=1,2,3,4)* are the flutter derivatives that are function of the reduced frequency $K = B\omega/U$. According to Eq. (2.1) the equation of motion used for identification flutter derivatives as follow

$$\begin{aligned} m[\ddot{h} + 2\xi_h\omega_h\dot{h} + \omega_h^2 h] &= \frac{1}{2}\rho U^2 B\left[KH_1^*(K)\frac{\dot{h}}{U} + KH_2^*(K)\frac{B\dot{\alpha}}{U} + K^2H_3^*(K)\alpha + K^2H_4^*(K)\frac{h}{B}\right] \\ I[\ddot{\alpha} + 2\xi_\alpha\omega_\alpha\dot{\alpha} + \omega_\alpha^2\alpha] &= \frac{1}{2}\rho U^2 B^2\left[KA_1^*(K)\frac{\dot{h}}{U} + KA_2^*(K)\frac{B\dot{\alpha}}{U} + K^2A_3^*(K)\alpha + K^2A_4^*(K)\frac{h}{B}\right] \end{aligned} \tag{2.7}$$

In the Eq. (2.7), there are eight unknown parameters (H^*_i and A^*_i *(i=1,2,3,4)*) from free vibration data. Suppose the model is oscillating in two degree of freedom such as vertical h and torsional α – dominant modes which whose circular frequencies are ω_h and ω_α, respectively. Therefore, exist two modal frequencies which is corresponding two reduced frequencies $K_h = B\omega_h/U$ and $K_\alpha = B\omega_\alpha/U$ and whose components are (h_1, a_1) and (h_2, a_2), respectively.

The aerodynamic forces is acting on a two DOF of a bridge deck section oscillating are given from Eq. (2.6) can be detailed as follows

$$\begin{aligned} L_{se} &= \frac{1}{2}\rho U^2 B\left[K_hH_1^*(K_h)\frac{\dot{h}_1}{U} + K_hH_2^*(K_h)\frac{B\dot{\alpha}_1}{U} + K_h^2H_3^*(K_h)\alpha_1 + K_h^2H_4^*(K_h)\frac{h_1}{B}\right] \\ &\quad + \frac{1}{2}\rho U^2 B\left[K_\alpha H_1^*(K_\alpha)\frac{\dot{h}_2}{U} + K_\alpha H_2^*(K_\alpha)\frac{B\dot{\alpha}_2}{U} + K_\alpha^2H_3^*(K_\alpha)\alpha_2 + K_\alpha^2H_4^*(K_\alpha)\frac{h_2}{B}\right] \\ M_{se} &= \frac{1}{2}\rho U^2 B^2\left[K_hA_1^*(K_h)\frac{\dot{h}_1}{U} + K_hA_2^*(K_h)\frac{B\dot{\alpha}_1}{U} + K_h^2A_3^*(K_h)\alpha_1 + K_h^2A_4^*(K_h)\frac{h_1}{B}\right] \\ &\quad + \frac{1}{2}\rho U^2 B^2\left[K_\alpha A_1^*(K_\alpha)\frac{\dot{h}_2}{U} + K_\alpha A_2^*(K_\alpha)\frac{B\dot{\alpha}_2}{U} + K_\alpha^2A_3^*(K_\alpha)\alpha_2 + K_\alpha^2A_4^*(K_\alpha)\frac{h_2}{B}\right] \end{aligned} \tag{2.8}$$

The Eq. (2.8) contains sixteen flutter derivatives and it is cannot to identify all of them from two modes vibration because the response motion contains only eight parameters of information: two set of modal frequency, modal damping, amplitude ratio, and phase lag.

In order to solve the problem for lack of information, various researchers proposed different

method. Scanlan and Tomko (1971) conducted experimental test with two steps: first, uncoupled derivatives are identified separately by pure vertical and torsional free vibration test; and second, coupled derivatives are obtained by coupled free vibration test of the model must have the same frequency at all wind velocities.

Iwamoto and Fujino (1995) proposed method to reduce the number of unknown parameters from sixteen to eight bases on the observation evidence of their wind tunnel test.

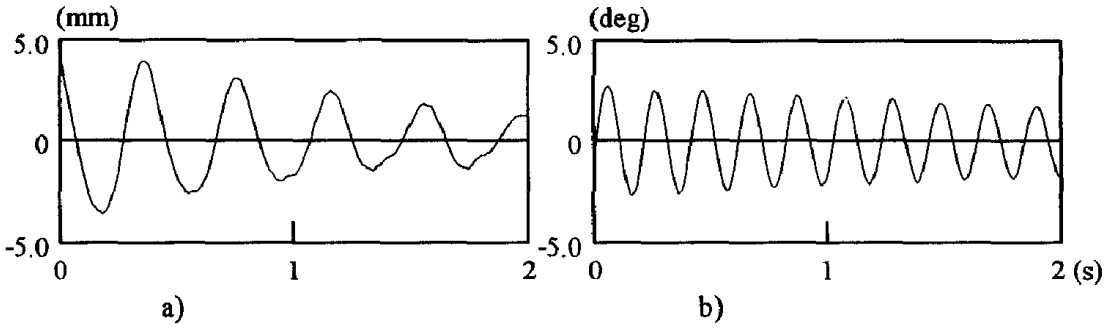

Figure 2.2 Free decay response at wind speed of 8 m/s; a) vertical displacement, b) torsional displacement (From Iwamoto and Fujino (1995))

Figure 2.2 shows uncouple phenomenon between vertical and torsional modes at mediate wind velocity. In figure 2.2a h_1 is dominant while α_1 is very small in figure 2.2b and vice versa with h_2 and α_2. Base on this observation they neglected the terms related to α_1 and h_2, and Eq. (2.8) can be rewritten as

$$\begin{aligned} L_{se} &= \frac{1}{2}\rho U^2 B\left[K_h H_1^*(K_h)\frac{\dot{h}_1}{U} + K_h^2 H_4^*(K_h)\frac{h_1}{B}\right] \\ &\quad + \frac{1}{2}\rho U^2 B\left[K_\alpha H_2^*(K_\alpha)\frac{B\dot{\alpha}_2}{U} + K_\alpha^2 H_3^*(K_\alpha)\alpha_2\right] \\ M_{se} &= \frac{1}{2}\rho U^2 B^2\left[K_h A_2^*(K_h)\frac{B\dot{\alpha}_1}{U} + K_h^2 A_3^*(K_h)\alpha_1\right] \\ &\quad + \frac{1}{2}\rho U^2 B^2\left[K_\alpha A_1^*(K_\alpha)\frac{\dot{h}_2}{U} + K_\alpha^2 A_4^*(K_\alpha)\frac{h_2}{B}\right] \end{aligned} \tag{2.9}$$

Eq. (2.9) also saying that ω_h should be used for H_i^* related to vertical motion, and ω_a for A_i^* related to torsional motion.

This verification is still not clearly because of the explanation base on amplitude of two modes oscillation; while in free vibration method the amplitude of vibration depend on initial amplitude. Therefore, in this study will be introduced another method to make this issue.

The equation of motion due to aerodynamic force can be written as

$$\begin{bmatrix} M & 0 \\ 0 & I \end{bmatrix}\begin{Bmatrix} \ddot{h} \\ \ddot{\alpha} \end{Bmatrix}+\begin{bmatrix} C_h & 0 \\ 0 & C_\alpha \end{bmatrix}\begin{Bmatrix} \dot{h} \\ \dot{\alpha} \end{Bmatrix}+\begin{bmatrix} K_h & 0 \\ 0 & K_\alpha \end{bmatrix}\begin{Bmatrix} h \\ \alpha \end{Bmatrix}=\begin{Bmatrix} L_{se} \\ M_{se} \end{Bmatrix} \tag{2.10}$$

where M and I are mass and mass inertial moment, respectively; C_h and C_a are mechanical damping of vertical and torsional modes, respectively; K_h and K_a are mechanical stiffness of vertical and torsional modes, respectively; L_{se} and M_{se} are self-excited force given as Eq. (2.6)

By substituting Eq. (2.6) into Eq. (2.10) and moving the aerodynamic damping and stiffness terms to the left hand side, Eq. (2.10) can be rewritten as follow:

$$\begin{bmatrix} M & 0 \\ 0 & I \end{bmatrix}\begin{Bmatrix} \ddot{h} \\ \ddot{\alpha} \end{Bmatrix}+\begin{bmatrix} \overline{C_{11}} & \overline{C_{12}} \\ \overline{C_{21}} & \overline{C_{22}} \end{bmatrix}\begin{Bmatrix} \dot{h} \\ \dot{\alpha} \end{Bmatrix}+\begin{bmatrix} \overline{K_{11}} & \overline{K_{12}} \\ \overline{K_{21}} & \overline{K_{22}} \end{bmatrix}\begin{Bmatrix} h \\ \alpha \end{Bmatrix}=\begin{Bmatrix} 0 \\ 0 \end{Bmatrix} \tag{2.11}$$

Where

$$\begin{aligned} \overline{C_{11}} &= C_h-\frac{1}{2}\rho\omega B^2 H_1^*(K) & \overline{K_{11}} &= K_h-\rho\omega^2 B^2 H_4^*(K) \\ \overline{C_{12}} &= -\frac{1}{2}\rho\omega B^3 H_2^*(K) & \overline{K_{12}} &= -\frac{1}{2}\rho\omega^2 B^3 H_3^*(K) \\ \overline{C_{21}} &= -\frac{1}{2}\rho\omega B^3 A_1^*(K) & \overline{K_{21}} &= -\frac{1}{2}\rho\omega^2 B^3 A_4^*(K) \\ \overline{C_{22}} &= C_\alpha-\rho\omega B^4 A_2^*(K) & \overline{K_{22}} &= K_\alpha-\frac{1}{2}\rho\omega^2 B^4 A_3^*(K) \end{aligned} \tag{2.12}$$

Under free vibration condition and eigenvalue problem of Eq. (2.11), the natural frequency and mode shape can be calculated as follows

$$-\omega^2\begin{bmatrix} M & 0 \\ 0 & I \end{bmatrix}\begin{Bmatrix} \Phi_1 \\ \Phi_2 \end{Bmatrix}+\begin{bmatrix} \overline{K_{11}} & \overline{K_{12}} \\ \overline{K_{21}} & \overline{K_{22}} \end{bmatrix}\begin{Bmatrix} \Phi_1 \\ \Phi_2 \end{Bmatrix}=\begin{Bmatrix} 0 \\ 0 \end{Bmatrix} \tag{2.13}$$

Where Φ_1 and Φ_2 are natural modes

Hence, the system characteristic equation is

$$\det\begin{bmatrix} -\omega^2 M+\overline{K_{11}} & \overline{K_{12}} \\ \overline{K_{21}} & -\omega^2 I+\overline{K_{22}} \end{bmatrix}=0 \tag{2.14}$$

Having the solutions

$$\begin{matrix} \omega_1^2 \\ \omega_2^2 \end{matrix}=\frac{\overline{K_{22}}}{2I}+\frac{\overline{K_{11}}}{2M}\pm\left[\left(\frac{\overline{K_{22}}}{2I}+\frac{\overline{K_{11}}}{2M}\right)^2-\frac{\overline{K_{11}}\,\overline{K_{22}}}{MI}+\frac{\overline{K_{12}}\,\overline{K_{21}}}{MI}\right]^{1/2} \tag{2.15}$$

Let $\dfrac{\overline{K_{11}}}{M}=\omega_h^2$; $\dfrac{\overline{K_{22}}}{I}=\omega_\alpha^2$ and substitute into Eq. (2.15)

$$\begin{matrix}\omega_1^2 \\ \omega_2^2\end{matrix} = \frac{\omega_\alpha^2 + \omega_h^2}{2} \pm \left[\left(\frac{\omega_\alpha^2 - \omega_h^2}{2} \right)^2 - \tau_{\alpha h}^2 \right]^{1/2} = 0 \tag{2.16}$$

where $$\tau_{\alpha h}^2 = -\frac{\overline{K_{12}}\,\overline{K_{21}}}{MI} \tag{2.17}$$

The mode shape of the 2 DOF systems can be calculated by inserting ω_1^2 from Eq. (2.16) into the first row of Eq. (2.13) and ω_2^2 from Eq. (2.16) into the second row of Eq. (2.13); Eq. (2.16) can be expressed by Mohr circle as show in figure 2.3.

Hence, letting arbitrarily $\Phi_{11} = 1$ and $\Phi_{22} = 1$, the natural modes become

$$\Phi_{21} = \frac{-\overline{K_{21}}}{-\omega_1^2 I + \overline{K_{22}}} \tag{2.18}$$

$$\Phi_{12} = \frac{-\overline{K_{12}}}{-\omega_2^2 M + \overline{K_{11}}} \tag{2.19}$$

The responses of two modes vertical and torsional can be written as follow

$$\begin{aligned} h &= \Phi_{11} z_1 + \Phi_{12} z_2 \\ \alpha &= \Phi_{21} z_1 + \Phi_{22} z_2 \end{aligned} \tag{2.20}$$

where z_1 and z_2 are natural coordinates.

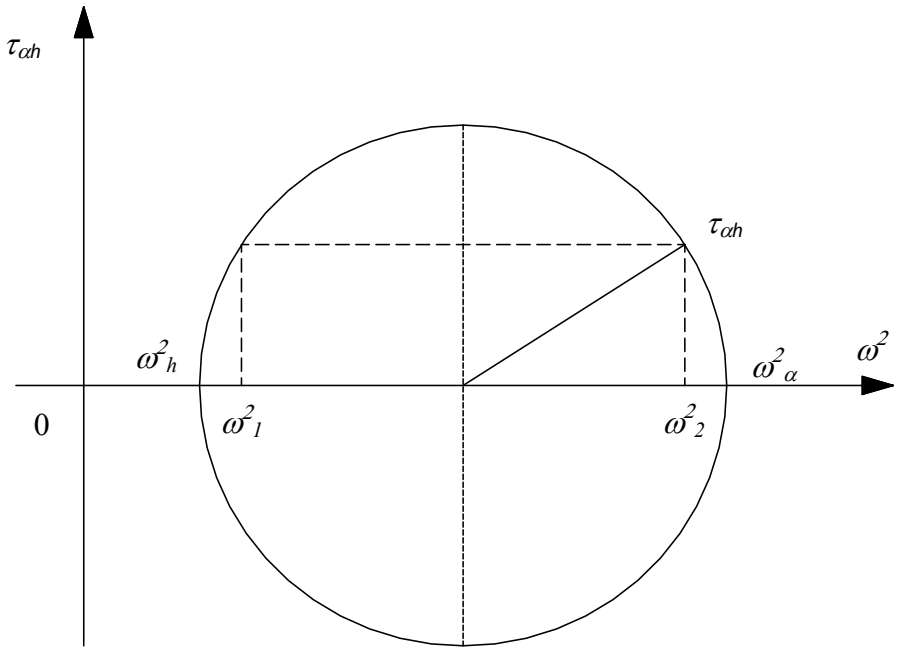

Figure 2.3 Mohr circle of vertical and torsional frequency

From the previous approve can be given some conclusion as follow:

1) If the effective stiffness in the of diagonal terms ($\overline{K_{12}}$ *and* $\overline{K_{21}}$) are considerably small, the value $\tau_{\alpha h}$ (Eq. 2.17) is also small, and the value of the frequency ω_1 is close to ω_α (pure torsional oscillation) and the frequency ω_2 is close to ω_h (pure vertical oscillation) (Eq. 2.16)
2) From Eqs. (2.18 & 2.19), if $\overline{K_{12}}$ *and* $\overline{K_{21}}$ are significant small, the natural mode Φ_{12} and Φ_{21} will be also small, then the responses of h and α in Eq. (2.20) will be dominated by Φ_{11} and Φ_{22}, respectively. It can be saying that the responses h and α can assumed solely by function of the frequencies ω_2 and ω_1, respectively.
3) The diagonal stiffness terms $\overline{K_{11}}$ *and* $\overline{K_{22}}$ are much larger compared with $\overline{K_{12}}$ *and* $\overline{K_{21}}$ because they contain the mechanical stiffness of structure. By this fact and the point 1 and 2 aforementioned, the assumption that the responses of two mode h and α as the solely function of the frequencies ω_2 and ω_1, respectively can be justified. The results of this assumption is that the reduced frequency which related to the vertical response h or $\dot{h}$ should be considered as the function of frequency ω_2 *(or* ω_h *)* and the reduced frequency which related to the torsional response α or $\dot{\alpha}$ should be considered as the function of frequency ω_1 *(or* ω_α *)*. Therefore, the aerodynamic forces in Eq. (2.6) can be rewritten as

$$L_{se} = \frac{1}{2}\rho U^2 B\left[K_h H_1^*(K_h)\frac{\dot{h}}{U} + K_\alpha H_2^*(K_\alpha)\frac{B\dot{\alpha}}{U} + K_\alpha^2 H_3^*(K_\alpha)\alpha + K_h^2 H_4^*(K_h)\frac{h}{B}\right]$$
$$M_{se} = \frac{1}{2}\rho U^2 B^2\left[K_h A_1^*(K_h)\frac{\dot{h}}{U} + K_\alpha A_2^*(K_\alpha)\frac{B\dot{\alpha}}{U} + K_\alpha^2 A_3^*(K_\alpha)\alpha + K_h^2 A_4^*(K_h)\frac{h}{B}\right] \quad (2.21)$$

Where

$$K_h = \frac{\omega_h B}{U};\ \ K_\alpha = \frac{\omega_\alpha B}{U} \quad (2.22)$$

CHAPTER 3

APPLICATION OF SYSTEM IDENTIFICATION TO IDENTIFY FLUTTER DERIVATIVES

In this chapter the most favored stochastic system identification methods that have been used to estimate the modal parameters of vibration structure in operational conditions. The chapter starts by presenting the mathematical techniques of stochastic state space models. Then output only time domain method which is stochastic subspace identification system utilized to identify dynamic properties of the model will be presented. The Covariance driven Stochastic System Identification (SSI_cov) method, which is computed the output covariance first as known that is impulse response. Thus, SSI_cov can be applied for ambient input or gust response. Second, Data driven stochastic subspace algorithms (SSI_data) which avoid the computation the output covariances will be presented. Next subsection presents how to extract flutter derivatives from modal parameters and final part presents uncertainties exiting and method increase accuracy of these methods.

3.1 Stochastic state space models

Considering a 2 DOF section model of bridge deck in turbulent flow, fluctuating wind load that acts on the deck can be expressed by a combination of a selt-excited force and a buffeting force:

$$\begin{aligned} m[\ddot{h} + 2\xi_h\omega_h\dot{h} + \omega_h^2 h] &= L_{se} + L_b \\ I[\ddot{\alpha} + 2\xi_\alpha\omega_\alpha\dot{\alpha} + \omega_\alpha^2\alpha] &= M_{se} + M_b \end{aligned} \tag{3.1}$$

where m and I are mass and mass moment of inertial per unit length, respectively; $\omega_h=2\pi f_h$ and $\omega_a=2\pi f_a$ are circular frequencies of vertical and torsional mode (in still air), respectively; ξ_h and ξ_a are heaving and torsional damping ratio to critical, respectively;

Another form dynamic equation of motion can be expressed likely that

$$\begin{aligned} m\ddot{h} + C_h\dot{h} + K_h h &= L_{se} + L_b \\ I\ddot{\alpha} + C_\alpha\dot{\alpha} + K_\alpha\alpha &= M_{se} + M_b \end{aligned} \tag{3.2}$$

where $C_h = 2(m\omega_h\xi_h)$ and $C_\alpha = 2(I\omega_a\xi_a)$ are mechanical damping of vertical and torsional modes, respectively; $K_h = m\omega_h^2$ and $K_a = I\omega_\alpha^2$ are mechanical stiffness of vertical and torsional modes,

respectively.

L_{se} and M_{se} are the aerodynamic self-excited lift and moment, respectively, given by

$$\begin{aligned} L_{se} &= \frac{1}{2}\rho U^2 B\left[K_h H_1^*(K_h)\frac{\dot{h}}{U} + K_\alpha H_2^*(K_\alpha)\frac{B\dot{\alpha}}{U} + K_\alpha^2 H_3^*(K_\alpha)\alpha + K_h^2 H_4^*(K_h)\frac{h}{B}\right] \\ M_{se} &= \frac{1}{2}\rho U^2 B^2\left[K_h A_1^*(K_h)\frac{\dot{h}}{U} + K_\alpha A_2^*(K_\alpha)\frac{B\dot{\alpha}}{U} + K_\alpha^2 A_3^*(K_\alpha)\alpha + K_h^2 A_4^*(K_h)\frac{h}{B}\right] \end{aligned} \tag{3.3}$$

where ρ is the air density; U is the mean wind velocity; B is the width of bridge deck; $K_i=\omega_i B/U$ is the reduce frequency ($i=h,\ \alpha$); H^*_i and A^*_i (i =1,2,3,4) are flutter derivatives.

L_b and M_b are buffeting forces in the vertical and torsional directions, respectively, given by

$$\begin{aligned} L_b &= \frac{1}{2}\rho U^2 B\left[2C_L\frac{u}{U} + \left(\frac{dC_L}{d\alpha} + \frac{D}{B}C_D\right)\frac{w}{U}\right] \\ M_b &= \frac{1}{2}\rho U^2 B^2\left[2C_M\frac{u}{U} + \left(\frac{dC_M}{d\alpha}\right)\frac{w}{U}\right] \end{aligned} \tag{3.4}$$

where D is the height of bridge deck; u and w are along and vertical turbulent components, respectively. C_D, C_L and C_M are shape factors depending on the angle of incidence. $dC_L/d\alpha$ and $dC_M/d\alpha$ are the slope of aerodynamic lift and moment, respectively.

By substituting Eq. (3.3) into Eq. (3.2) and moving the aerodynamic damping and stiffness terms to the left hand side, Eq. (3.2) can be rewritten as follow:

$$[M]\{\ddot{q}(t)\} + [C^e]\{\dot{q}(t)\} + [K^e]\{q(t)\} = \{f(t)\} = B_2 u(t) \tag{3.5}$$

where $\{q(t)\}=\{h(t)\ \alpha(t)\}^{\mathrm{T}}$ is the displacement vector; $\{f(t)\}=\{L_b\ \ M_b\}^{\mathrm{T}}$ is the buffeting force vector; $\{f(t)\}$ is factorized into matrix B_2 and input vector $u(t)$; $[M]$ is mass matrix; $[C^e]$ is gross damping matrix including the structural damping and aerodynamic damping; $[K^e]$ is gross stiffness matrix including the structural stiffness and aerodynamic stiffness. With the following definitions

$$M=\begin{bmatrix} m & 0 \\ 0 & I \end{bmatrix}; \qquad C^e=\begin{bmatrix} \overline{C_{11}} & \overline{C_{12}} \\ \overline{C_{21}} & \overline{C_{22}} \end{bmatrix}; \qquad K^e=\begin{bmatrix} \overline{K_{11}} & \overline{K_{12}} \\ \overline{K_{21}} & \overline{K_{22}} \end{bmatrix} \tag{3.6}$$

Where

$$\begin{aligned} \overline{C_{11}} &= C_h - \frac{1}{2}\rho\omega B^2 H_1^*(K) & \overline{C_{12}} &= -\frac{1}{2}\rho\omega B^3 H_2^*(K) \\ \overline{C_{21}} &= -\frac{1}{2}\rho\omega B^3 A_1^*(K) & \overline{C_{22}} &= C_\alpha - \rho\omega B^4 A_2^*(K) \end{aligned} \tag{3.7}$$

$$\overline{K_{11}} = K_h - \rho\omega^2 B^2 H_4^*(K) \qquad \overline{K_{12}} = -\frac{1}{2}\rho\omega^2 B^3 H_3^*(K)$$
$$\overline{K_{21}} = -\frac{1}{2}\rho\omega^2 B^3 A_4^*(K) \qquad \overline{K_{22}} = K_\alpha - \frac{1}{2}\rho\omega^2 B^4 A_3^*(K) \tag{3.7}$$

The second-order differential equation Eq. (3.5) can be transformed into a first-order state equation Eq. (3.8).

$$\dot{x}(t) = A_c x(t) + B_c u(t) \tag{3.8}$$

where

$$x(\mathrm{t}) = \begin{Bmatrix} q(t) \\ \dot{q}(t) \end{Bmatrix}; \quad A_c = \begin{bmatrix} 0 & I_u \\ -[M]^{-1}[K^e] & -[M]^{-1}[C^e] \end{bmatrix}; \quad \mathrm{B}_c = \begin{bmatrix} 0 \\ [M]^{-1} B_2 \end{bmatrix} \tag{3.9}$$

A_c is designated state matrix with size *4*-by-*4*; *x(t)* is the state vector; B_c is the input matrix; I_u is a unit matrix

The combination of the state equation and the observation equation fully describes the input and output behaviors of the structural system and are named a state-space system.

$$\begin{aligned} \dot{x}(t) &= A_c x(t) + B_c u(t) \\ y(t) &= C_c x(t) + D_c(u(t)) \end{aligned} \tag{3.10}$$

C_c is the output matrix and D_c is the direct transmission matrix at continuous time.
Eq. (3.10) is a deterministic state space model in a continuous time. Continuous time means that the expression can be evaluated at each time instant, deterministic means that the input and output quantities can be measured exactly. This is not practical; the measurements are mostly sampled at discrete-time. In addition, it is impossible to measure all DOFs and measurements always have disturbance effects. For all these reasons, the continuous deterministic system is converted to a suitable form: discrete-time combined deterministic-stochastic state-space model as follow:

$$\begin{aligned} x_{k+1} &= Ax_k + Bu_k + w_k \\ y_k &= Cx_k + Du_k + v_k \end{aligned} \tag{3.11}$$

where $x_k = x(k\Delta t) = \{q_k \ \dot{q}_k\}^T$ is the discrete-time state vector containing the discrete sample displacement q_k and velocity $\dot{q}_k$; w_k and v_k is the process noise due to disturbances and modelling inaccuracies and the measurement noise due to sensor inaccuracy respectively.

Assuming that w_k and v_k being zero mean and covariance matrix as

$$E\left[\begin{pmatrix} w_p \\ v_p \end{pmatrix}\begin{pmatrix} w_q^T & v_q^T \end{pmatrix}\right] = \begin{pmatrix} Q & S \\ S^T & R \end{pmatrix}\delta_{pq} \tag{3.12}$$

where the indices p and q are time-instants; E is the expectation operator; δ_{pq} is the Kronecker delta. The correlation $E(w_p\, w_q{}^{\mathrm{T}})$ and $E(v_p\, v_q{}^{\mathrm{T}})$ are equal to zero in case of different time-instant. $Q = E(w_k\, w_k^T)$; $R = E(v_k\, v_k^T)$; $S = E(w_k v_k^T)$

3.2 Stochastic system identification

In the modal analysis, the input is sometimes unknown and the system will be excited by white noise. The stochastic state-space model can be expressed as

$$\begin{aligned} x_{k+1} &= Ax_k + w_k \\ y_k &= Cx_k + v_k \end{aligned} \tag{3.13}$$

Assumption, the stochastic model assumes that $\{x_k\}$, $\{w_k\}$ and $\{v_k\}$ are mutually independent, and they are zero mean.

Hence, $E(x_k) = 0$; $E(w_k) = 0$; $E(v_k) = 0$; $E(x_k w_k^T) = 0$; $E(x_k v_k^T) = 0$

The state covariance matrix is defined as

$$\Sigma = E(x_k \quad x_k^T) \tag{3.14}$$

The output covariance matrix is as following

$$\Lambda_i = E(y_{k+i} \quad y_k^T) \tag{3.15}$$

The state-output covariance matrix is defined as

$$G = E(x_{k+1} \quad y_k^T) \tag{3.16}$$

From Eqs.(3.13)-(3.16), the following are obtained

$$\begin{aligned} \Sigma &= A\Sigma A^T + Q \\ \Lambda_0 &= C\Sigma C^T + R \\ G &= A\Sigma C^T + S \end{aligned} \tag{3.17}$$

$$\Lambda_i = CA^{i-1}G \tag{3.18}$$

Eq. (3.18) is called Lyapunov equation which means that the output covariance can be considered as impulse responses.

Therefore, the theoretical application of stochastic system can go back to Eigen-system realization algorithm (ERA) method (Juang & Pappa 1985).

Three figures (3.2-3.3) show the linear time-invariant deterministic system, combined deterministic-stochastic system and stochastic system problems, respectively.

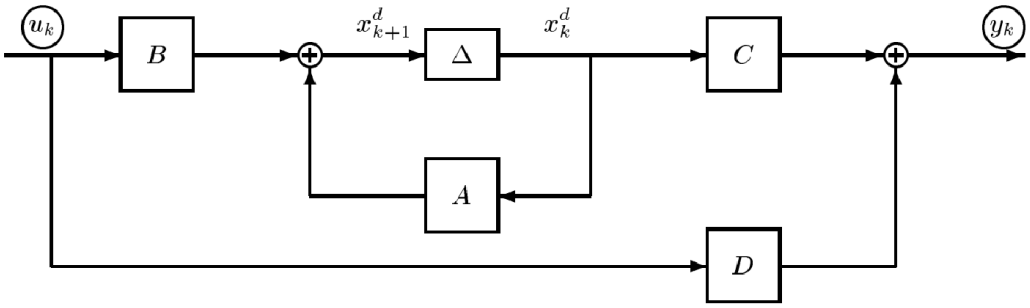

Figure 3.1 A linear time-invariant deterministic system illustrate Eq. (3.10)

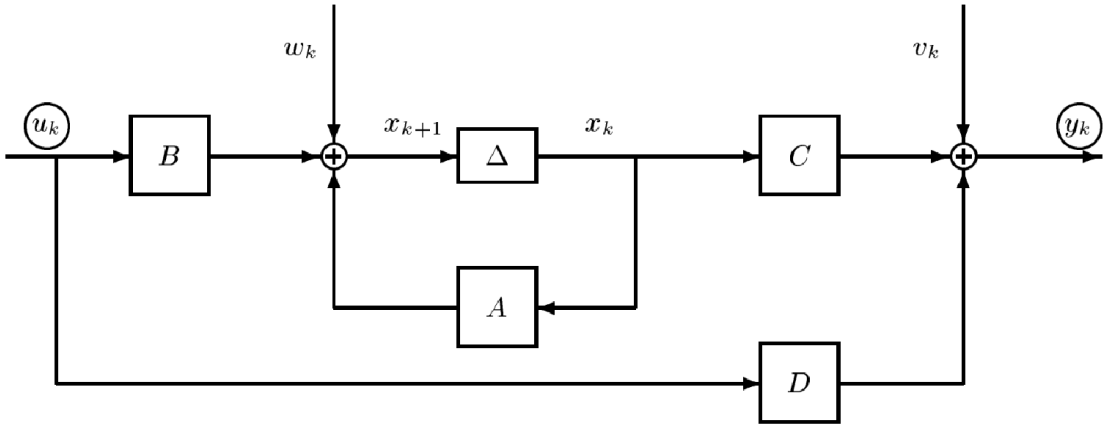

Figure 3.2 A linear time-invariant combined deterministic-stochastic system illustrate Eq. (3.11)

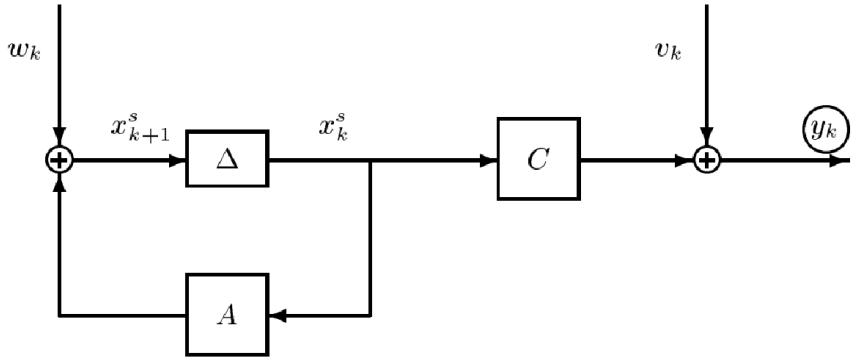

Figure 3.3 A linear time-invariant stochastic system illustrate Eq. (3.13)

3.3 Covariance driven Stochastic System Identification (SSI_cov)

The heart of SSI_cov method is the ERA developed by Juang & Pappa (1985). It is the famous technique for modal parameter identification from free vibration response or impulse response.

The output measurement data obtained from l sensors (in this study l=2)

$$y = (y_0, y_1, y_2, y_2 \ldots y_n) \in R^{lxn} \tag{3.19}$$

The output data are assembled in block Hankel matrix with 2i block rows, and j column as

$$H = \left[\begin{array}{cccc} y_0 & y_1 & \cdots & y_{j-1} \\ y_1 & y_2 & \cdots & y_j \\ \cdots & \cdots & & \cdots \\ y_{i-1} & y_i & \cdots & y_{i+j-2} \\ \hline y_i & y_{i+1} & \cdots & y_{i+j-1} \\ y_{i+1} & y_{i+2} & \cdots & y_{i+j} \\ \cdots & \cdots & & \cdots \\ y_{2i-1} & y_{2i} & \cdots & y_{2i+j-2} \end{array}\right]_{2ixj} = \left[\begin{array}{c} Y_{0|i-1} \\ \hline Y_{i|2i-1} \end{array}\right] = \left[\begin{array}{c} Y_p \\ \hline Y_f \end{array}\right] \begin{array}{c} \updownarrow li \\ \hline \updownarrow li \end{array} \tag{3.20}$$

where $2i$ is the number of block rows, j is the number of data points, l is the number of output sensors. The Hankel matrix can be divided into two parts, the upper is the past output and lower is the future output.

The number of block row (i) is a user defined index which large enough but it should at least be larger than the maximum order of the system one want identify. One block contain l rows (number of output (l=2)), the matrix H consist $2il$ rows.

The number of columns j is typically equal to s-$2i$+1 (s is length of data), which mean that all of data s are used

The key step in the SSI_cov system is the computation of output covariance that is similarly compared with CBHM (Jakobsen 1995).which can be expressed assuming ergodicity process as:

$$\Lambda_i = E[y_{k+1}\ y_k^T] = \lim_{N\to\infty} \frac{1}{N} \sum_{k=0}^{N-1} y_{k+i} y_k^T \approx \frac{1}{N} \sum_{k=0}^{N-1} y_{k+i} y_k^T \tag{3.21}$$

where i is time lag; N is finite number of data

All output covariance Λ_i in Eq. (3.21) is stored in block Toeplitz matrix as:

$$T_{1|i} = \begin{bmatrix} \Lambda_i & \Lambda_{i-1} \cdots \Lambda_1 \\ \Lambda_{i+1} & \Lambda_i \ \cdots \ \Lambda_2 \\ \cdots & \cdots \ \ \cdots \\ \Lambda_{2i-1} & \Lambda_{2i-2} \cdots \Lambda_i \end{bmatrix}_{ixi} \tag{3.22}$$

Combining Eq. (3.18) and Eq. (3.22), then block Toeplitz matrix can be decomposed as follows

$$T_{1|i} = \begin{bmatrix} C \\ CA \\ \cdots \\ CA^{i-1} \end{bmatrix} [A^{i-1}G \quad A^{i-2}G \cdots AG \quad G] = O_i C_i \tag{3.23}$$

On the other hand, observability matrix O_i and controllability matrix C_i can be obtained from singular value decomposition (SVD) of the Toeplitz matrix:

$$T_{1|i} = \begin{bmatrix} U_1 & U_2 \end{bmatrix} \begin{bmatrix} S_1 & 0 \\ 0 & 0 \end{bmatrix} \begin{bmatrix} V_1^T \\ V_2^T \end{bmatrix} = U_1 S_1 V_1^T \tag{3.24}$$

where *U, V* are orthonormal matrices and *S* is a diagonal matrix containing singular values. The number of non-zero give the rank of the decomposed matrix and coincide with the size *n* (n=2xDOF=4) of the state-space matrix *A*. Comparing with the Eq. (3.23) and Eq. (3.24), we can be rewritten that

$$\begin{aligned} O_i &= U_1 S_1^{1/2} \\ C_i &= S_1^{1/2} V_1^T \end{aligned} \tag{3.25}$$

Now the realization of state matrix *A* and controllability matrix *C* are achieved. The state matrix *A* can be obtained by decomposing a shift block Toeplitz matrix:

$$T_{2|i+1} = O_i A C_i \tag{3.26}$$

Combining the Eq. (3.25) and Eq. (3.26) gives:

$$A = O_i^{\dagger} T_{2|i+1} C_i = S_i^{-1/2} U_1^T T_{2|i+1} V_1 S_1^{-1/2} \tag{3.27}$$

where $(.)^{\dagger}$ is the pseudo-inverse of a matrix. The output matrix *C* equals the first *l* rows of O_i where *l* number of outputs (in this study *l*=2 for 2 DOF system).

3.4 Data driven Stochastic System Identification (SSI_data)

The Stochastic Subspace Identification (SSI) algorithm was originally introduced by Van Overschee and De Moor (1991) and then developed (SSI_data method) by Peeters and De

Roeck (1999).

SSI_data implement directly with output of experimental data, without need to convert output data to correlation, covariance or spectra. The main step of SSI_data is a projection of the row space of the future outputs into the row of past outputs. The orthogonal projection P_i is defined as:

$$P_i = Y_f / \mathbf{Y}_p = Y_f Y_p (Y_p Y_p{}^T)^{-1} Y_p \tag{3.28}$$

where the matrix Y_f and Y_p are the lower and upper half part of a bock Hankel matrix H.

QR factorization of the block Hankel matrix Eq. (3.20) is defined as

$$H = \begin{bmatrix} Y_p \\ \hline Y_f \end{bmatrix} = RQ^T \tag{3.29}$$

Where $Q \in R^{j \text{ x } j}$ is an orthogonal matrix $Q^TQ = QQ^T = I_j$ and $R \in R^{2li \text{ x } j}$ is a lower triangular matrix. Because $2li < j$ so it can reject the zeros in R and the corresponding zeros in Q

$$H = \begin{array}{c} \\ li \\ l \\ l(i-1) \end{array} \begin{array}{c} \begin{array}{ccc} li & l & l(\mathrm{i}-1) \end{array} \\ \begin{pmatrix} R_{11} & 0 & 0 \\ R_{21} & R_{22} & 0 \\ R_{31} & R_{32} & R_{33} \end{pmatrix} \end{array} \begin{array}{c} \begin{array}{c} j \to \infty \end{array} \\ \begin{pmatrix} Q_1^T \\ Q_2^T \\ Q_3^T \end{pmatrix} \end{array} \begin{array}{l} \\ li \\ l \\ l(i-1) \end{array} \tag{3.30}$$

Substituting the QR factorization of the output Hankel matrix (3.30) into Eq. (3.28) will be obtained the simple expression of the projection

$$P_i = \begin{pmatrix} R_{21} \\ R_{31} \end{pmatrix} Q_1^T \tag{3.30}$$

Stochastic subspace identification has been an exited the main theorem is that the projection P_i can be factorized as the product of observability matrix O_i and the Kalman filter state sequence $\hat{X}_i$ (Peeters & Roeck 1999):

$$P_i = \begin{pmatrix} C \\ CA \\ \cdots \\ CA^{i-1} \end{pmatrix} \begin{pmatrix} \hat{x} & \hat{x}_{i+1} & \cdots & \hat{x}_{i+j-1} \end{pmatrix} = O_i \hat{X}_i \tag{3.31}$$

The observability matrix O_i and the Kalman filter sequence $\hat{X}_i$ are obtained by applying SVD to the projection matrix:

$$P_i = U_1 S_1 V_1^T \tag{3.32}$$

Comparing Eq. (3.31) and Eq. (3.32) gives:

$$O_i = U_1 S_1^{1/2}, \qquad \hat{X}_i = O_i^{\dagger} P_i \tag{3.33}$$

If the past and future outputs of Hankel matrix are shifted, time-shift projection is achieved:

$$P_{i-1} = Y_f^- / \boldsymbol{Y}_p^+ = O_{i-1} \hat{X}_{i+1} \tag{3.34}$$

where

$$P_{i-1} = \begin{pmatrix} R_{31} & R_{32} \end{pmatrix} \begin{pmatrix} Q_1^T \\ Q_2^T \end{pmatrix} \tag{3.35}$$

$O_{i\text{-}1}$ is obtained from O_i after deleting the last l rows and the shifted state sequence can be computed in Eq. (3.34) as:

$$\hat{X}_{i+1} = O_{i-1}^{\dagger} P_{i-1} \tag{3.36}$$

From Eq. (3.33) and Eq. (3.36), the Kalman state sequences $\hat{X}_i, \hat{X}_{i+1}$ are calculated using only output data. The state and controllability matrices can be recovered from over determined set of linear equations, obtained by extending Eq. (3.13):

$$\begin{aligned} \begin{pmatrix} \hat{X}_{i+1} \\ Y_{i|i} \end{pmatrix} &= \begin{pmatrix} A \\ C \end{pmatrix} \left(\hat{X}_i \right) + \begin{pmatrix} \rho_w \\ \rho_v \end{pmatrix} \\ Y_{i|i} &= \begin{pmatrix} R_{21} & R_{22} \end{pmatrix} \begin{pmatrix} Q_1^T \\ Q_2^T \end{pmatrix} \end{aligned} \tag{3.37}$$

where $Y_{i/i}$ is a Hankel matrix with only one block row. Since the Kalman state sequence and the outputs are known, and the residual $(\rho^{\mathrm{T}}{}_{\mathrm{w}} \ \rho^{\mathrm{T}}{}_{\mathrm{v}})^{\mathrm{T}}$ are uncorrelated with $\hat{X}_i$, the set of equation can be solved for A and C in a least-squares:

$$\begin{pmatrix} A \\ C \end{pmatrix} = \begin{pmatrix} \hat{X}_{i+1} \\ Y_{i|i} \end{pmatrix} \left(\hat{X}_i \right)^{\dagger} \tag{3.38}$$

Kalman filter state: Kalman filter plays an important role for stochastic system identification (more detail can be found from Appendix B). The Kalman filter provides an optimal prediction of the states x_{k+1} are estimate by using the observation of the outputs up to time k and the available system matrices to gather with the known noise cavariances. If the initial state is $\hat{x}_0 = 0$, the corresponding covariance is given by $P_0 = E\left[\hat{x}_0 \ \hat{x}_0^T \right] = 0$ and the output measurements (y_0, ..., y_k,) are given the non-steady- state Kalman filter states $\hat{x}_{k+1}$ by the following formula:

$$\begin{aligned}
&\hat{x}_{k+1} = A\hat{x}_k + K_k(y_k - C\hat{x}_k) \\
&K_k = (G - AP_kC^T)(\Lambda_0 - CP_kC^T)^{-1} \\
&P_{k+1} = AP_kA^T + (G - AP_kC^T)(\Lambda_0 - CP_kC^T)^{-1}(G - AP_kC^T)^T
\end{aligned} \tag{3.39}$$

where K_k is the Kalman filter gain and P_k is the Kalman state covariance matrix. The Kalman filter state are gathered to form of Kalman filter state sequence, such as

$$\hat{X}_i = (\hat{x}_i \;\; \hat{x}_{i+1} \;\; \ldots \;\; \hat{x}_{i+j-1}) \tag{3.40}$$

3.5 Identification of flutter derivatives

The modal parameters of the system can be obtained by solving the eigenvalue problem for the state matrix A from Eqs. (3.27 & 3.38):

$$A = \Psi\Lambda\Psi^{-1}; \quad \Phi = C\Psi \tag{3.41}$$

where Ψ is the complex eigenvector; Λ is the complex eigenvalue; Φ is the mode shape matrix. When the complex modal parameters are known, the gross damping C^e and gross stiffness K^e in Eq. (3.6) are determined by

$$\begin{bmatrix} K^e & C^e \end{bmatrix} = -M \begin{bmatrix} \Phi\Lambda^2 & \Phi^*(\Lambda^*)^2 \end{bmatrix} \begin{bmatrix} \Phi & \Phi^* \\ \Phi\Lambda & \Phi^*\Lambda^* \end{bmatrix}^{-1} \tag{3.42}$$

Letting

$$\begin{aligned}
&\overline{C}^e = M^{-1}C^e; \quad \overline{K}^e = M^{-1}K^e \\
&\overline{C} = M^{-1}C^0; \quad \overline{K} = M^{-1}K^0
\end{aligned} \tag{3.43}$$

where C^0 and K^0 are the physical damping and stiffness matrices of the model under the no-wind condition, the flutter derivatives of 2 DOF can be defined as:

$$\begin{aligned}
H_1^*(K_h) &= -\frac{2m}{\rho B^2\omega_h}(\overline{C}_{11}^e - \overline{C}_{11}), & A_1^*(K_h) &= -\frac{2I}{\rho B^3\omega_h}(\overline{C}_{21}^e - \overline{C}_{21}) \\
H_2^*(K_\alpha) &= -\frac{2m}{\rho B^3\omega_\alpha}(\overline{C}_{12}^e - \overline{C}_{12}), & A_2^*(K_\alpha) &= -\frac{2I}{\rho B^4\omega_\alpha}(\overline{C}_{22}^e - \overline{C}_{22}) \\
H_3^*(K_\alpha) &= -\frac{2m}{\rho B^3\omega_\alpha^2}(\overline{K}_{12}^e - \overline{K}_{12}), & A_3^*(K_\alpha) &= -\frac{2I}{\rho B^4\omega_\alpha^2}(\overline{K}_{22}^e - \overline{K}_{22}) \\
H_4^*(K_h) &= -\frac{2m}{\rho B^3\omega_h^2}(\overline{K}_{11}^e - \overline{K}_{11}), & A_4^*(K_h) &= -\frac{2I}{\rho B^4\omega_h^2}(\overline{K}_{21}^e - \overline{K}_{21})
\end{aligned} \tag{3.44}$$

The flowchart of these procedures to be follow to use the stochastic system identification flutter derivatives are presented in figures 3.4&3.5

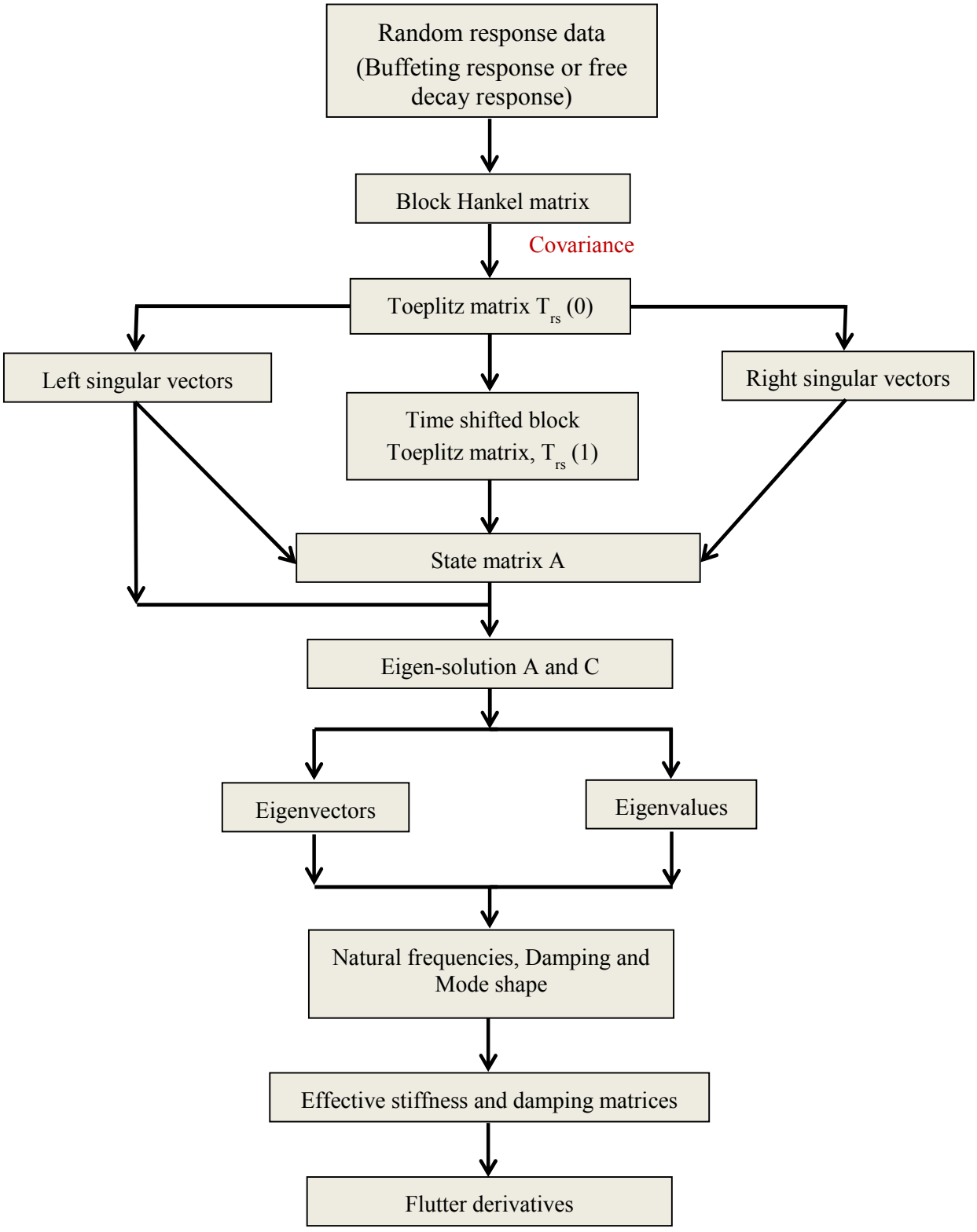

Figure 3.4 Flow chart of the SSI_cov method

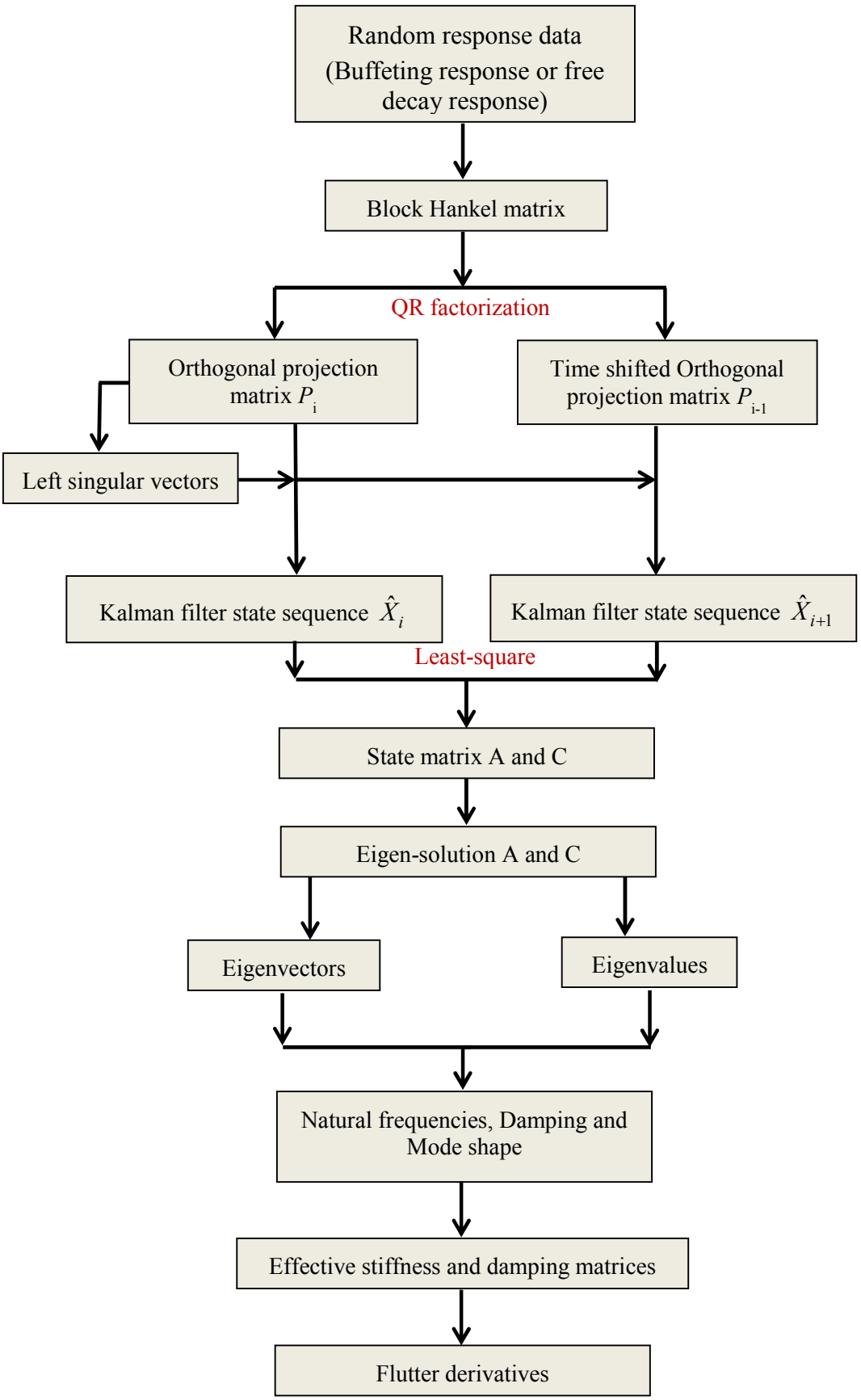

Figure 3.5 Flow chart of the SSI_data method

3.6 Elimination noise effects

In the output-only system identification method, which assumption the system will be excited by white noise. If this white noise assumption is violated, such as if the output data contains some dominant frequency components, these frequency components cannot be separated from Eigen-frequency of the system and then spurious modes will appear in the state matrix *A*. System order to remove spurious modes can be decided by a stabilization diagram (Reynders *et al.* 2008). The spurious modes can be rejected by selecting the mode at a model order that is high enough.

The stochastic system identification does not yield exact values for the parameters but only estimates with uncertainties. The origins of these uncertainties (Reynders 2008) can be described as follow:

From the experimental point of view: the number of data samples is finite for stochastic problem; the input might not be white noise and non-stationary effect.

From a statistical point of view: an uncertainty can be induced by the bias of the model or by the bias of the modes and the variance of the modes.

These uncertainties are caused by the appearance of spurious modes. The stabilization diagram can be detected spurious modes if sufficiently high values of the model order are taken into account.

The stabilization diagram is a graphical tool method used to help in the selection of the order of system. The quality of a stabilization diagram depends on the algorithm used in the identification, on the values of the input parameters of the algorithm, and also on noise ratio of the time series under analysis.

There are three ways to construct a stabilization diagram:

1. Fix the dimension of Toeplitz matrix an increase the system order. The advantage of this method is computational time saving. The drawback is that the required dimension of Toeplitz matrix is unknown, the computed pole increase with the system order, if the additional criteria is not used.

fix

Increase system order

$$T_{1|i} = fix \begin{bmatrix} \Lambda_i & \Lambda_{i-1} \cdots \Lambda_1 \\ \Lambda_{i+1} & \Lambda_i \ \cdots \ \Lambda_2 \\ \cdots & \cdots \ \ \cdots \\ \Lambda_{2i-1} & \Lambda_{2i-2} \cdots \Lambda_i \end{bmatrix}_{ixi} = USV^T = (U_1 \quad U_2)\begin{pmatrix} S_1 & 0 \\ 0 & 0 \end{pmatrix}\begin{pmatrix} V_1^T \\ V_2^T \end{pmatrix} \tag{3.45}$$

2. Fix the system order and increase the size of Toeplitz matrix (square matrix). The

advantage of this method is larger the size and more components the Toeplitz matrix be decomposed, therefore more effectives noise elimination is achieve increasing the size of Toeplitz matrix. Main drawback is time consuming and determination of system order.

$$T_{1|i} = \begin{bmatrix} \Lambda_i & \Lambda_{i-1} \cdots \Lambda_1 \\ \Lambda_{i+1} & \Lambda_i \cdots \Lambda_2 \\ \cdots & \cdots \\ \Lambda_{2i-1} & \Lambda_{2i-2} \cdots \Lambda_i \end{bmatrix}_{ixi} = USV^T = (\mathrm{U}_1 \quad \mathrm{U}_2)\begin{pmatrix} S_1 & 0 \\ 0 & 0 \end{pmatrix}\begin{pmatrix} V_1^T \\ V_2^T \end{pmatrix} \tag{3.46}$$

Increase size (↘) — *fix* (⇔)

3. Fix the system order and increase the only rows of Toeplitz matrix (rectangular matrix)

$$T_{1|i} = \begin{bmatrix} \Lambda_i & \Lambda_{i-1} \cdots \Lambda_1 \\ \Lambda_{i+1} & \Lambda_i \cdots \Lambda_2 \\ \cdots & \cdots \\ \Lambda_{2i-1} & \Lambda_{2i-2} \cdots \Lambda_i \end{bmatrix}_{ixi} = USV^T = (\mathrm{U}_1 \quad \mathrm{U}_2)\begin{pmatrix} S_1 & 0 \\ 0 & 0 \end{pmatrix}\begin{pmatrix} V_1^T \\ V_2^T \end{pmatrix} \tag{3.47}$$

Increase size (↓) — *fix* (⇔)

4. The advantage of this method is less time consuming than second method, the drawback is required the number of columns depend on the signal content, and also determination of system order.

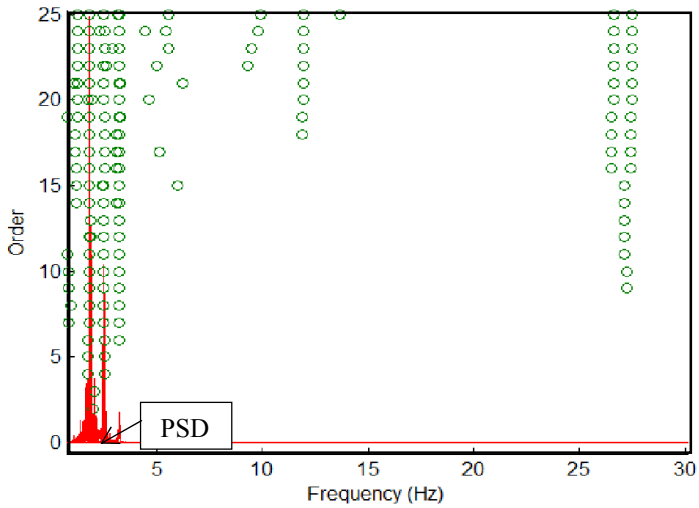

Figure 3.6 Stabilization diagram

In this dissertation, based on section model wind tunnel test that is a real order of system always known before (equal a number degree of freedom of model testing). The elimination spurious mode is using the first scheme corresponding to fix the size of Toeplitz matrix (with

SSI_cov) or fix the size Hankel matrix (with SSI_data), and changing the order of system will be obtained stabilization diagram (model order versus frequency) (figure 3.6). Base on this diagram, the real model order can be chosen by selecting the mode at an order high enough.

CHAPTER 4

WIND TUNNEL EXPERIMENT

This chapter describes the equipment used in this study including the wind tunnel, the model bridge deck and grid for turbulent generation and data acquisition system.

4.1 Experiment set-up

4.1.1 The Atmospheric Wind Tunnel

The atmospheric wind tunnel is close-circuit wind tunnel located at Yokohama National University as shown in Figure. (4.1). The working section is 1.8m wide and 1.8m high, maximum wind velocity is 35m/s.

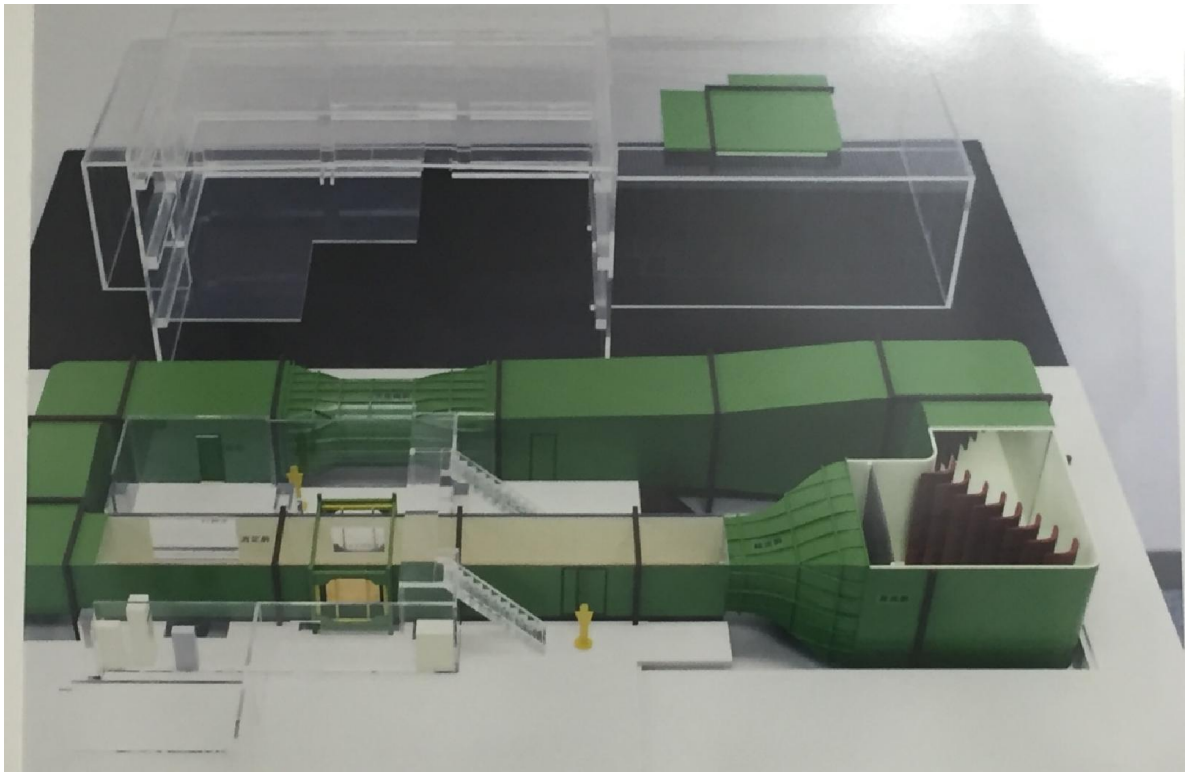

Figure 4.1 Three dimension model of YNU wind tunnel

Turbulent flows used in this study were generated by using biplane wooden grid. The grid with bar size is 6 cm and bar spacing is 24 cm as show in Figure 4.2. Turbulence properties are controlled by changing the distance to model. In this study, three grid positions to model

corresponding to three different turbulent intensities are generated. I = 6.2%, I = 9.1% and I = 15.6% corresponding grid position to the model is 4.84 m, 3.34 m and 1.97 m, respectively.

a. Biplane wooden grid b. Installation grid in wind tunnel

Figure 4.2 Grid generates turbulent flow

4.1.2 Section Model

The prototype of bridge deck section is truss deck which the cross-section dimension is shown in figure. (4.3).

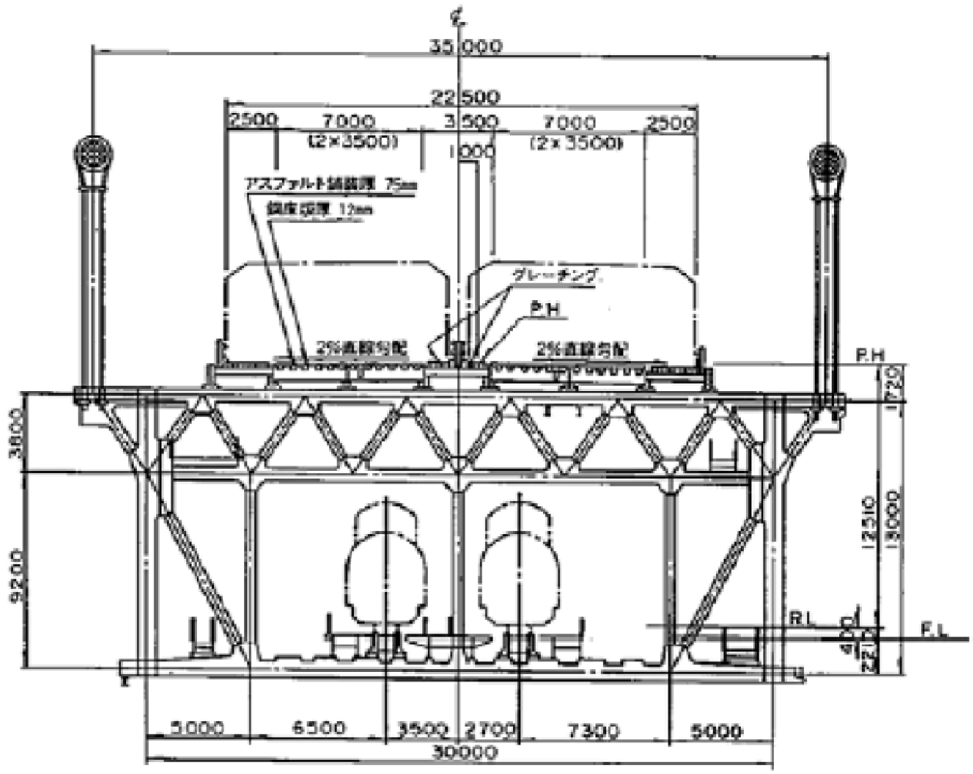

Figure 4.3 Prototype trussed deck section

The prototype cross section includes two layers, the upper use for vehicle and lower for train. The orthotropic slab which the grating located at middle and both side of vehicle layer.

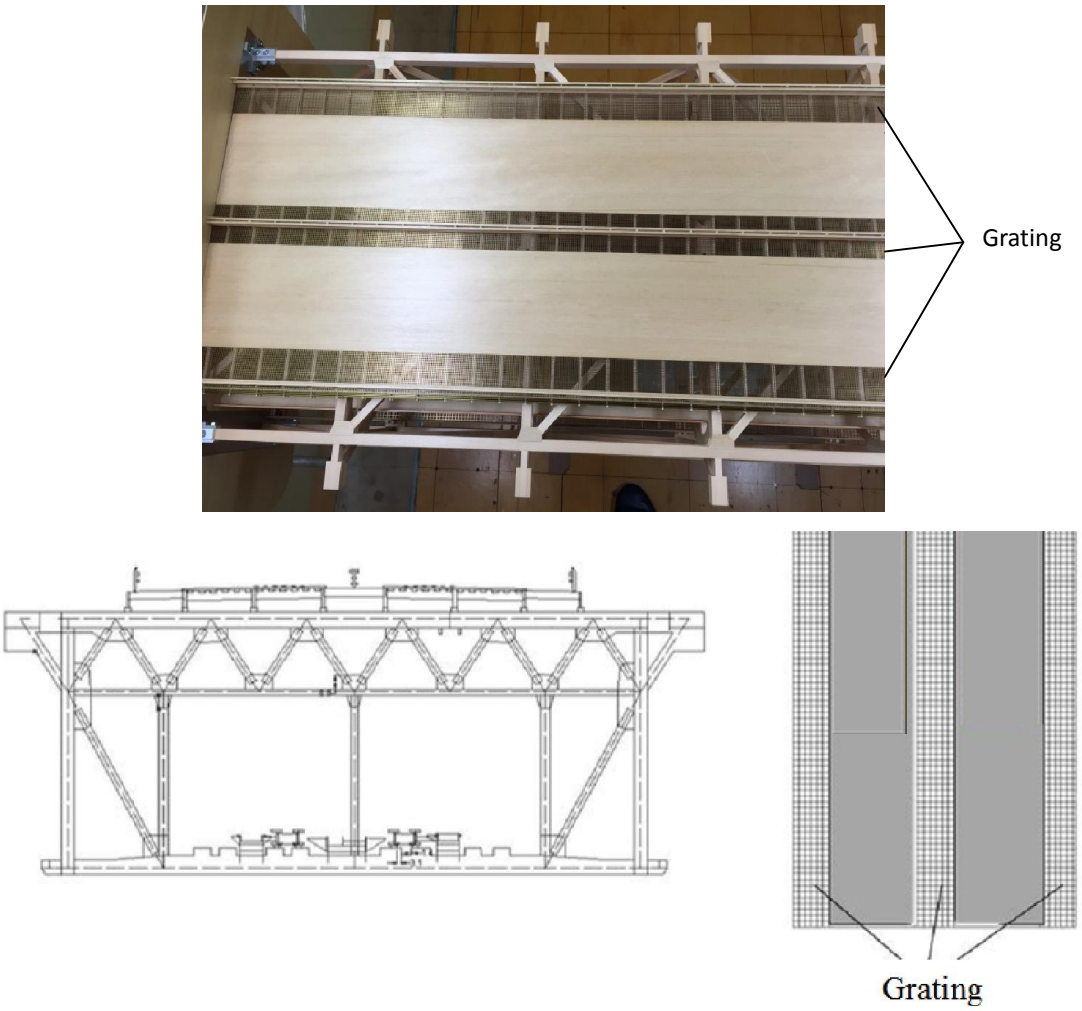

Figure 4.4 Original slab of trussed deck section

Identification of flutter derivatives of long span bridge deck are through the section bridge which is designed a certain length. The section model is used in this study base on section of bridge shown in figure 4.4 which the grating will be covered and noise fence installed under the rail way as shown in figures (4.5 &4.6).

The model section is scaling down from prototype much be considered some scale factors, such as length scale, velocity scale and density scale.

The model was fabricated by wood with a scale of 1:80. The length of section model is 1.25m. The width and depth of the section model are 363 mm and 162.5 mm, respectively. The unit mass and moment of inertia are 8.095 kg/m and 0.2281 kgm^2/m, respectively. The detail test condition is described into table 4.1

Table 4.1 Model property

		Prototype	Model requirement	Real model	Deviation
Width B (m)		30.0	0.375	0.375	0 (%)
Height D (m)		13.0	0.1625	0.1625	0 (%)
Mass m (kg/m)		$40.63x10^3$	6.348 (7.936 kg)	(8.095)	+2 (%) (≤2%)
Moment of inertia (kgm^2/m)		$7.63 x10^3$	0.1863 ($0.2328 kgm^2$)	(0.2281)	-2 (%) (≤22%)
Frequency (Hz)	Vertical	0.166		1.869	7.11
	Torsional	0.329		3.296	7.99
	Ratio	1.98	1.98	1.76	-11% (≤5%)
Damping (logarithm decrement)	Vertical	0.03	0.03	0.0322	+0.0022 (±0.005%)
	Torsional	0.03	0.03	0.0263	+0.0037 (±0.005%)

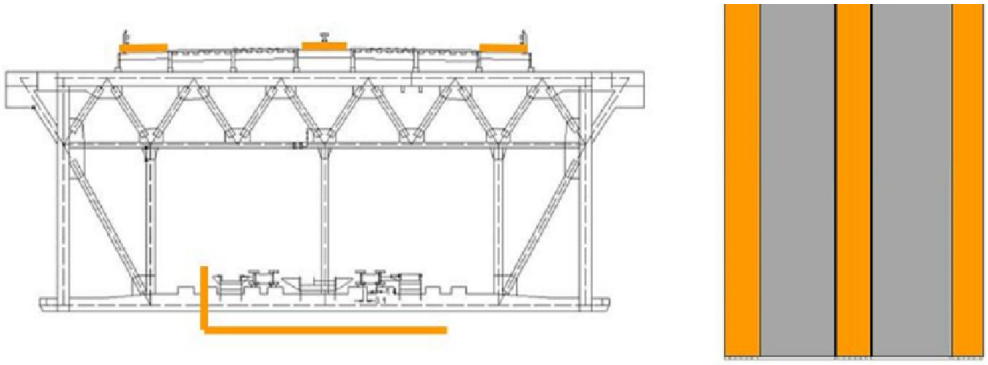

Figure 4.5 Covered the grating and noise fence installed under the rail way

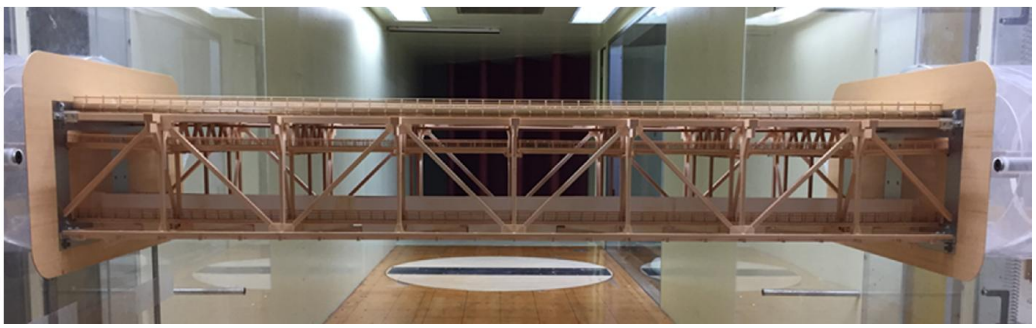

a. Elevation

Figure 4.6 Trussed deck section model (cont.)

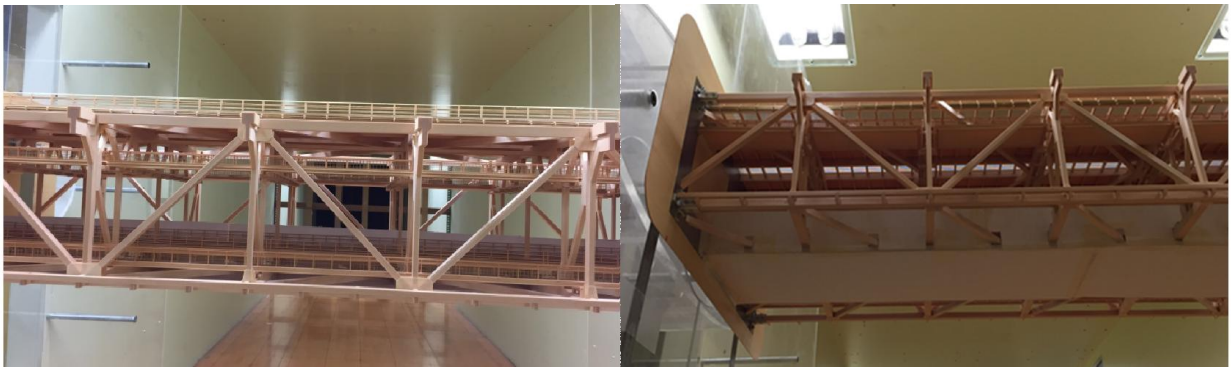

b. Leading edge c. Trailing edge

Figure 4.6 Trussed deck section model

4.1.3 Experimental setup

The model is attacked to a rigid test frame and suspended across wind tunnel by eight equal helical springs with stiffness k which arranged at arm distance equal from upstream and downstream of the geometric centerline. The contributions of spring mass to total mas and inertia are accounted by adding one-third of their mass at their point of attachment. Piano wires were also used to arrest motion in a desired degree of freedom. The configuration set-up can be seen in Figures (4.7 & 4.8). Vertical and torsional displacement obtained by laser transducers.

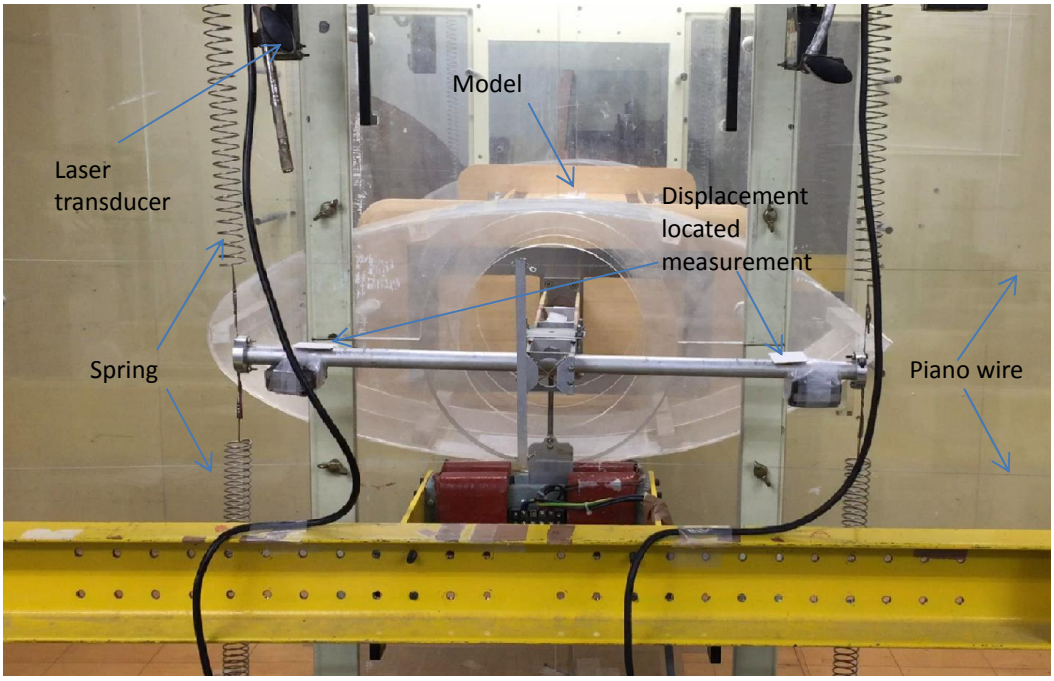

Figure 4.7 Suspension systems for wind tunnel test on the section model

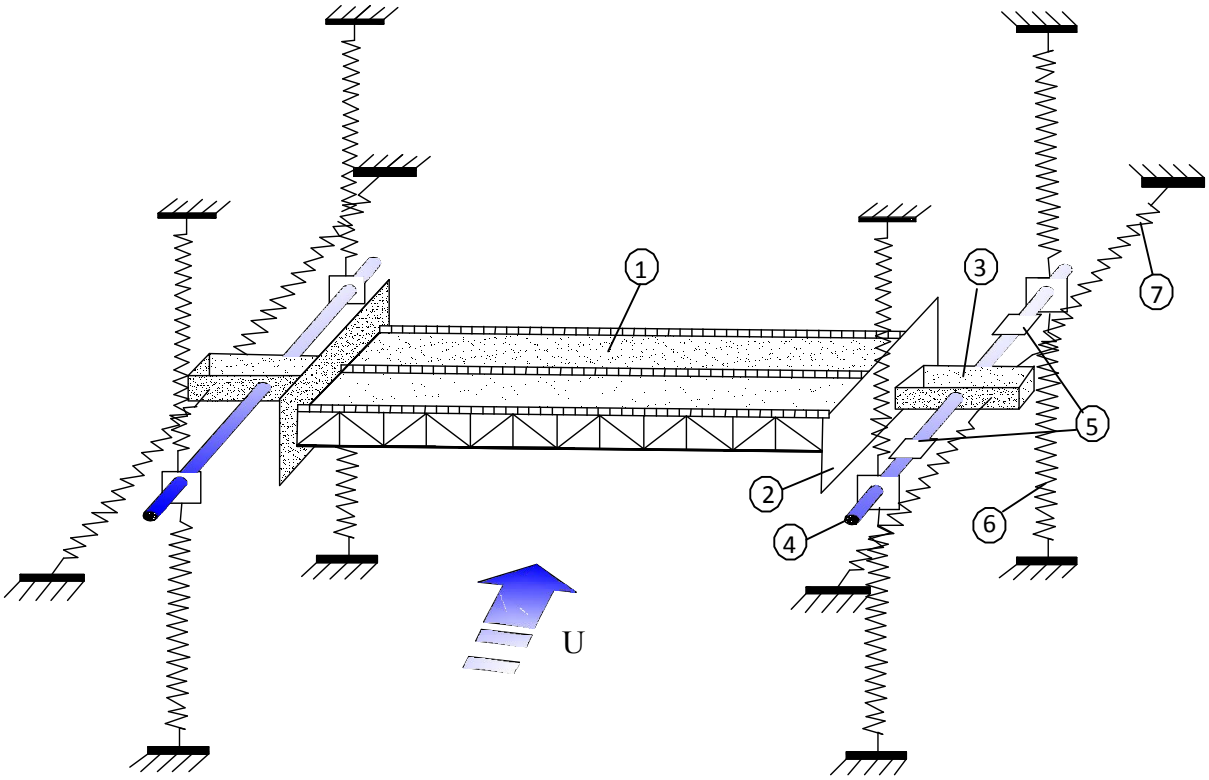

Figure 4.8 Experimental model setup

1. Model section
2. Thin plate
3. Extension rigid aluminum connecting the model to lateral bar
4. Lateral bar connecting to the spring
5. Target laser sensor for measurement vertical and torsional oscillation
6. Vertical spring mounted model
7. Horizontal confine motion

Other instrumentation supported in observation process included the following:

- A pitot tube measure air pressure
- A set laser displacement measurement
- Multichannel analog digital convert
- Microcomputer and data acquisition software
- Pen record
- Hotwire anemometer

4.2 Experimental procedure

The experimental measurement of time history of section model in wind tunnel can be briefed as

follow:

1. The wind flow is generated by the propeller driven by electronic power with desired wind velocity. A pitot tube is placed under of the section model and connected to an electronic manometer with an analog output and the relative pressure will be displayed. The mean wind velocity can be calculated from pressure by the equation

$$U = \sqrt{\frac{2\Delta p}{\rho}} \tag{4.1}$$

   Where U is mean wind speed, Δp is air pressure, and ρ is air density

2. In this study, the oscillation of the model will be achieved by two techniques, free vibration and random vibration (gust response). In free vibration technique, the model will be excited oscillation with the initial amplitude and relived for free vibration under a certain wind velocity. In random vibration technique, the model will be excited by turbulent flow without necessary initial excitation.
3. The vertical and torsional displacements time history can be obtained through at a certain located by laser device measurement (figures (4.7 & 4.8)).
4. The time history measurement of vertical h (heaving) and torsional α (pitching) responses can be calculated by

$$\begin{aligned} h &= \frac{h_1 + h_2}{2} \\ \alpha &= \tan^{-1}\left(\frac{h_1 - h_2}{2}\right) \end{aligned} \tag{4.2}$$

   where h_1 and h_2 are the displacement time history measured by laser 1 and laser 2, respectively.

5. The data obtained by laser device need to convert to time history displacement by multiply by calibration factor.

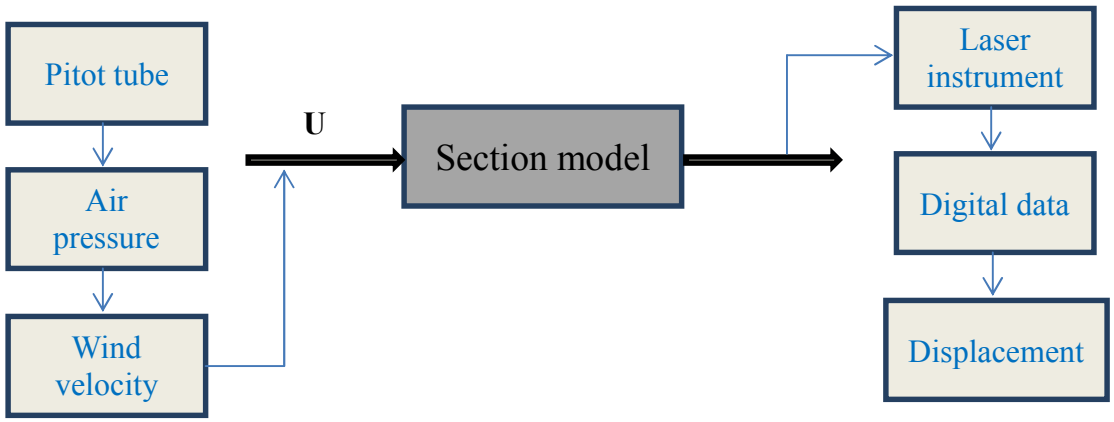

Figure 4.9 Data acquisition

4.3 Determination of mechanical frequency and damping

4.3.1 Determination of mechanical frequency

In order to calibration the required frequency and mass of model system, the additional mass method will be applied. The torsional oscillation can be controlled by adding a certain mass at a certain distance from the center of gravity of section model. The vertical oscillation and mass of model can be control by adding a certain mass at both including in first case and placing at center of gravity of section model. The mass will be varied and each mass will be determined frequency by free vibration technique.

Vertical frequency and mass: the vertical natural frequency of model is expressed as follow

$$\omega = \sqrt{\frac{K}{m}} \tag{4.3}$$

where K is stiffness of model system; m is mass of model.

If the additional mass Δm_i; the vertical frequency of the system can be written as

$$\omega_i = \sqrt{\frac{K}{m + \Delta m_i}} \tag{4.4}$$

The frequency ω_i can be identified from free vibration response of the model with adding Δm_i mass.

Eq. (4.4) can be rewritten as

$$\frac{1}{\omega_i^2} = \frac{m}{K} + \frac{1}{K}\Delta m_i \tag{4.5}$$

Eq. (4.5) is the linear equation with the variable $\frac{1}{\omega_i^2}$ and Δm_i; $\frac{m}{K}$ and $\frac{1}{K}$ are a constants.

When the adding mass is varied the frequency will be determined and obtained linear regression between $\frac{1}{\omega_i^2}$ and Δm_i (figure 4.11)

From figure (4.11) frequency and mass can be calculated as follow

$$\begin{aligned} c &= \frac{m}{K} \\ \omega &= \sqrt{\frac{1}{c}} \end{aligned} \tag{4.6}$$

$$m = c\tan\alpha \tag{4.7}$$

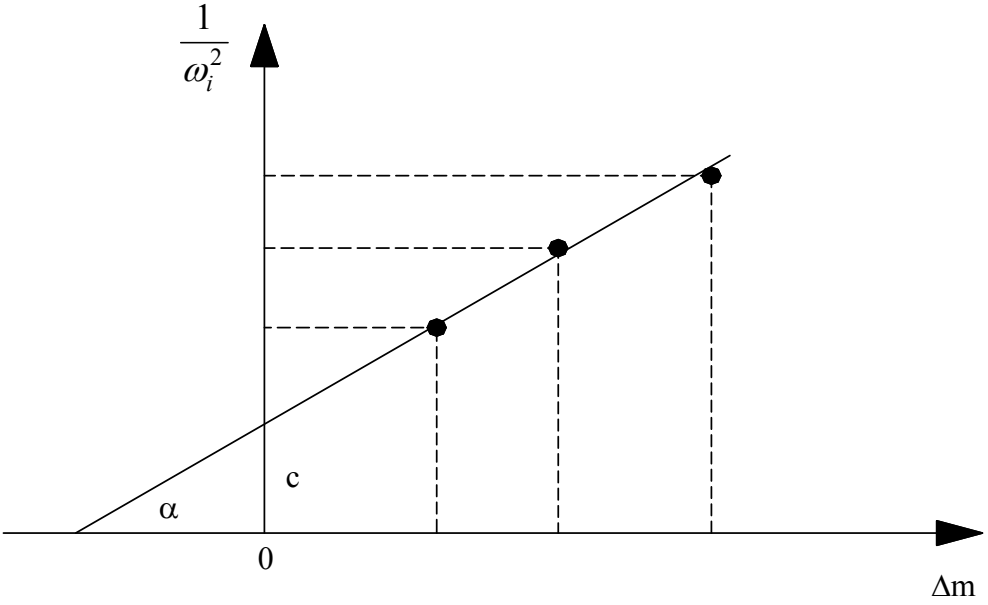

Figure 4.10 Regression linear of additional mass

Torsional frequency and moment of inertial of mass:

Determination of the torsional frequency and moment inertial of mas is similar compared with vertical frequency. The difference is additional mass located distance from center of gravity of section model. The moment inertial of mass of additional mass is defined as

$$\Delta I_i = d_i^2 \Delta m_i \tag{4.8}$$

where d_i is distance from center of gravity of model to additional mass

Torsional frequency is defined as

$$\omega = \sqrt{\frac{K}{I}} \tag{4.9}$$

Linear equation of torsional frequency and additional moment inertial of mass can be defined

$$\frac{1}{\omega_i^2} = \frac{I}{K} + \frac{1}{K}\Delta I_i \tag{4.10}$$

Similarity with previous process, the torsional frequency and moment inertial of mass will be obtained.

4.3.2 Determination of mechanical damping

Base on free vibration of damped system, the logarithmic decrement can be calculated as follow

$$\delta = \ln \frac{x_n}{x_{n+1}} = \frac{1}{j} \ln \frac{x_n}{x_{n+j}} \tag{4.11}$$

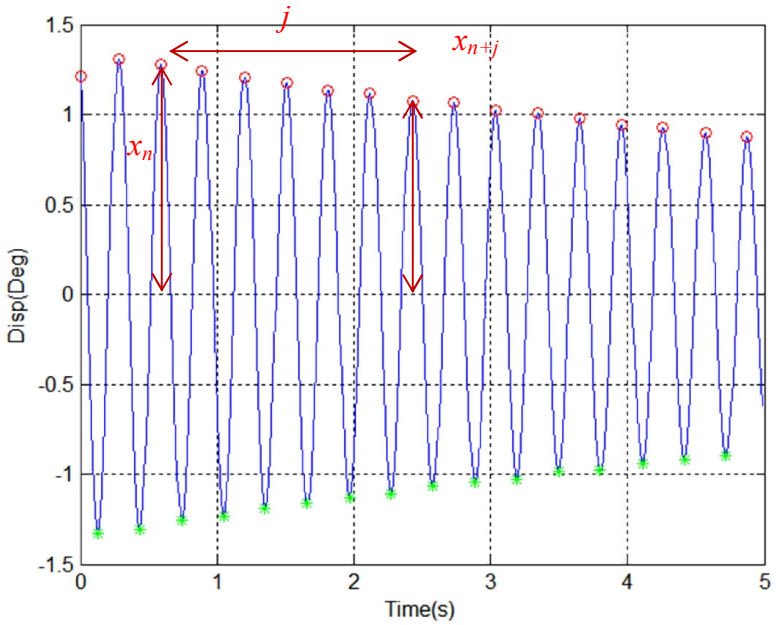

Figure 4.11 Damped free vibration

where x_n and x_{n+j} are amplitudes of responses corresponding to the time t_n and t_{n+j} ($t_{n+j}=t_n+jT$ where T is the period; j is and integer) (figure 4.12).

The damping ratio can be obtained by

$$\xi = \frac{\delta}{\sqrt{(2\pi)^2 + \delta^2}} \cong \frac{\delta}{2\pi} \tag{4.12}$$

4.4 Turbulence property

The turbulent flows used in this study were generated by biplane wooden grids (Figure. 4.2). The turbulent properties are controlled by changing the distance to the model. Hotwire anemometer attacked at different location along the model (figure. 4.13). Hotwire anemometer can be measured two dimensions those are along wind turbulence and vertical wind turbulence with sample frequency 2000 (Hz). The data achieved at very along mean wind velocity.

The turbulence properties are described below by means of their standard deviation, integral length scale, power spectrum density function and correlation between turbulence at two points.

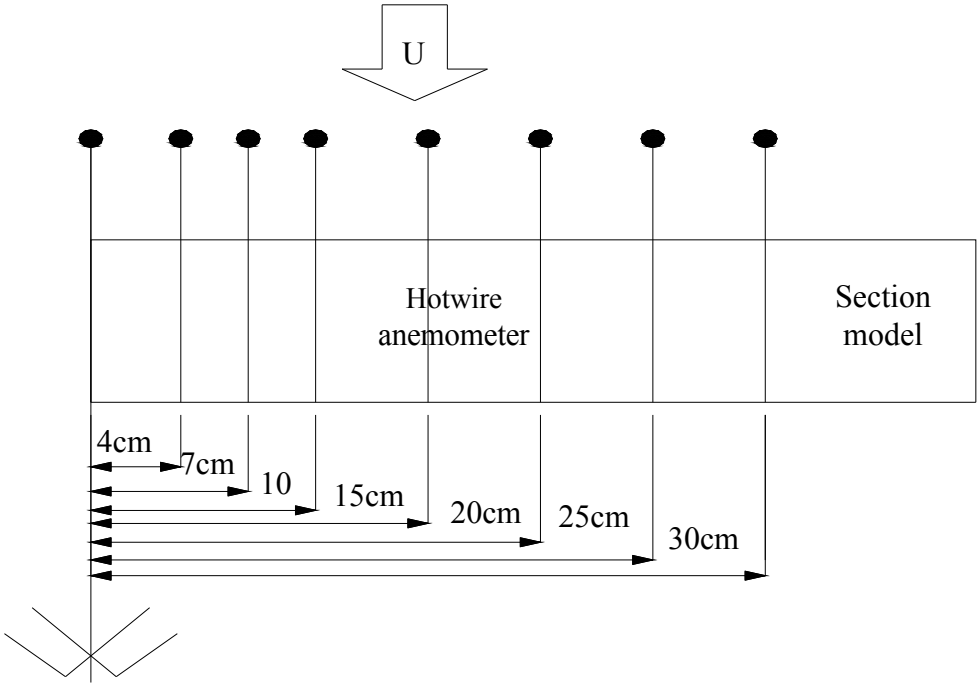

Figure 4.12 Hotwire anemometer

4.4.1 Standard deviation of turbulence component

Probability density function

The probability density function of fluctuated wind speed is customarily with Gauss distribution. Figure 4.14 shows both longitudinal and vertical wind speed fluctuation fairly good agreement with Gauss distribution.

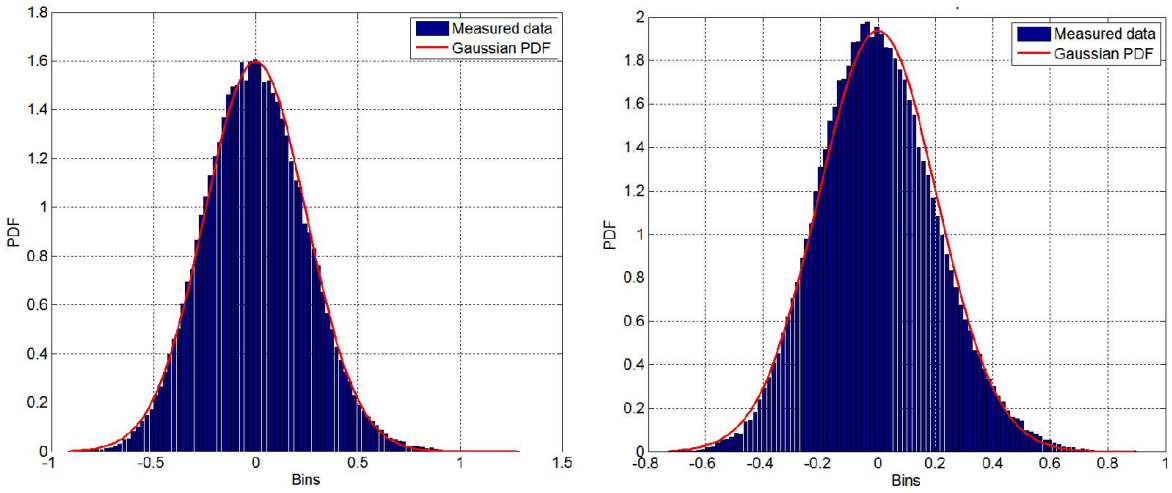

(a) along wind turbulence (b) vertical wind turbulence

Figure 4.13 Probability density function of longitudinal and vertical velocity fluctuation

Turbulence intensity

The turbulence intensity I_i (%) for the along wind turbulence component u and across-wind w is defined as:

$$I_i = \frac{\sigma_i}{U} \qquad (\text{i} = \text{u, w}) \tag{4.12}$$

where: U is the horizontal average wind speed; σ_i is the standard deviation of the fluctuating components.

Turbulence integral length scale

Turbulence integral length scales are a measure of the size of the vortices in the wind, or in other words the average size of a gust in given direction. Base on the measured wind speed with time interval of 10 minutes, the turbulence integral length scale was calculated using autocorrelation function integral method as follows:

$$L_i^x = \frac{U}{\sigma_i^2}\int_0^\infty R_i(\tau)d\tau \qquad (\text{i} = \text{u, w}) \tag{4.12}$$

where U is the horizontal average wind speed; σ_i is the standard deviation of the fluctuating components; $R_i(\tau)$ is the autocorrelation function of turbulence components (figure 4.14a&b).

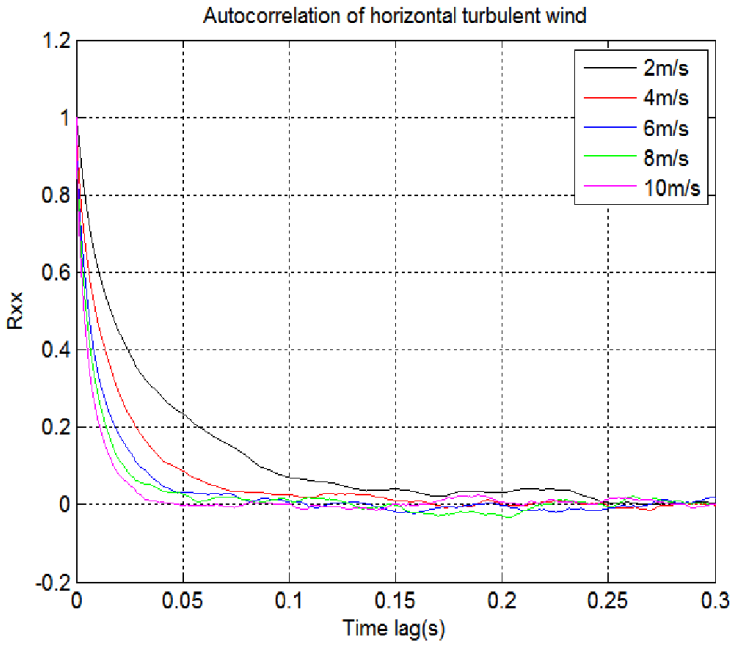

Figure 4.14a Autocorrelation function of horizontal turbulent component

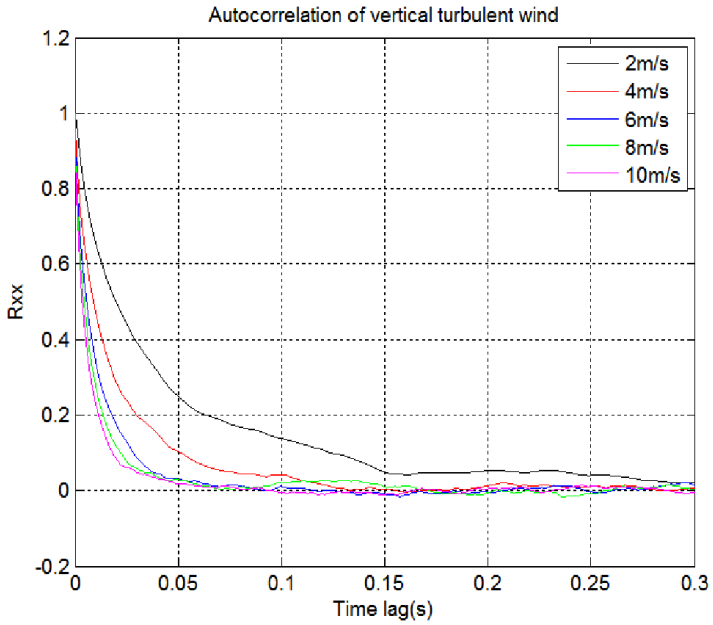

Figure 4.14b Autocorrelation function of vertical turbulent component

The length scale calculated from Eq. (4.12) in some cases is large value, because the autocorrelation of turbulence component in several cases is just asymptotic to abscissa due to the area under autocorrelation curve and abscissa quite large.

In this study the integral scale is defined as:

$$L_u^x = \frac{1}{2\pi}\frac{U}{n_{peak}} \tag{4.13}$$

Where n_{peak} is the frequency at which the curve reduced spectrum reaches a maximum.

The flow conditions and turbulence properties of three difference cases are shown in Table 1.

Table 4.1 Turbulence intensity and integral length scale

	I_u (%)	I_w (%)	L_u (cm)	L_w (cm)
Case 1	6.2	4. 6	11.3	9.1
Case 2	9.1	6.9	9.0	8.7
Case 3	15.6	13.2	6.8	6.4

4.4.2 Turbulence power spectral density

The turbulence intensity and integral length scale do not fully describe a properties of turbulent oncoming flows, because thanks to Y. Nakamura and S. Ozono (1987) studied on bluff-body aerodynamic shown that small-scale turbulence affects flow fields and aerodynamic paremeters more than larger one. Therefore the power spectral distribution of turbulence scales was also quantified for this research.

The frequency distribution of turbulent along-wind velocity component *u* is described by the non-dimensional power spectral density function $R_N(z, f)$ defined as:

$$R_N(z,f) = \frac{fS_u(z,f)}{\sigma_u^2(z)} \tag{4.14}$$

where *f* is frequency in hertz and $S_u(z, f)$ is the power spectrum for the along-wind turbulent component

The von Karman formula for the dimensionless spectrum of longitudinal component of wind turbulence:

$$\frac{fS_u}{\sigma_u^2} = \frac{4f_L}{\left[1+70.8f_L^2\right]^{5/6}} \tag{4.15}$$

where S_u is the spectral density function of the longitudinal component, *f* is the frequency in Hertz and σ^2 is the variance of the longitudinal velocity component. The non-dimension frequency *is* $f_L=fL^x_u(z)/U(z)$; $L^x_u(z)$ is the integral scale.

The non-dimensional power spectral density function is used in Eurocode 1:

$$\frac{fS_u}{\sigma_u^2} = \frac{6.8f_L}{\left[1+10.2f_L\right]^{5/3}} \tag{4.16}$$

Figure 4.15 shows the non-dimensional frequency distribution of turbulent along-wind velocity component versus non-dimensional power spectral density function and matching between the power spectrum of simulated data from wind tunnel and empirical atmospheric turbulence von Karman and Eurocode 1. Compared with von Karman spectrum, the measured data coinccided well with it in the high frequency and it was a little higher in the low frequency. Turbulent energy is generated in larger eddies (low frequency). For most structure, these low-frequency fluctuations give no significant response contribution.

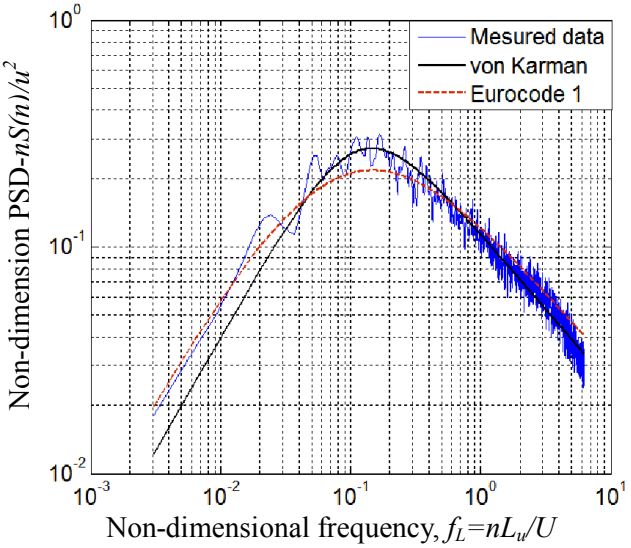

Figure 4.15 Non-dimension PSD function for the longitudinal turbulence component

In Figure 4.16, three spectra obtained at different reduced turbulent intensity (turbulent intensity) are shown. Values of the spectral density function increase as the turbulence intensity is increased. In the intermediate region, called the inertial subrange, the spectra is the presence with a -5/3 slope, known as Kolmogorov's spectrum (Figure 4.15), instead of -2/3 exponent as demonstrated in non-dimensional von Kaman spectrum (Figure 4.16).

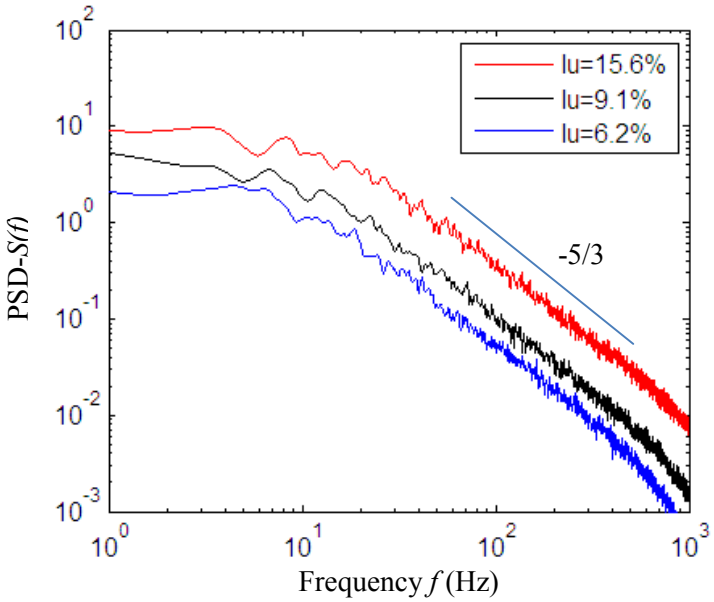

Figure 4.16 Dimension PSD function for the longitudinal turbulence component

4.4.3 Spatial correlation

The normalized cross-spectrum describes the statistical dependence between the

turbulence components at two points at a given frequency *f*.

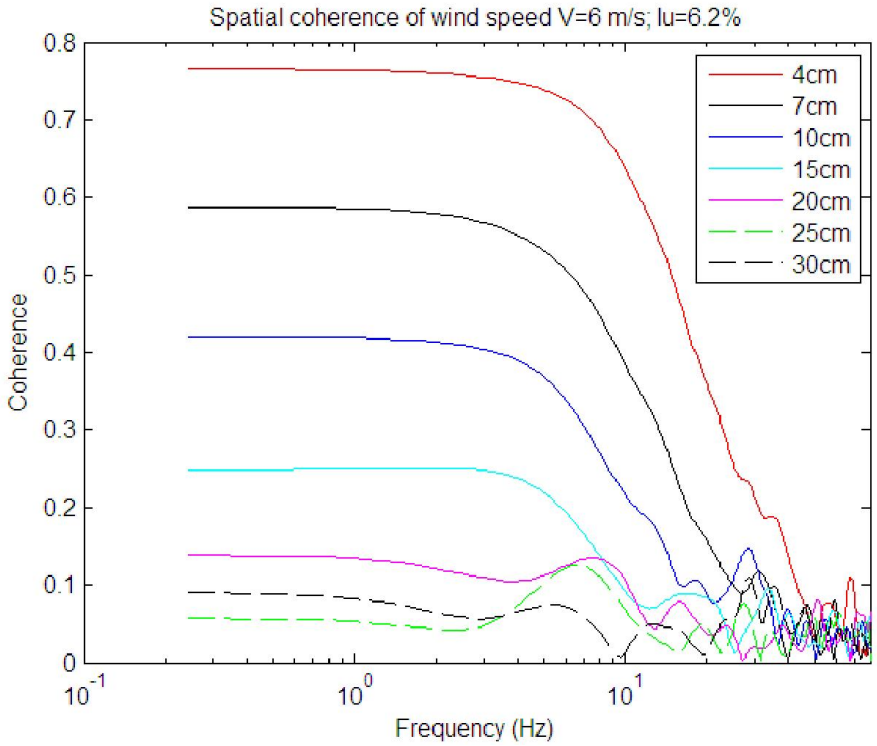

Figure 4.17 Spatial correlation (V=6m/s; Iu=6.2%)

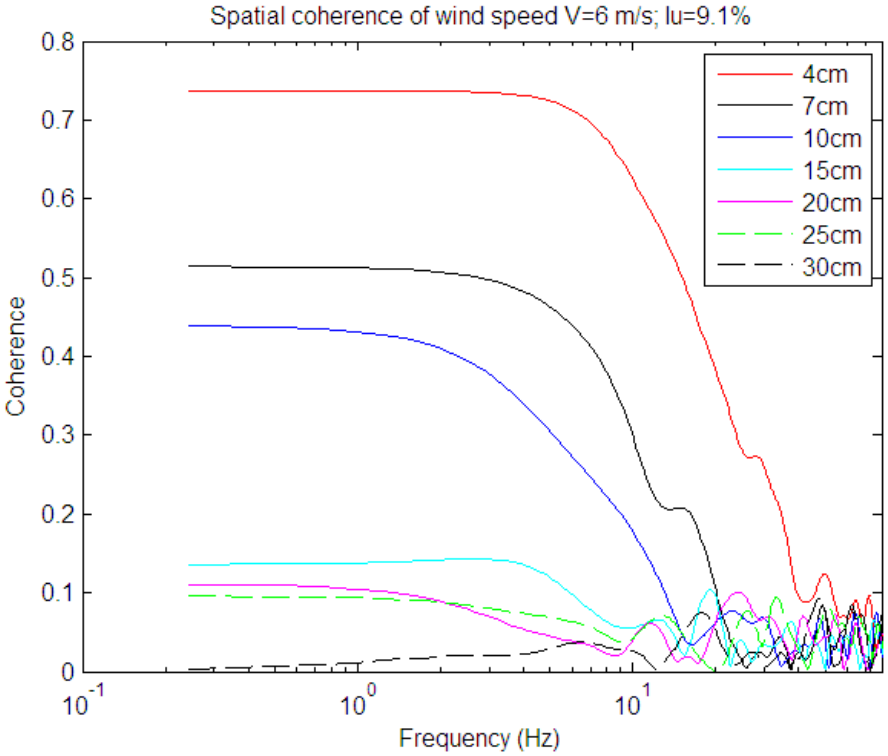

Figure 4.18 Spatial correlation (V=6m/s; Iu=9.1%)

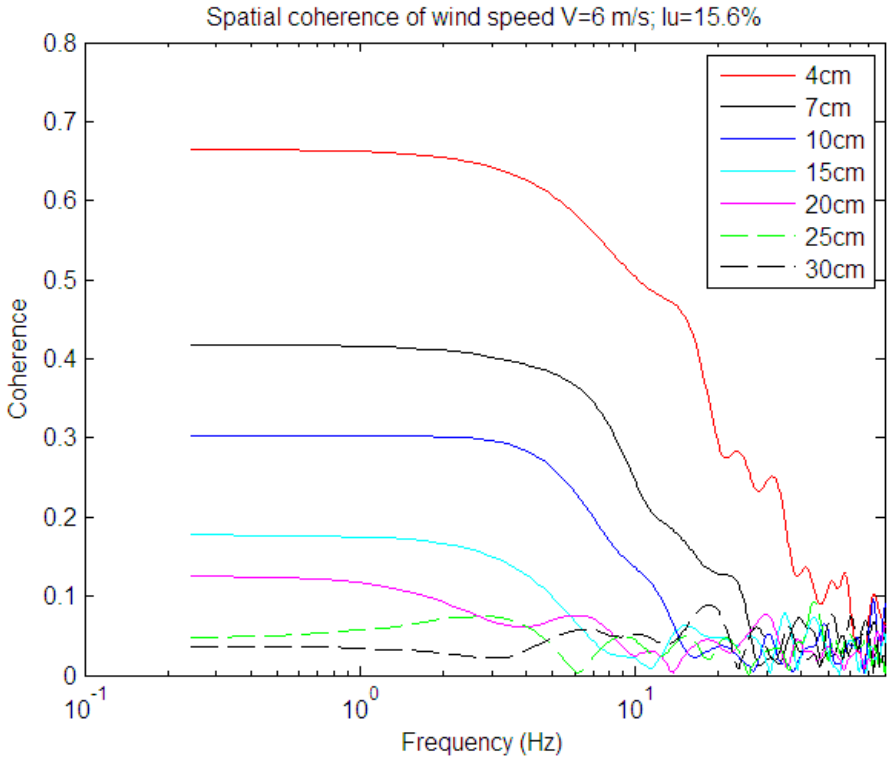

Figure 4.19 Spatial correlation (V=6m/s; Iu=15.6%)

The root-coherence function is defined as the absolute value of the normalized cross-spectrum and given by:

$$\sqrt{Coh} = |S_N| = \left| \frac{S_{uu}(P_1, P_2, f)}{\sqrt{S_u(P_1, f) S_u(P_2, f)}} \right| \tag{4.17}$$

where S_{uu} is cross-spectrum of the two longitudinal turbulence components at point P_1 and P_2, respectively.

As shown in figures 4.17 to 4.19 the normalized cross-spectrum decrease when the distance between two points increase and coherence decrease as frequency increase. It can be seen that coherence does not go to unity when the frequency equal to zero. The comparison of coherence at same velocity, turbulence intensity increases the coherence decrease.

4.5 Model dynamic properties

Tests have been executed under both smooth and turbulence flows. The aim of this testing is to quantify the effect of oncoming turbulence flows on the dynamic responses of section model. Figures (4.18a & 4.18b) illustrate the displacement of two degree of freedom (heaving and torsional modes) versus reduced wind velocities under smooth and different turbulence flows. Abbreviation of 'RSM' is root-mean-square; 'Max' is maximum amplitude

of vibration; 'Smooth' is smooth flow condition. In smooth flow, the vertical vibration is limited when reduced mean wind speed is from 0 to 9 and then considerably increases but vertical flutter does not occur in this test (figure 4.18a). On the other hand, the torsional displacement is very small till sudden increment and flutter occur at reduced wind velocity about 5.7 (figure 4.18b).

When model is immersed in turbulent flows, the vertical and torsional motions vibrate in spite of small reduced wind velocities. The vertical response increases proportionally with V_r and when the turbulent intensity increases, the amplitude of vibration lightly increase. In the turbulent flows vertical flutter also does not occur.

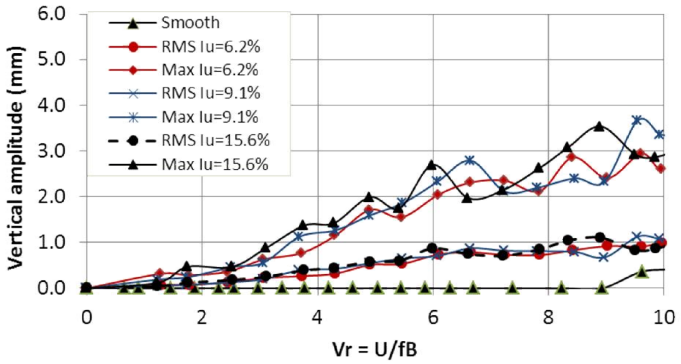

Figure 4.18a Model amplitude (heaving mode) with vary turbulence intensity

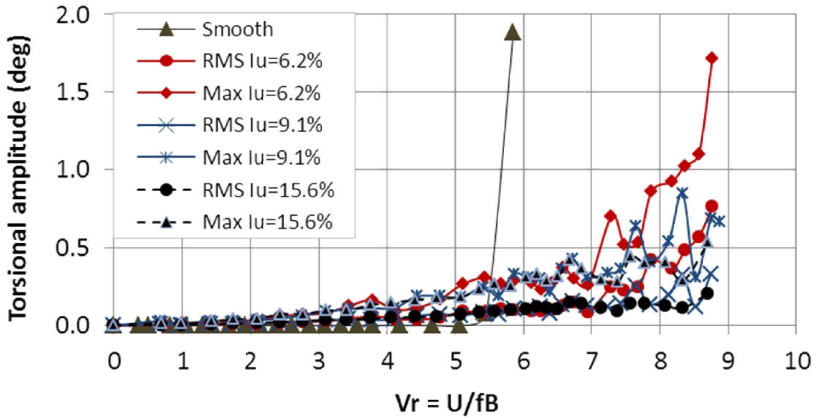

Figure 4.18b Model amplitude (torsional mode) with vary turbulence intensity

In cases of I_u = 6.2% and I_u = 9.1%, the torsional vibration gradually increases with V_r and flutter occurs at V_r = 7.2 and V_r = 7.7, respectively, which is higher than that in smooth flow (V_r = 5.7). On the other hand, in case of I_u = 15.6% flutter occur up to V_r = 8.6 (the critical wind speed is defined at the amplitude of 0.5 deg).

In order to clearly demonstrate the effect of coupling between two modes heaving and torsional non-dimension parameters corresponding heaving and torsional displacement are expressed as following (G. Bartoli 2006):

$$h_{nd} = 1000\frac{h}{B}; \qquad \alpha_{nd} = 1000\frac{\tan(\alpha)(B/2)}{B} \tag{4.18}$$

where h and α are the vertical and torsional displacement of section model respectively. The two figures (4.19a & 4.19b) illustrate the relationship between two modes heaving and torsional in smooth and turbulent flows (I = 6.2%). Two graphs indicate that only pure torsional flutter occurs, without exit of coupling flutter. In smooth flow, the torsional flutter occurs at reduced wind speed around 5.7 but in turbulent flow (with small turbulent intensity I = 6.2%) torsional flutter occurs at larger V_r = 8.3. Considering figure 4.19b, in the turbulent flow when V_r < 7 the motion is mainly due to vertical, but from V_r > 7.5 torsional vibration is larger and then divergence occurs.

In general, the effects of turbulent flows on section model induce larger vibration than smooth flow but the vibration proportionally increase with mean velocities and without sudden increase occurring like smooth flow. The motions under turbulent flows are known as buffeting response which can effect on service state design of bridge (such as fatigue problem). Turbulent flows significantly affect dynamic responses of the truss bridge deck section. Buffetting raises the amplitude response level progressively in proportion to the reduced wind speed and turbulent intensity. Specifically, turbulence induces buffeting response but increase flutter critical velocity.

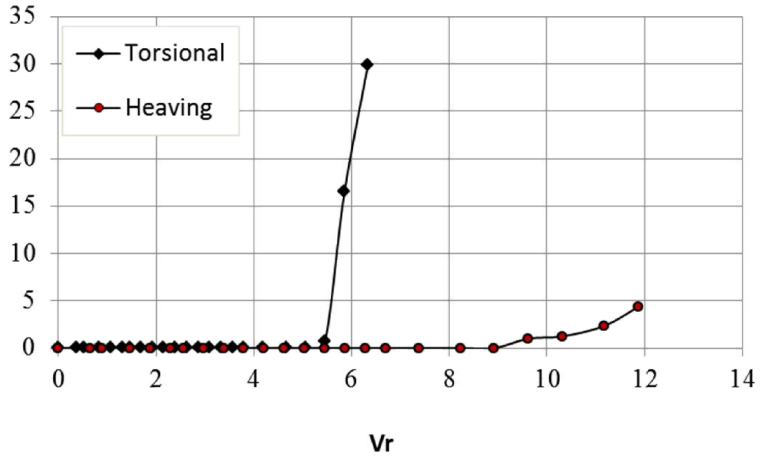

Figure 4.19a Non-dimensional amplitude (smooth flow)

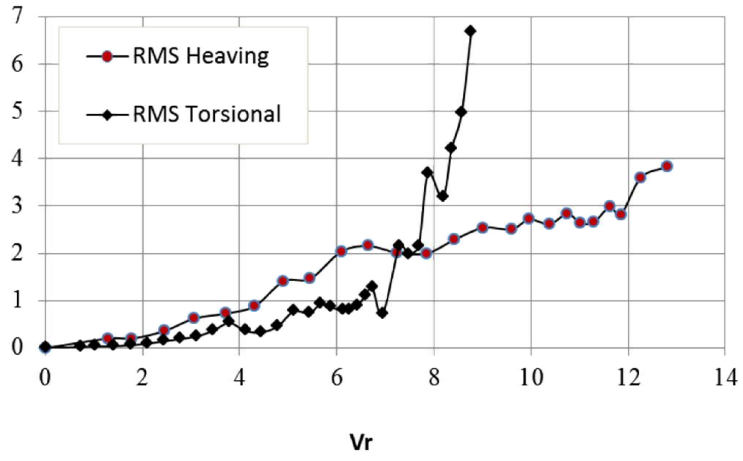

Figure 4.19b Non-dimensional amplitude (turbulence flow $I = 6.2\%$)

CHAPTER 5

IDENTIFICATION OF FLUTTER DERIVATIVES

This chapter presents the results by application of stochastic system identification method for extracting flutter derivatives. The output only time domain analysis stochastic system identifications: covariance stochastic system (SSI_cov) and data driven stochastic system method (SSI_data) are used to extract simultaneously all flutter derivatives from two degrees of freedom system. The output data which gust response is obtained by an experimental wind tunnel test and simulation for a trussed deck section with various turbulence intensity. The results are also compared with those from smooth flow as well as free decay response.

5.1 General of identification of flutter derivatives

The decay and buffeting signals are acquired at a sampling frequency 100Hz and these samples are set to zero mean before operating with Matlab (figures 5.1&5.2).

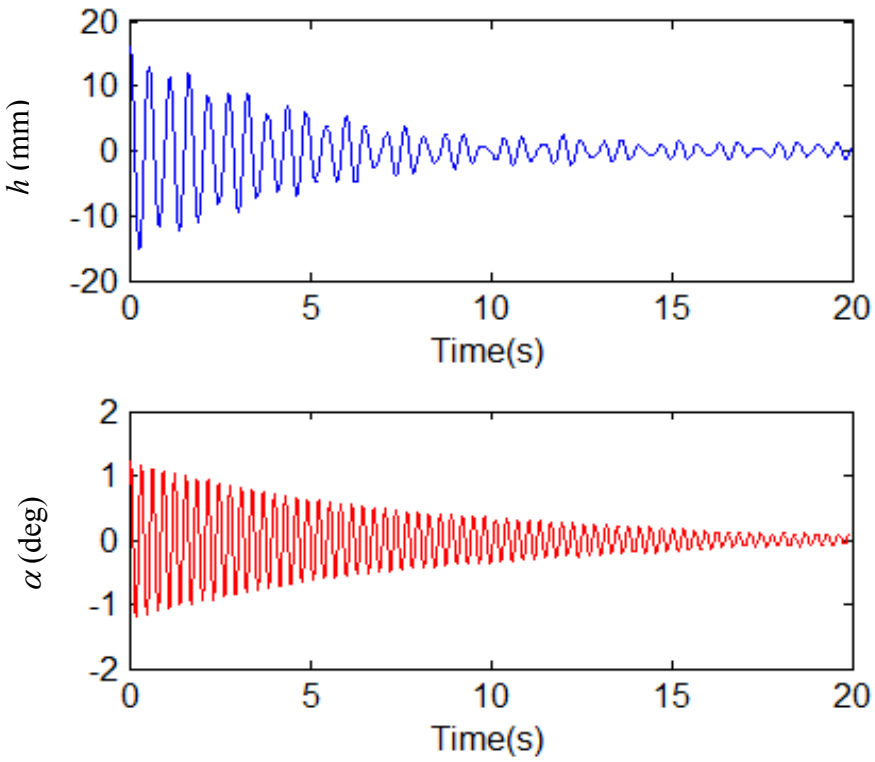

Figure 5.1 Free decay response of the bridge deck section model (h-heaving; α–torsional) under turbulent flow (I_u = 9.1%; U=2.91m/s)

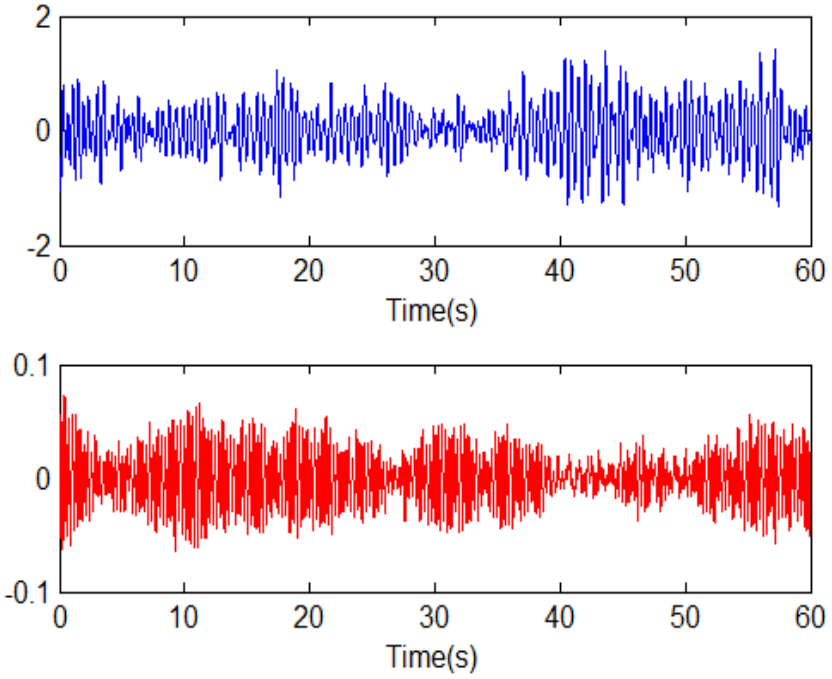

Figure 5.2 Buffeting response of the bridge deck section model (h-heaving; α–torsional) under turbulent flow (I_u = 9.1%; U = 2.91m/s)

First, the numbers of block rows (i) is a user defined index which large enough but it should at least be larger than the maximum order of the system one want identify. One block contain l rows (number of output (l=2)), the matrix H consist $2il$ rows. The number of columns j is typically equal to s-2i+1 (s is length of data), which mean that all of data are used.

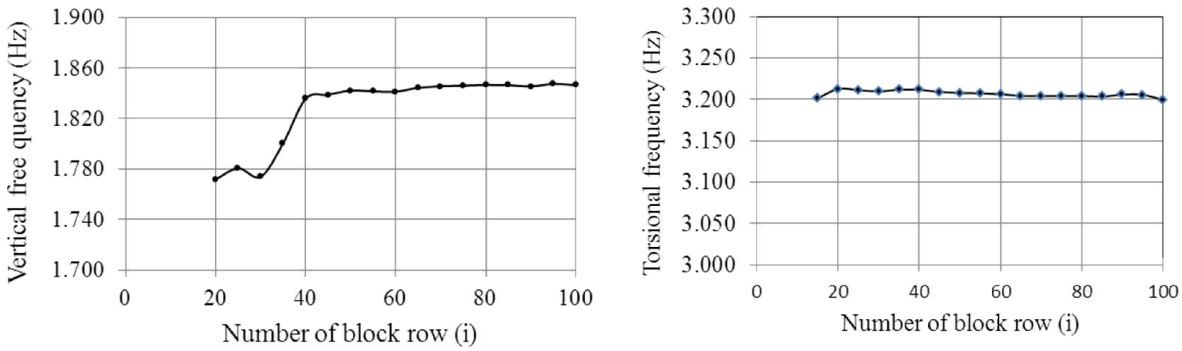

Figure 5.3 Modal parameters vs. Numbers of block rows

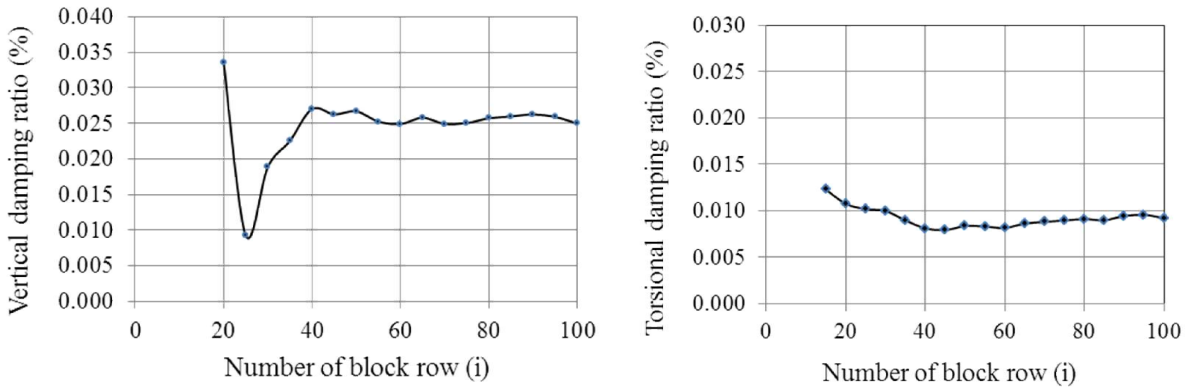

Figure 5.3 Modal parameters vs. Numbers of block rows (cont.)

In this study, numbers of block rows are chosen base on the stable of frequencies and damping ratios. Figure 5.3 shows the identified modal frequency and damping ratio of two mode heaving and torsional vibration by extracting from buffeting responses with different numbers of block rows. The numbers of block rows (i) where the stable of all modal parameters is larger than 40. In this study, the numbers of block rows (i) is chosen equal 50.

The SSI_cov is implemented including of the raw time histories of data Hankel matrix are converted to the Toeplitz matrix Eq. (3.22) and shifted block Toeplitz matrix Eq. (3.26). Computing SVD of block Toeplitz matrix, truncate the SVD to the model order, estimating O_i and C_i by splitting the SVD Eqs. (3.25 & 3.26) and finally estimating state matrix A and controllability matrix C Eq. (3.27).

The actual implementation of SSI_data consists of projecting (P_i) the row space of the under part outputs (Y_f) into the row space of the upper part outputs (Y_p) by applying robust numerical techniques QR factorization Eq. (3.30) and shifted projecting matrix P_{i-1}, computing SVD of P_i, truncating the SVD into the model order and to eliminate spurious poles by using stabilization diagram. The Kalman filter state sequence $\hat{X}_i$ is found from P_i and splitting the SVD and the state matrix A and C obtained by least square solution Eq. (3.38).

The system order n can be determined from the number nonzero singular values of Toeplitz matrix or projecting matrix. In practice, affect by noise thus singular values that are all different from zero. Therefore, it is suggested to look at the "gap" between two successive singular values (figure 5.4). The order will chose by the maximum number of singular values at "gap" occur. Some cases there is no "gap", the stabilization diagram as aforementioned will be applied.

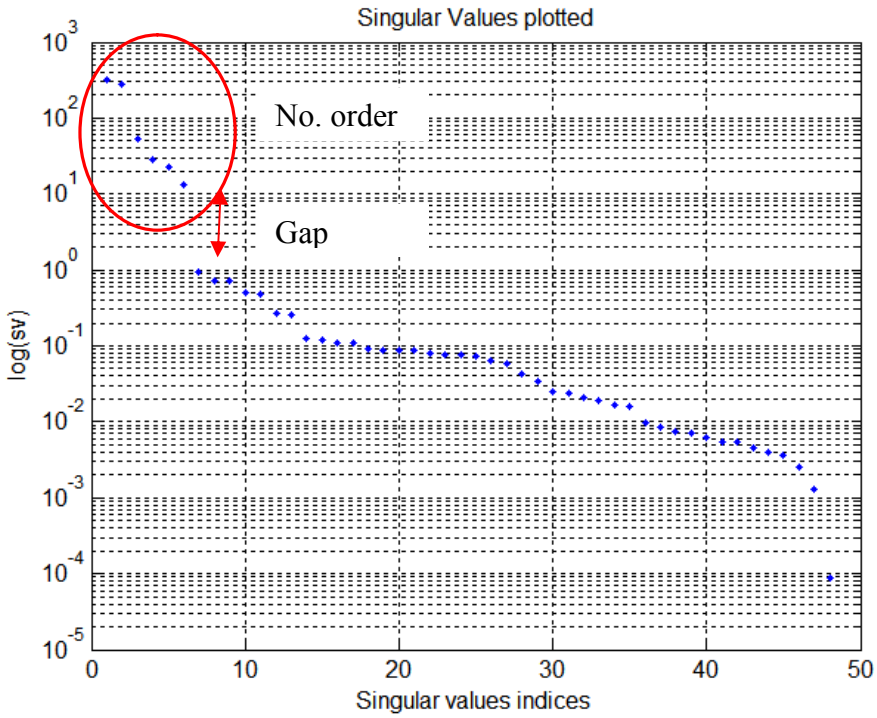

Figure 5.4 Number of order

5.2 Numerical simulation results

Before analysis the buffeting response time series, simulated data have been tested first in order to check the performance, the stability of the stochastic system identification method.

5.2.1 Validation to a white noise excitation

A validation of the stochastic system identification technique for application to extract flutter derivatives of bridge deck section have been achieved by comparing the result from the numerical simulation with experimental ones. The assumption of output only system is the input white noise. Base on this assumption, the buffeting response time-series of section model excited by lift and moment white-noise was computed by numerical integration method. The section model properties assumed following (Jakobsen and Hjorth-Hansen, 1995):

$$M_0 = \begin{bmatrix} 2.6526 & 0 \\ 0 & 0.0189 \end{bmatrix}; \quad C_0 = \begin{bmatrix} 0.3616 & 0 \\ 0 & 0.0072 \end{bmatrix}; \quad K_0 = \begin{bmatrix} 397.0573 & 0 \\ 0 & 24.7315 \end{bmatrix}$$

f_h=1.947 Hz; f_α=5.76 Hz; logarithm decrements δ_h=0.035 and δ_a=0.033.

At the mean wind velocity U=10.26 m/s, air density 1.181 kg/m^3. The effective stiffness and

damping were pre-set at:

$$M_0 = \begin{bmatrix} 2.6526 & 0 \\ 0 & 0.0189 \end{bmatrix}; \quad C^e = \begin{bmatrix} 8.9308 & -0.0799 \\ 0.4345 & 0.0386 \end{bmatrix}; \quad K^e = \begin{bmatrix} 420.1002 & -59.1805 \\ 1.7552 & 19.6592 \end{bmatrix}$$

The buffeting responses were computed by the constant acceleration method of numerical integration (Newmark-β with time step Δt=0.01s, β=1/4) under white noise excitation as show in figure (5.5b). The numerical simulation procedure as follow figure 5.5a.

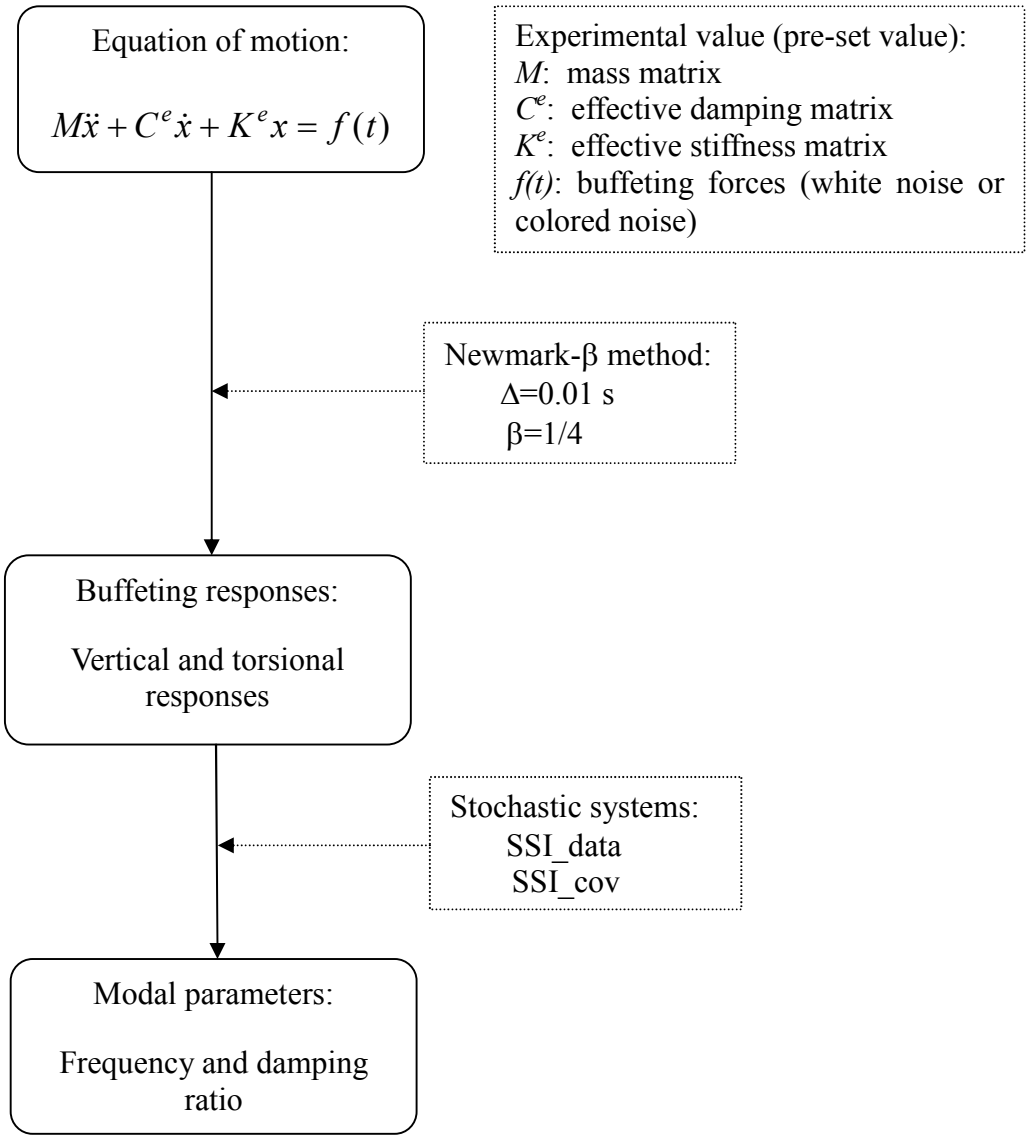

Figure 5.5a Numerical simulation diagram

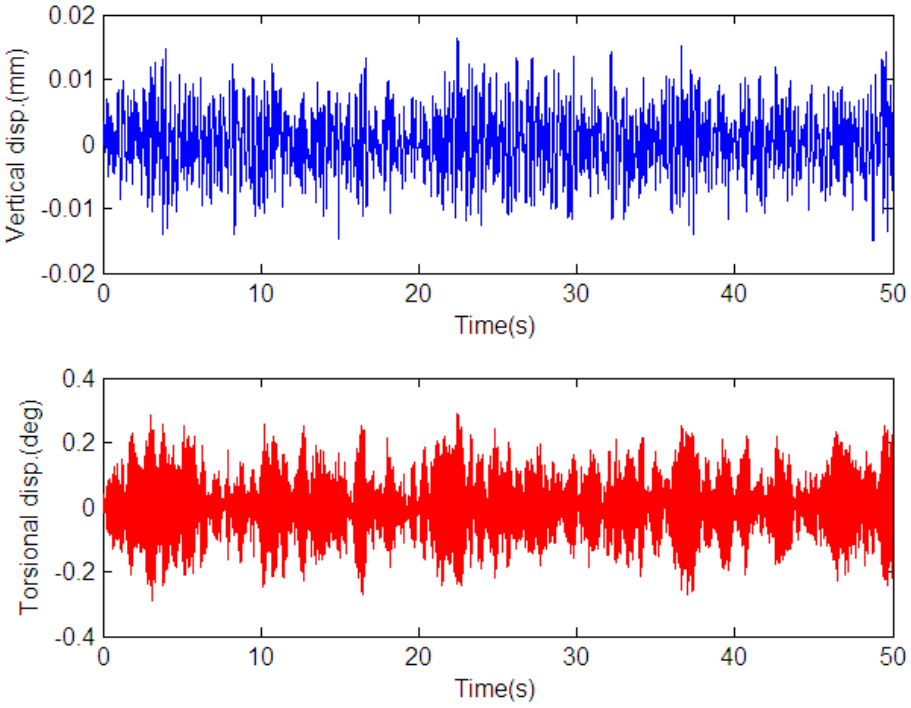

Figure 5.5b Buffeting response simulated under white noise excitation

The SSI method applied to these response data and obtained the effective structural matrix and the deviation of identified matrices from the pre-set ones:

SSI_data:

$$C_r^{\,e} = \begin{bmatrix} 8.7996 & -0.0795 \\ 0.5008 & 0.0358 \end{bmatrix};\quad K_r^{\,e} = \begin{bmatrix} 429.7659 & -53.8006 \\ 1.2898 & 19.3466 \end{bmatrix}$$

$$\Delta C\% = \begin{bmatrix} -1.46 & -0.6 \\ 15.26 & -7.25 \end{bmatrix};\quad \Delta K\% = \begin{bmatrix} 2.3 & -9.09 \\ -26.5 & -1.59 \end{bmatrix}$$

SSI_cov:

$$C_r^{\,e} = \begin{bmatrix} 8.4351 & -0.0795 \\ 0.2525 & 0.0339 \end{bmatrix};\quad K_r^{\,e} = \begin{bmatrix} 415.5835 & -54.8856 \\ 2.5008 & 19.47 \end{bmatrix}$$

$$\Delta C\% = \begin{bmatrix} -5.55 & -23.02 \\ 15.26 & -12.03 \end{bmatrix};\quad \Delta K\% = \begin{bmatrix} -1.07 & -7.26 \\ -25.38 & 0.962 \end{bmatrix}$$

The results are in good agreement to compare with the pre-set values. The direct term related to frequency and damping ratio estimated by SSI_data are less than 10%. The differences in

the off-diagonal term C_{21} and K_{21} are around 25%, these parameters related to A_1^* and A_4^*, but the magnitude value quite are small, those are trivial effect.

The deviations of estimated system matrices compared with preset value by SSI_cov are plausible. The deviation of diagonal parameter are less than 10%, except the parameter related to torsional damping term is equal 12%, but this value compared with very small value.

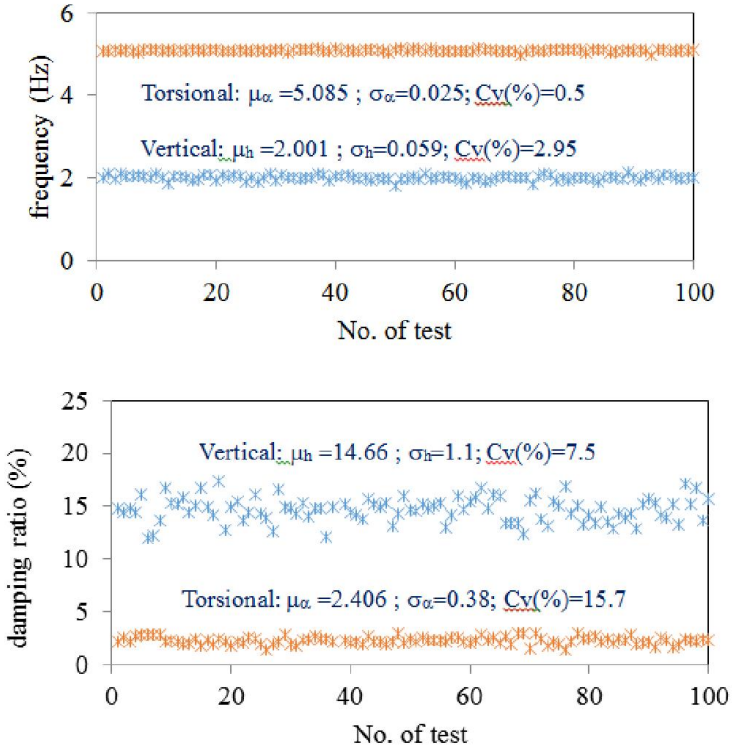

Figure 5.6a Stability of modal parameters from 100 buffeting response simulations by SSI_data

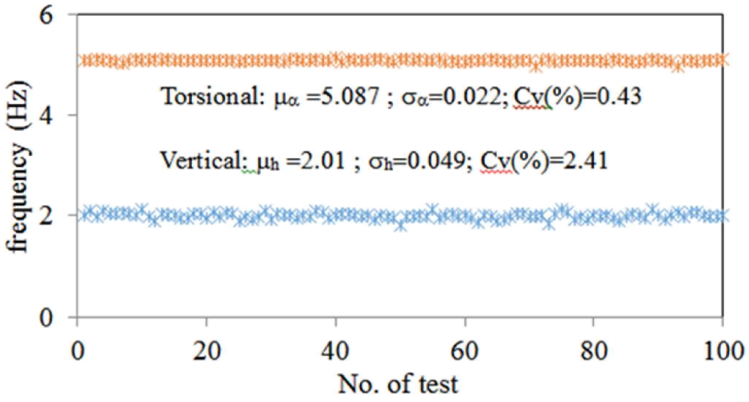

Figure 5.6b Stability of modal parameters from 100 buffeting response simulations by SSI_cov (cont.)

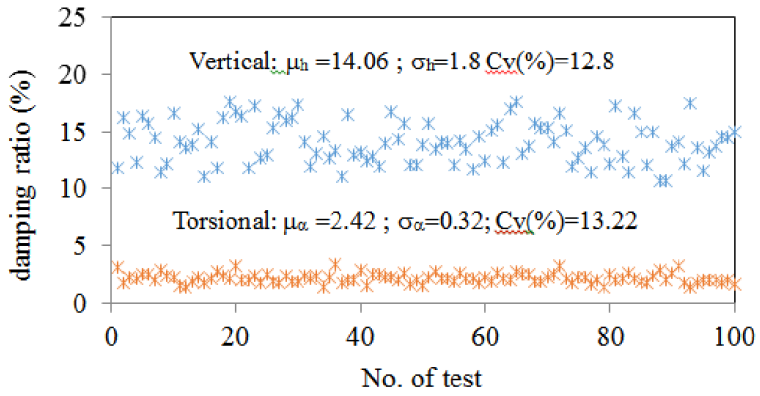

Figure 5.6b Stability of modal parameters from 100 buffeting response simulations by SSI_cov (cont.)

In order to estimate the stability of stochastic system, the frequency and damping ratio of pre-set values are simulated under white noise excitation with 100 different cases. Figures 5.6a & 5.6b show the frequency and damping ratio extracted from both techniques SSI_data and SSI_cov, respectively. The parameters obtained by SSI_data technique are in good agreements with preset values, the differences of mean values of vertical frequency and damping ratio is 0.09% and 1.88% respectively and torsional frequency and damping ratio is 0.92% and 11.54%, respectively. These parameters obtained by SSI_cov are more scatter, with vertical frequency and damping ratio is 0.36% and 6.25% respectively and torsional frequency and damping ratio is 0.89% and 11.17%, respectively. The computation time required for SSI_cov is longer compared with for SSI_data.

The stability of stochastic systems was also estimated by adding Gaussian noise to buffeting response. The frequency and damping ratio of preset value are simulated under white noise excitation and the buffeting response obtained by numerical method will be added various noise to signal level (AWGN), then modal parameter will be obtained by stochastic system identification.

The procedure of adding white noise as following:

- The buffeting response x to which an AWGN noise needs to be added for a given SNR (specified in dB).
- Calculate the power of vector x following as:

$$E_s = \frac{1}{L}\sum_{i=0}^{L-1}\left|x[\mathrm{i}]\right|^2 \qquad \text{where L=length(x)}$$

- Convert given SNR in dB to power of signal - linear scale (SNR_{lin}) and find the noise vector (from Gaussian distribution with noise variance) following the equation

$$noise = \sqrt{\frac{E_s}{SNR_{lin}}} * randn(1, \mathrm{L})$$

- Response with added noise to signal

  y= x + noise

- Final, modal parameters identify by SSI-data

Tables 5.1 to 5.4 show modal parameters by SSI-data and tables 5.5 to 5.8 by SSI-cov and the deviation compared with preset values. When SNR decrease up to 40% the results from both techniques were changed less than 10%.

Table 5.1 Vertical frequency vs. SNR (SSI-data)

SNR	90	85	80	75	70	65	60	55	50	40
fh	2.0002	2.0061	2.0017	2.0009	2.0033	2.0009	2.0012	2.0063	2.0017	2.0195
Δfh(%)	-0.1356	0.1601	-0.0605	-0.1026	0.0205	-0.1023	-0.0859	0.1696	-0.0603	0.8308

Table 5.2 Vertical damping ratio vs. SNR (SSI-data)

SNR	90	85	80	75	70	65	60	55	50	40
ξh	0.1342	0.1348	0.1342	0.1339	0.1315	0.1375	0.1403	0.1306	0.1274	0.1296
Δξh(%)	-2.5072	-2.0488	-2.4818	-2.7064	-4.4699	-0.1051	1.9300	-5.1108	-7.4474	-5.8367

Table 5.3 Torsional frequency vs. SNR (SSI-data)

SNR	90	85	80	75	70	65	60	55	50	40
fα	5.0767	5.0558	5.0723	5.0819	5.0420	5.0718	5.0835	5.0629	5.0675	5.0830
Δfα(%)	-1.0963	-1.5041	-1.1821	-0.9958	-1.7725	-1.1917	-0.9655	-1.3656	-1.2764	-0.9740

Table 5.4 Torsional damping ratio vs. SNR (SSI-data)

SNR	90	85	80	75	70	65	60	55	50	40
ξa	0.0281	0.0272	0.0279	0.0278	0.0262	0.0269	0.0264	0.0267	0.0270	0.0265
Δξα(%)	3.3287	-0.1119	2.4578	2.2107	-3.8105	-1.2023	-2.8803	-1.6587	-0.9096	-2.568

Table 5.5 Vertical frequency vs. SNR (SSI-cov)

SNR	90	85	80	75	70	65	60	55	50	40
fh	1.9652	1.9650	1.9661	1.9659	1.9612	1.9639	1.9612	1.9657	1.9643	2.0339
Δfh	-1.8830	-1.8942	-1.8377	-1.8477	-2.0841	-1.9459	-2.0825	-1.8580	-1.9257	1.5456

Table 5.6 Vertical damping ratio vs. SNR (SSI-cov)

SNR	90	85	80	75	70	65	60	55	50	40
ξh	0.1339	0.1336	0.1340	0.1335	0.1323	0.1329	0.1402	0.1313	0.1264	0.1331
Δξh	-2.6791	-2.9085	-2.5896	-2.9767	-3.8346	-3.4234	1.8834	-4.6193	-8.1424	-3.2541

Table 5.7 Torsional frequency vs. SNR (SSI-cov)

SNR	90	85	80	75	70	65	60	55	50	40
fα	5.0845	5.0845	5.0845	5.0845	5.0844	5.0844	5.0846	5.0843	5.0841	5.0844
Δfα	-0.9448	-0.9449	-0.9449	-0.9443	-0.9465	-0.9470	-0.9424	-0.9490	-0.9519	-0.9463

Table 5.8 Torsional damping ratio vs. SNR (SSI-cov)

SNR	90	85	80	75	70	65	60	55	50	40
ξa	0.0268	0.0268	0.0268	0.0268	0.0268	0.0268	0.0268	0.0268	0.0266	0.0270
Δξα	-1.5775	-1.5698	-1.5614	-1.5974	-1.5595	-1.5024	-1.4547	-1.6020	-2.1231	-0.8717

The deviation of identified results compared with pre-set values show in figure 5.7

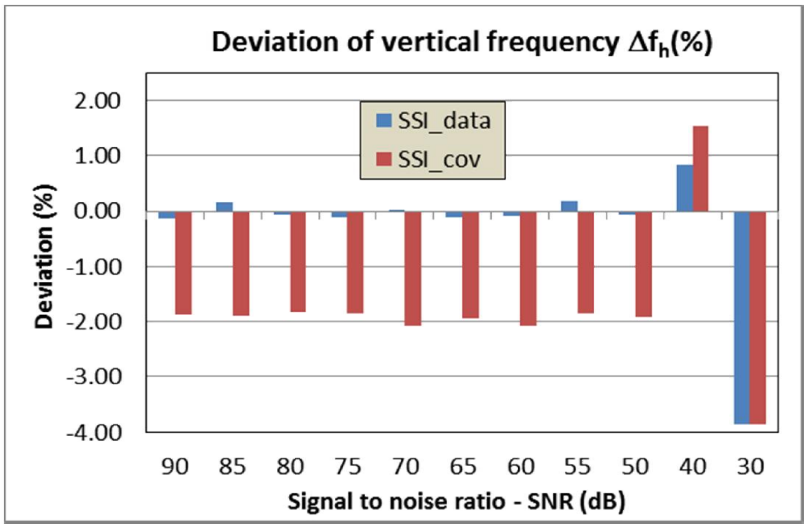

Figure 5.7 Deviation of modal parameters from simulations by SSI (cont.)

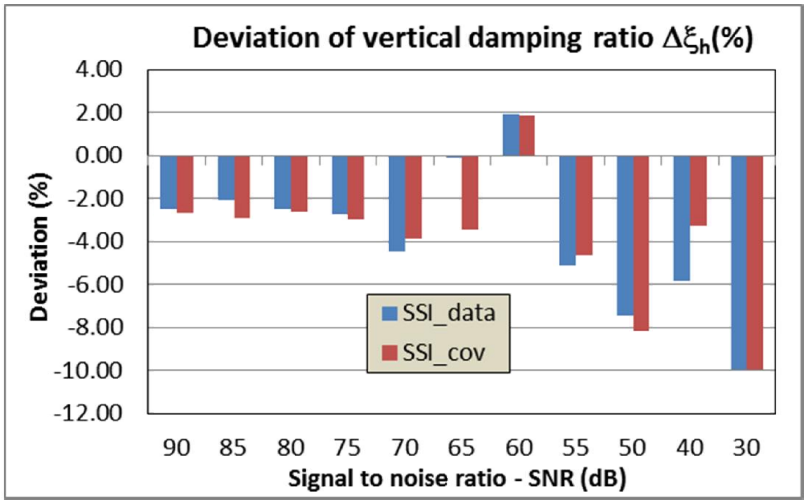

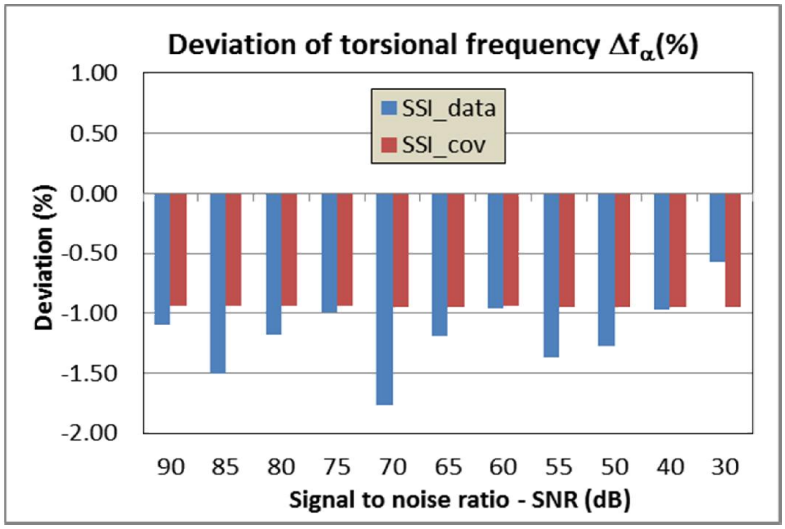

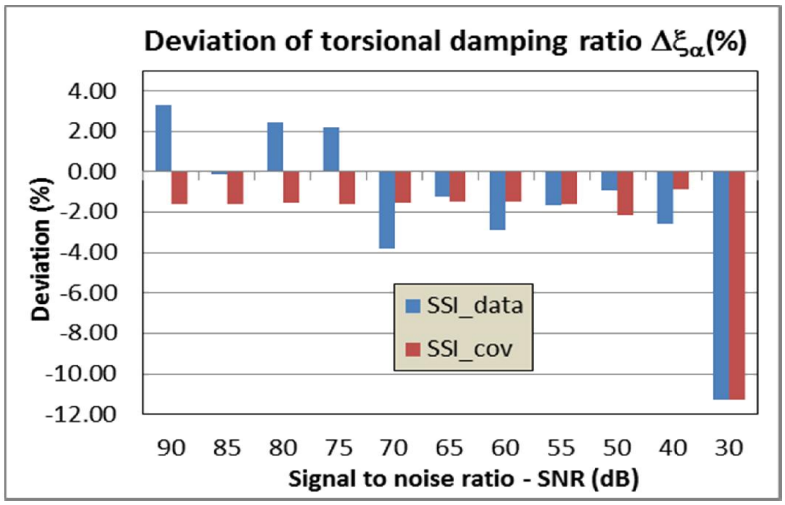

Figure 5.7 Deviation of modal parameters from simulations by SSI (cont.)

5.2.2 Estimate colored noise input effect on modal parameters

In order to estimate the operating feature of the stochastic systems which the input is colored noise, the frequency and damping ratio of preset value are simulated under colored noise excitation with 100 different cases.

The buffeting with colored noise that was generated by sending a white noise sequence y of variance 1 through the linear filter:

$$H(z) = \frac{0.02z - 0.041}{z - 0.85}$$

The power spectrum density function of colored noise illustrate in figure 5.8

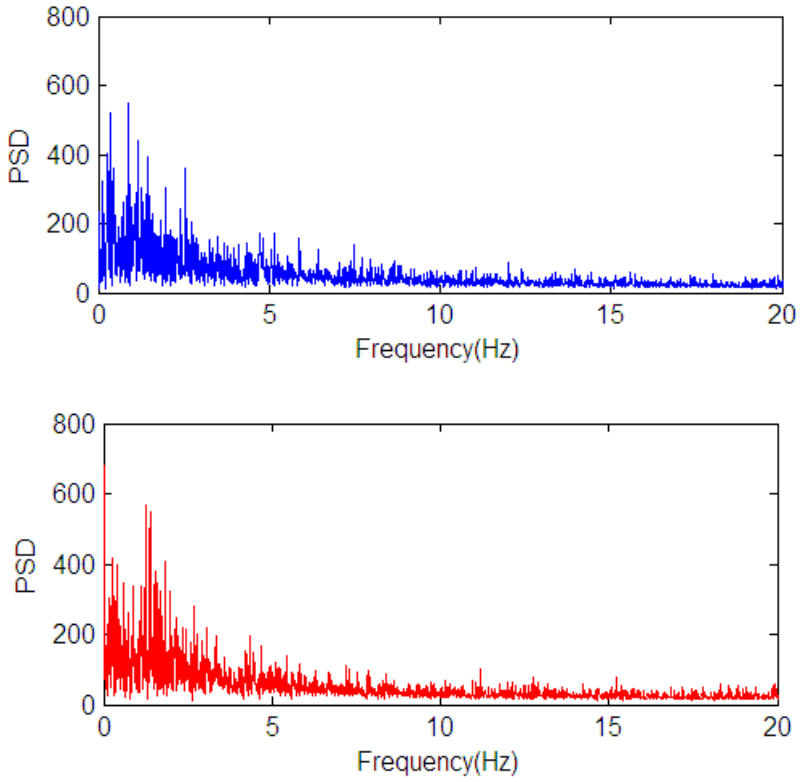

Figure 5.8 PSD of colored noise time series (buffeting force and buffeting moment)

The procedure described in Section 5.2.1 was repeated with the buffeting forces is colored noise. Figures 5.9 & 5.10 show the frequency and damping ratio extracted from both SSI_data and SSI_cov. The modal parameters obtained by SSI_data are in good agreements compared with preset values, the differences of mean values of vertical frequency and damping ratio is 0.67% and 10.2% respectively and torsional frequency and damping ratio is

0.94% and 16.1%, respectively. These modal parameters obtained by SSI_cov, with vertical frequency and damping ratio is 1.42% and 10.6% respectively and torsional frequency and damping ratio is 0.92% and 17.5%. The estimated results of SSI_data are higher accuracy compared with for SSI_cov.

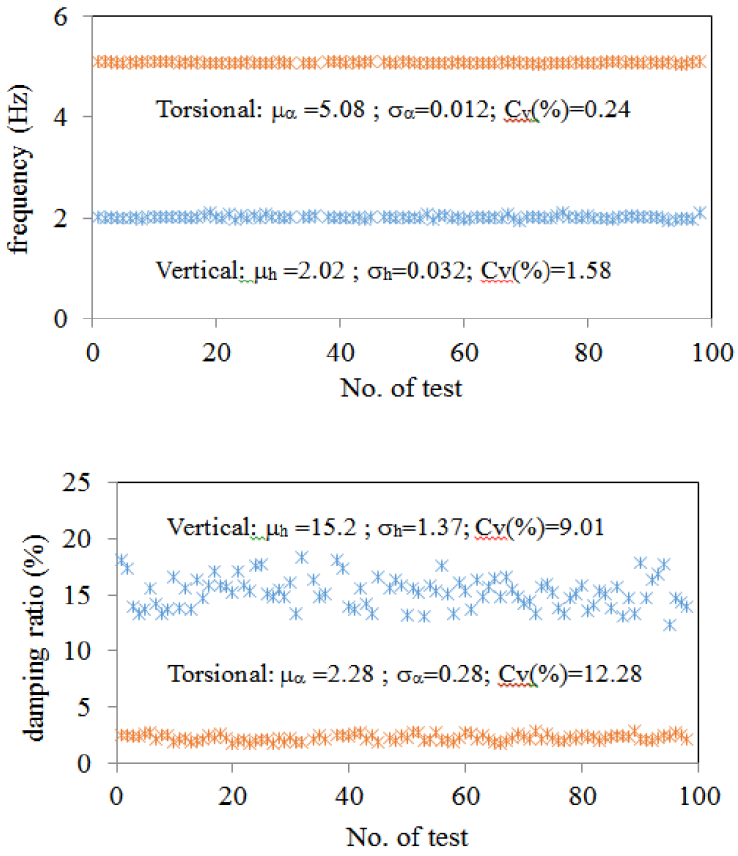

Figure 5.9 Stability of modal parameters from 100 buffeting response simulations by SSI_data

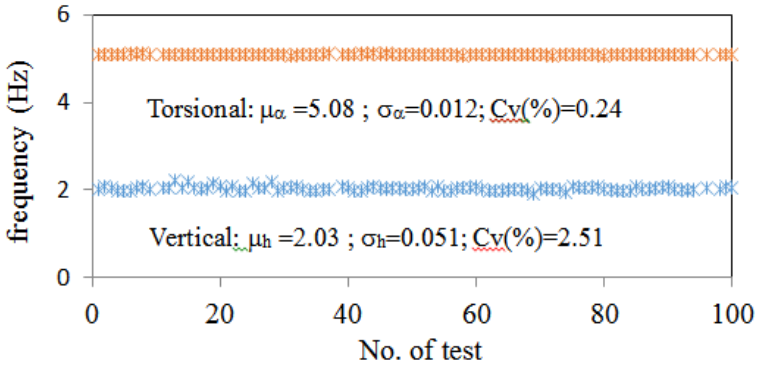

Figure 5.10 Stability of modal parameters from 100 buffeting response simulations by SSI_cov (cont.)

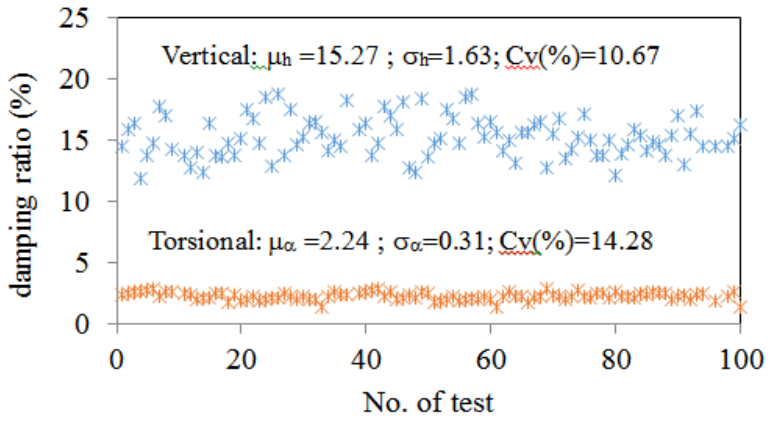

Figure 5.10 Stability of modal parameters from 100 buffeting response simulations by SSI_cov (cont.)

5.3 Extraction flutter derivatives from experiment data

5.3.1 Comparision flutter derivatives between SSI_cov and SSI_data

The process for extracting FDs by SSI_cov and SSI_data methods are mentioned before. Figure 5.11a&b shows the frequency and damping ratio of heaving and torsional mode obtained from both techniques. The value of frequency and damping ratio of heaving and torsional mode are in good agreement from both techniques.

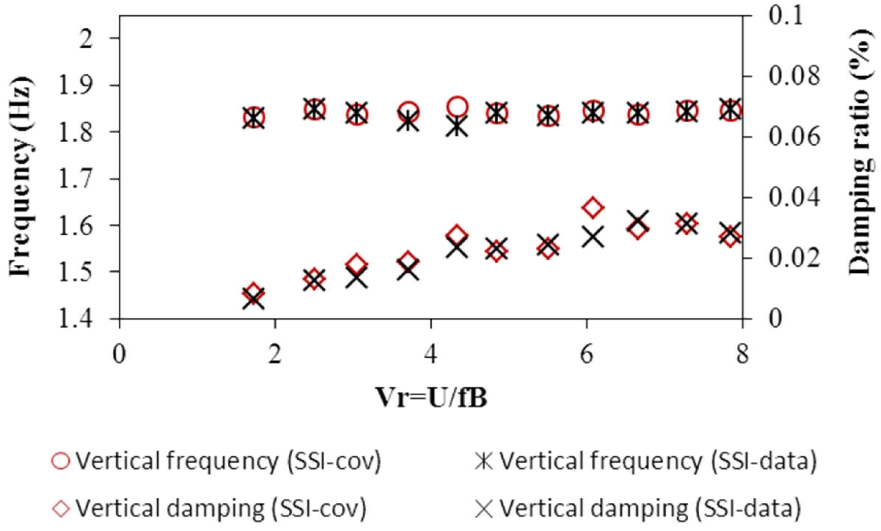

Figure 5.11a Frequency and damping ratio of heaving mode from free decay response under turbulent flow (I_u = 9.1%)

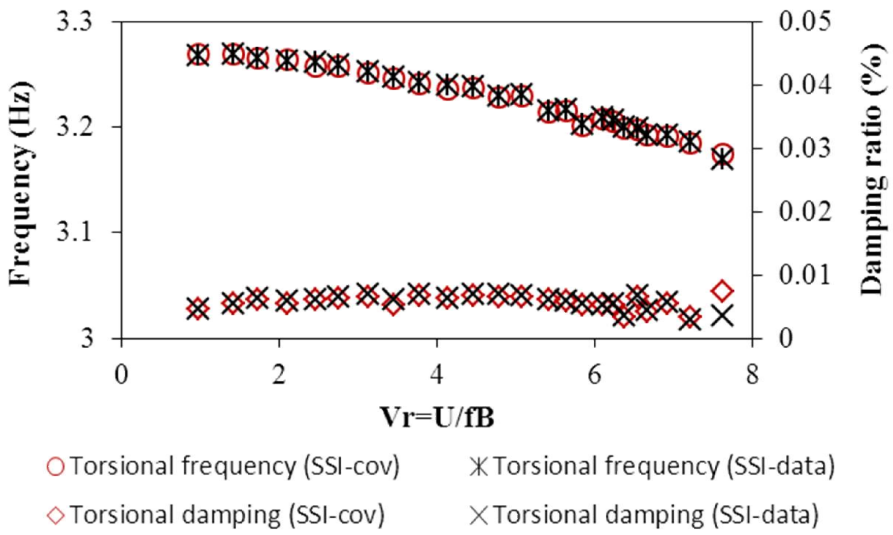

Figure 5.11b Frequency and damping ratio of torsional mode from free decay response under turbulent flow (I_u = 9.1%)

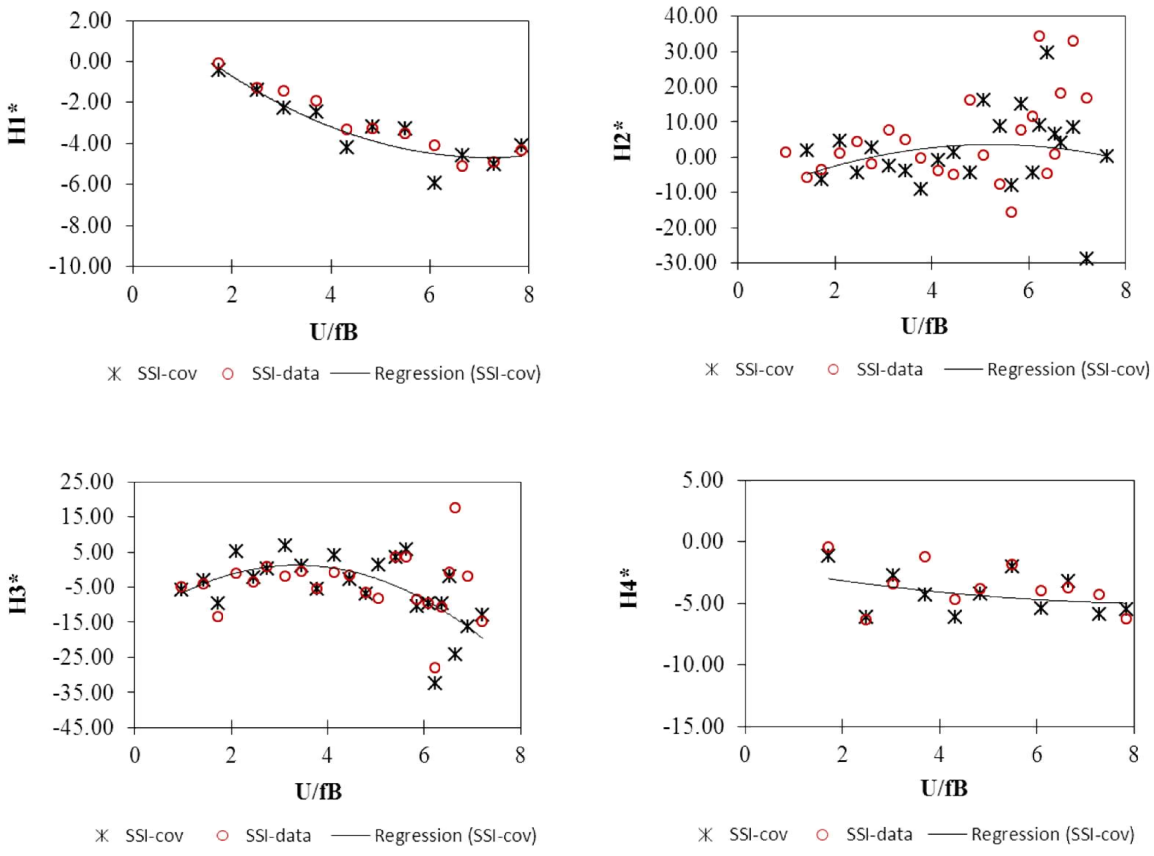

Figure 5.12 FDs (H_i) of the bridge section model under turbulent flow (I_u=9.1%) from free decay response

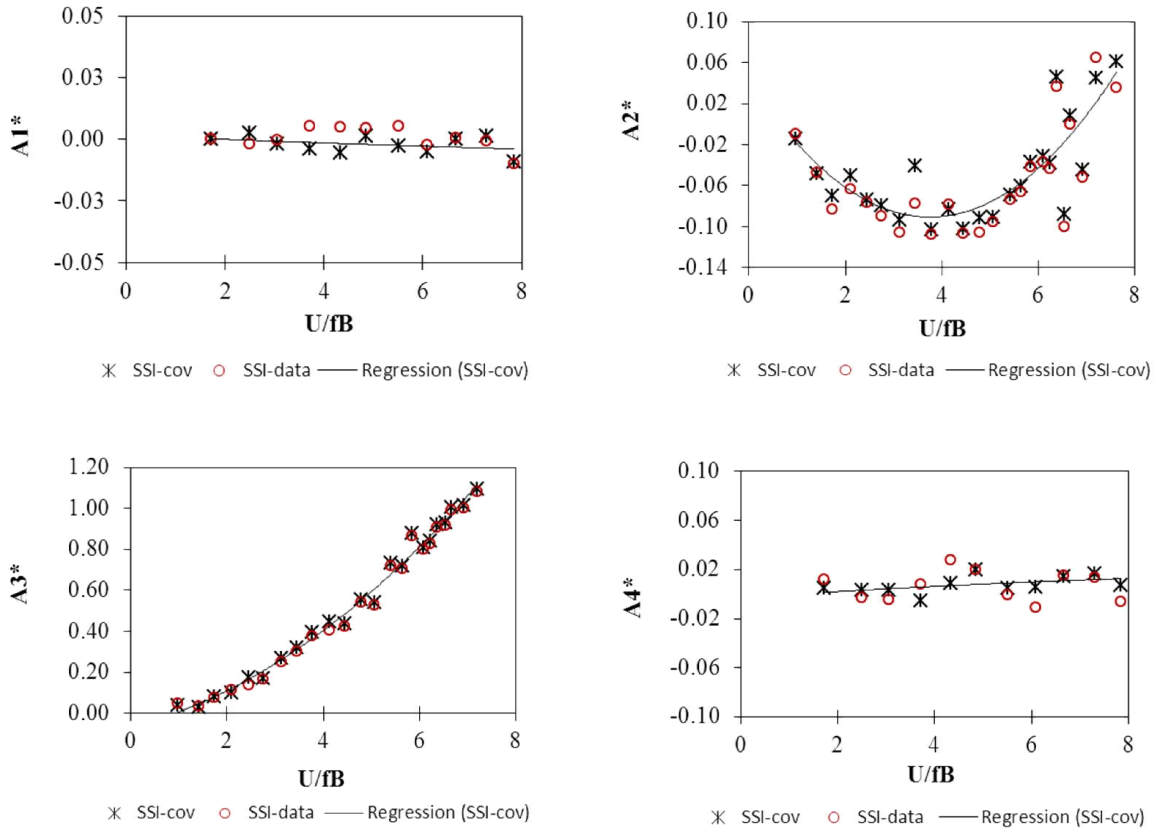

Figure 5.13 FDs (A_i) of the bridge section model under turbulent flow (I_u=9.1%) from free decay response

Figures (5.12 & 5.13) show FDs with respect to reduced wind speed. In general, the results from two methods show the same trend and both techniques are working well. The method SSI_cov shows the results (H^*_1 and A^*_2) somewhat scattering than those obtained by SSI_data. The SSI_data method is appreciably faster than the SSI_cov. Both methods start with data reduction step. In the SSI_cov, the reduction is due to take covariance of output of the Toeplitz matrix, while SSI_data algorithm is obtained by projecting the row space of the future outputs into the row of the past output. However SSI_data avoid the calculation of covariance between the outputs data.

5.3.2 Extract of flutter derivatives from buffeting response

In general, at high wind velocity, the aerodynamic damping of heaving mode is too high and vertical free response is too short. Therefore, the extraction of FDs cannot be accomplished accurately. In addition, free decay mechanism is not practical to describe real

bridges behavior in field. On the other hand, the extraction of FDs from buffeting response is more closely reflected to a real bridge behavior under turbulent wind field. The bridge deck section model will vibrate under the excitation of turbulent flow even at small wind velocity. The method is simpler than free vibration technique because of no operator corrupts by exciting the section model. It is reasonable to extract FDs from buffeting response.

Figures 5.14 & 5.15 show the flutter derivatives of the bridge deck to obtained by the SSI_data from both decaying response and buffeting responses of 1DOF and 2DOF systems under turbulent flow (I_u=9.1%).

Generally, most FDs are in agreement with both free decay and buffeting response of 1DOF and 2DOF systems. The flutter derivative H_1^* extracted from buffeting response is slightly higher than that obtained from free decay response. Coupled terms (H_2^* and H_3^*) extracted from buffeting responses are more scattering than those from free decay, particularly at high reduced wind velocity.

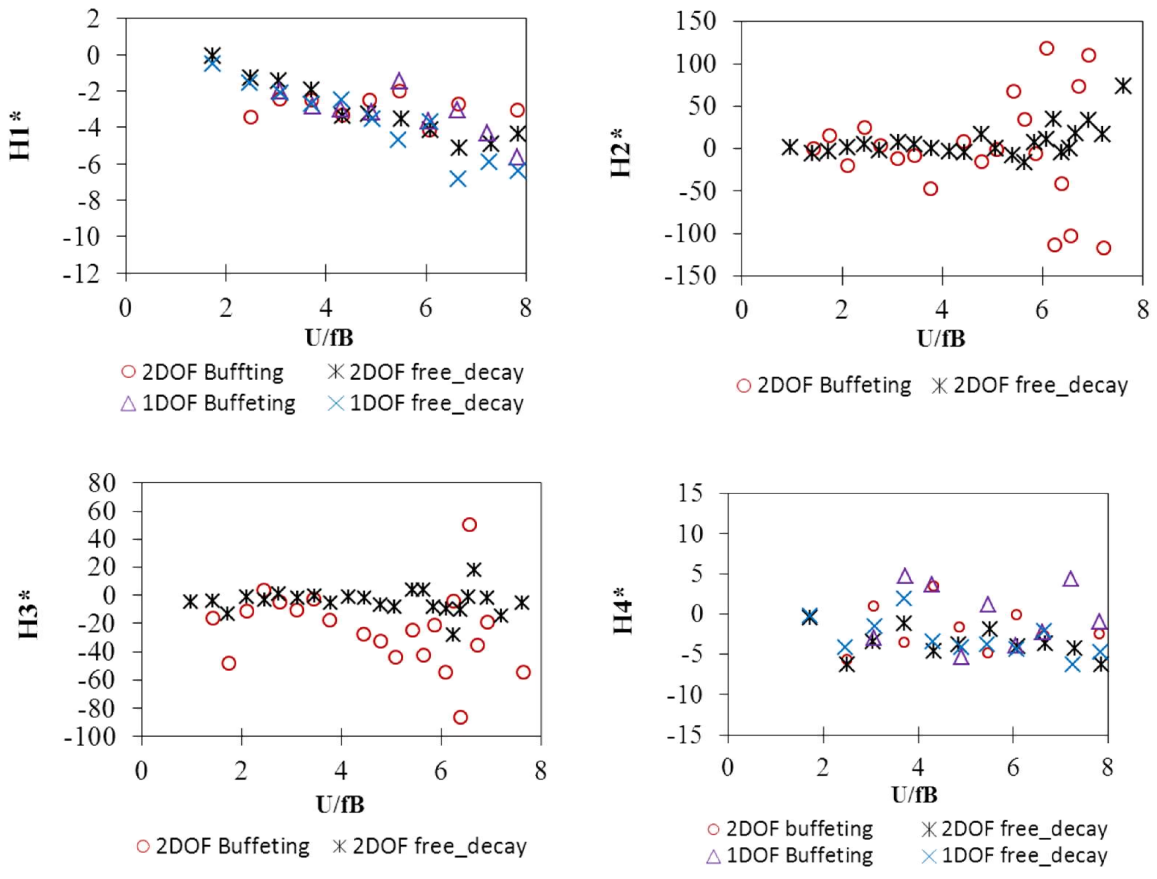

Figure 5.14 FDs (H_i) of the bridge section model by single mode and coupled mode from free decay and buffeting responses (I_u=9.1%)

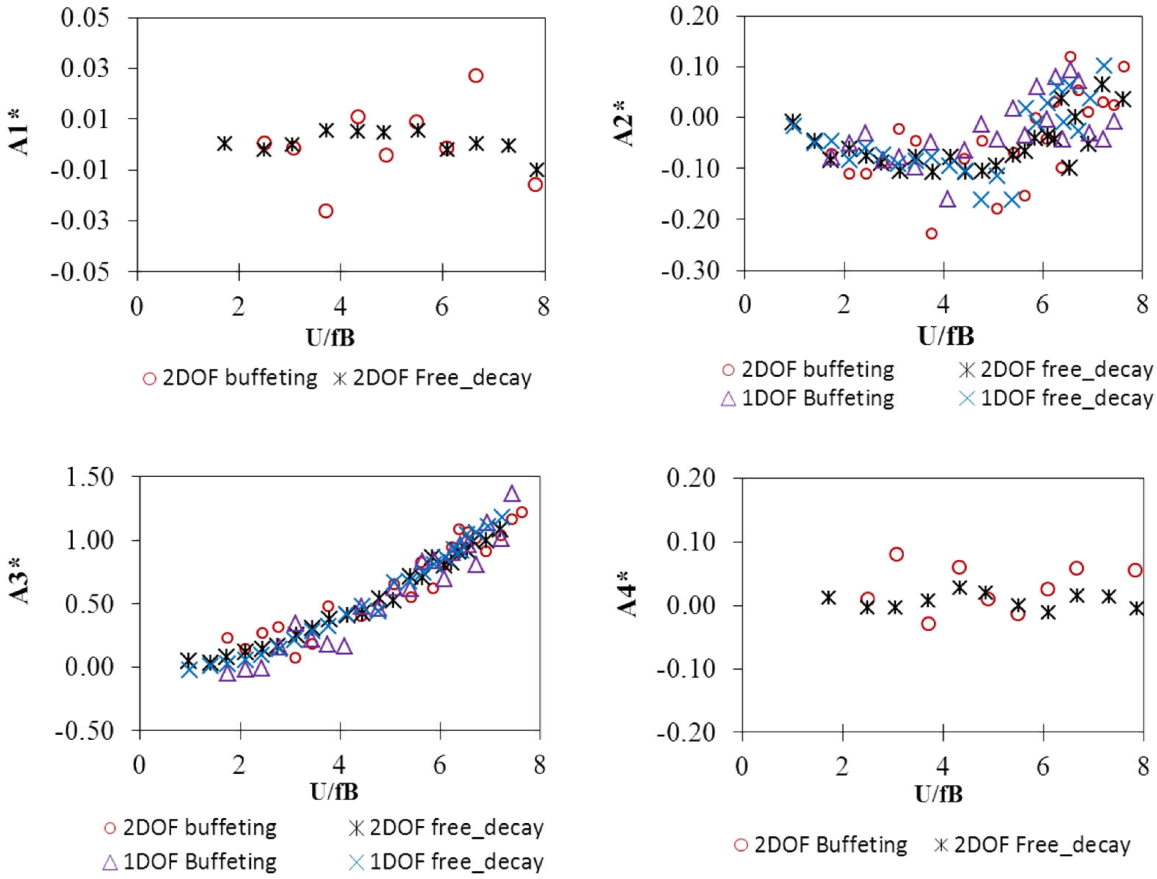

Figure 5.15 FDs (A_i) of the bridge section model by single mode and coupled mode from free decay and buffeting responses (I_u=9.1%)

In this study, the sectional profile is truss bridge deck section, which is only pure torsional flutter occurred, A_2^* is the most important derivative. The A_2^* extracted from buffeting response is scatter at small reduced wind velocities, but scatter become smaller at high reduced wind speed compared with that obtained from free decay response.

5.3.3 The effects of turbulence on flutter derivatives

In order to clarify the effects of oncoming flow turbulence on FDs, the SSI_data method is applied to extract FDs from buffeting response with different turbulence intensity. Figures (5.16 & 5.17) show the damping ratio of heaving and torsional mode versus reduced wind speed. Compared with in smooth flow, the damping ratio of heaving mode increase more slowly, at certian reduced velocity, torsional damping ratio decrease when increase tubulence intnesity. Figures (5.18 & 5.19) show the flutter derivatives under smooth and turbulent flows with the difference turbulence intensity versus reduced wind speed. $H_1^*, H_4^*, A_1^*, A_4^*$

associated with vertical oscillation were identified using the vertical frequency and $H_2^*, H_3^*, A_2^*, A_3^*$ associated with torsional oscillation were calculated using torsional frequency. In addition, the flutter derivatives obtained in both of these cases are shown in figures (5.20 & 5.21) by free decay responses. In general, the extraction of FDs in the both cases from buffeting and free decay responses are almost similar. The torsional damping term A_2^* plays an important role on torsional flutter instability since its positive/negative value corresponds to the aerodynamic instability/stability of torsional fluter. On the other hand, the coupled term, H_3^* and A_1^* together with the aerodynamically uncoupled term A_2^* have significant role on heaving-torsional 2 DOF coupled flutter instability (Matsumoto 2001). In this experiment, the onset flutter is defined as zero cross of reduced velocity axis with the A_2^*.

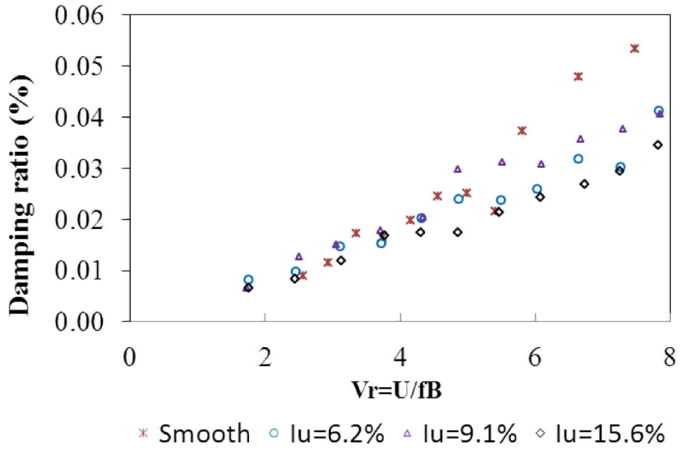

Figure 5.16 Damping ratio of heaving mode of the bridge section model under smooth and turbulence flows

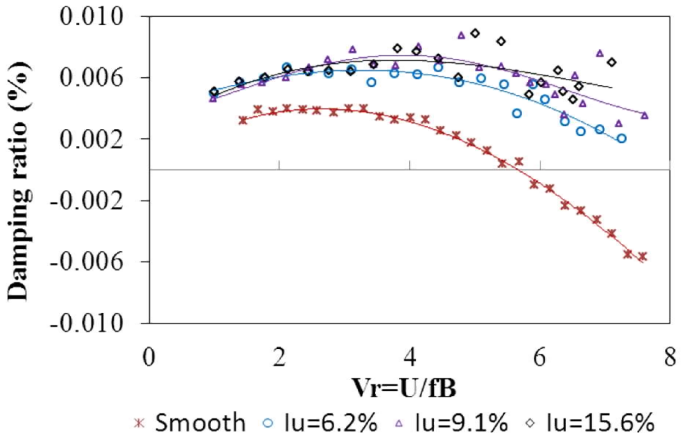

Figure 5.17 Damping ratio of torsional mode of the bridge section model under smooth and turbulence flows (solid curves are fitted polynomial)

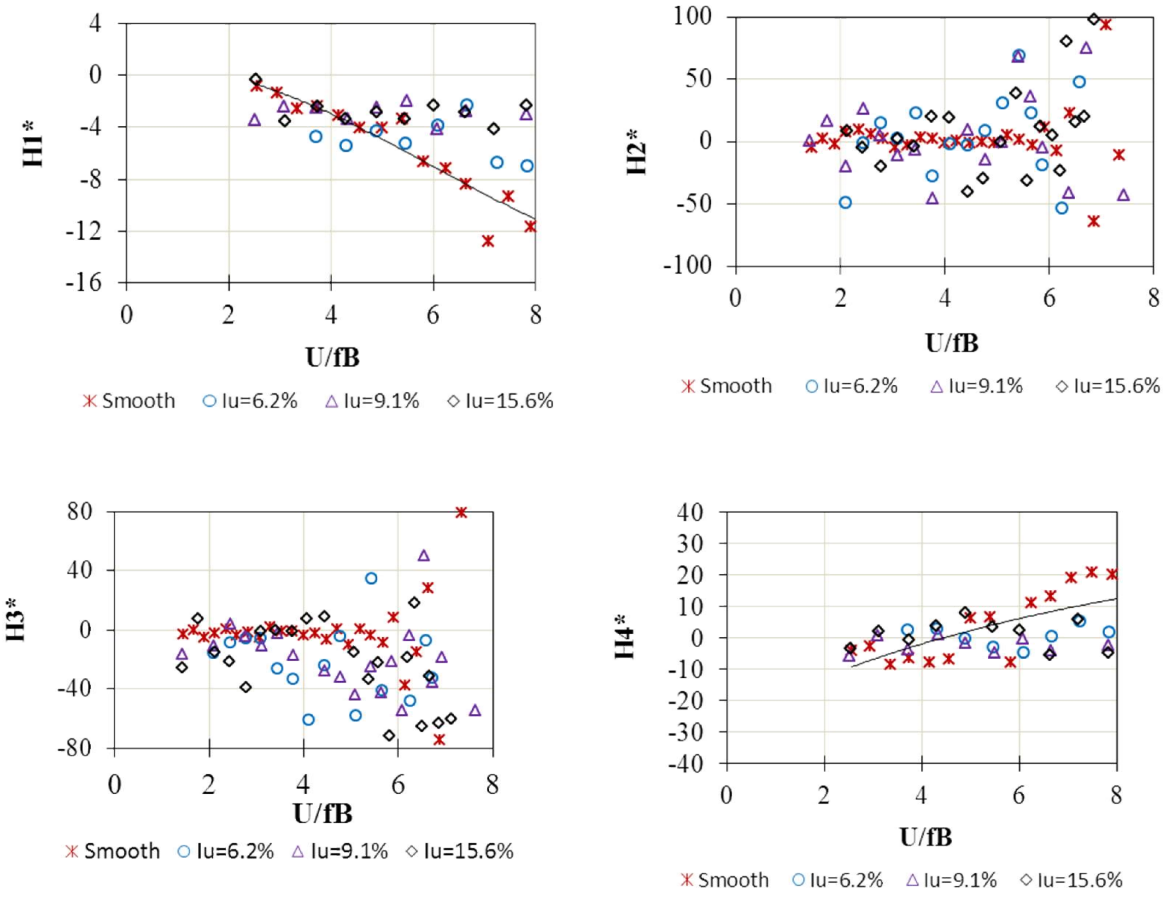

Figure 5.18 FDs (H_i) of the bridge section model under smooth and turbulent flows by buffeting response (solid curve are fitted polynomial of smooth case)

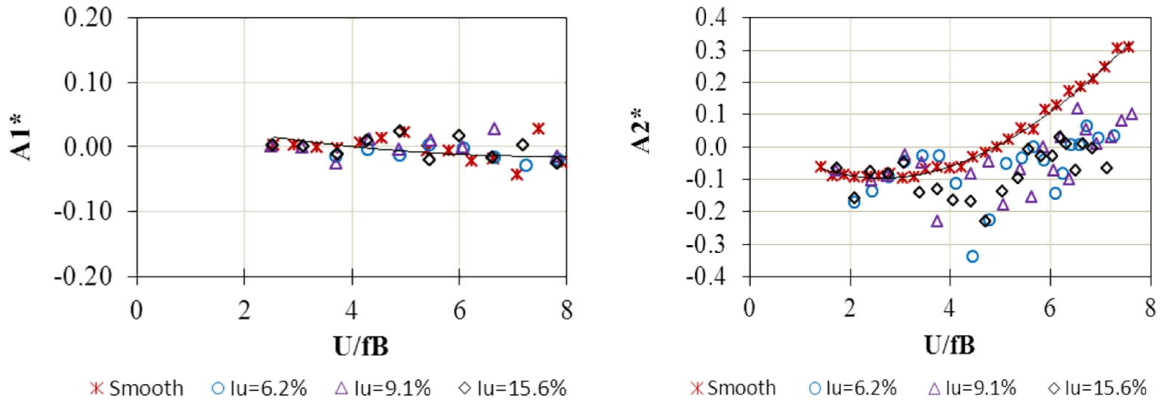

Figure 5.19 FDs (A_i) of the bridge section model under smooth and turbulent flows by buffeting response (solid curve are fitted polynomial of smooth case) (cont.)

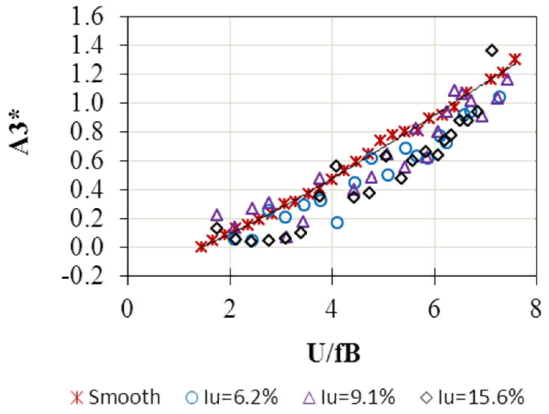

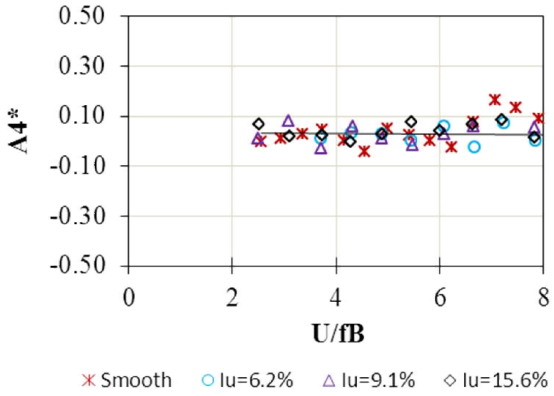

Figure 5.19 FDs (A_i) of the bridge section model under smooth and turbulent flows by buffeting response (solid curve are fitted polynomial of smooth case) (cont.)

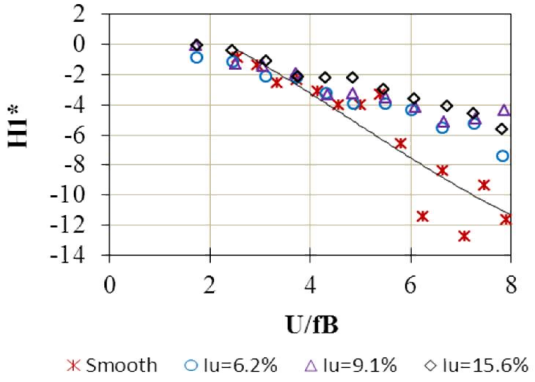

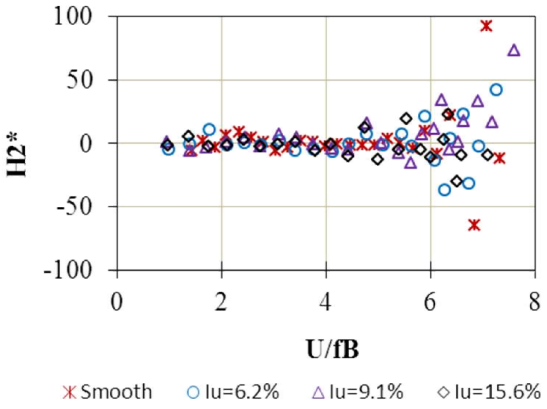

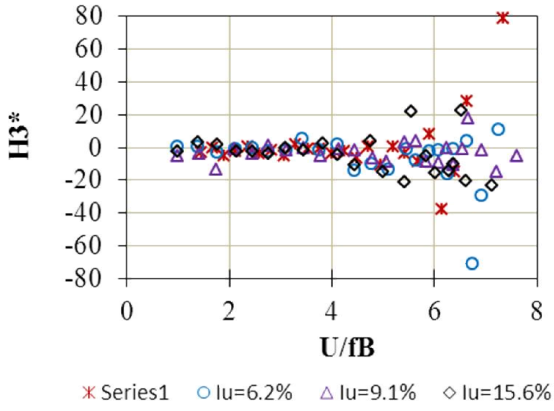

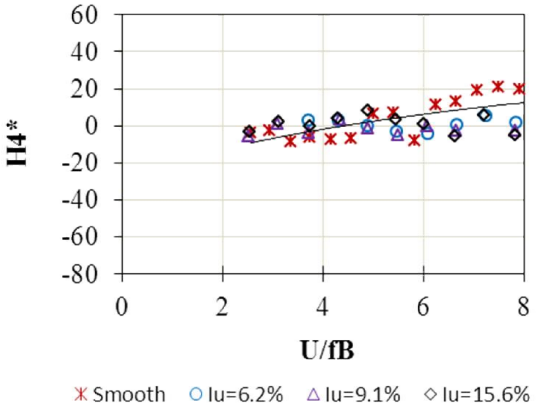

Figure 5.20 FDs (H_i) of the bridge section model under smooth and turbulent flows by free decay response (solid curve are fitted polynomial of smooth case)

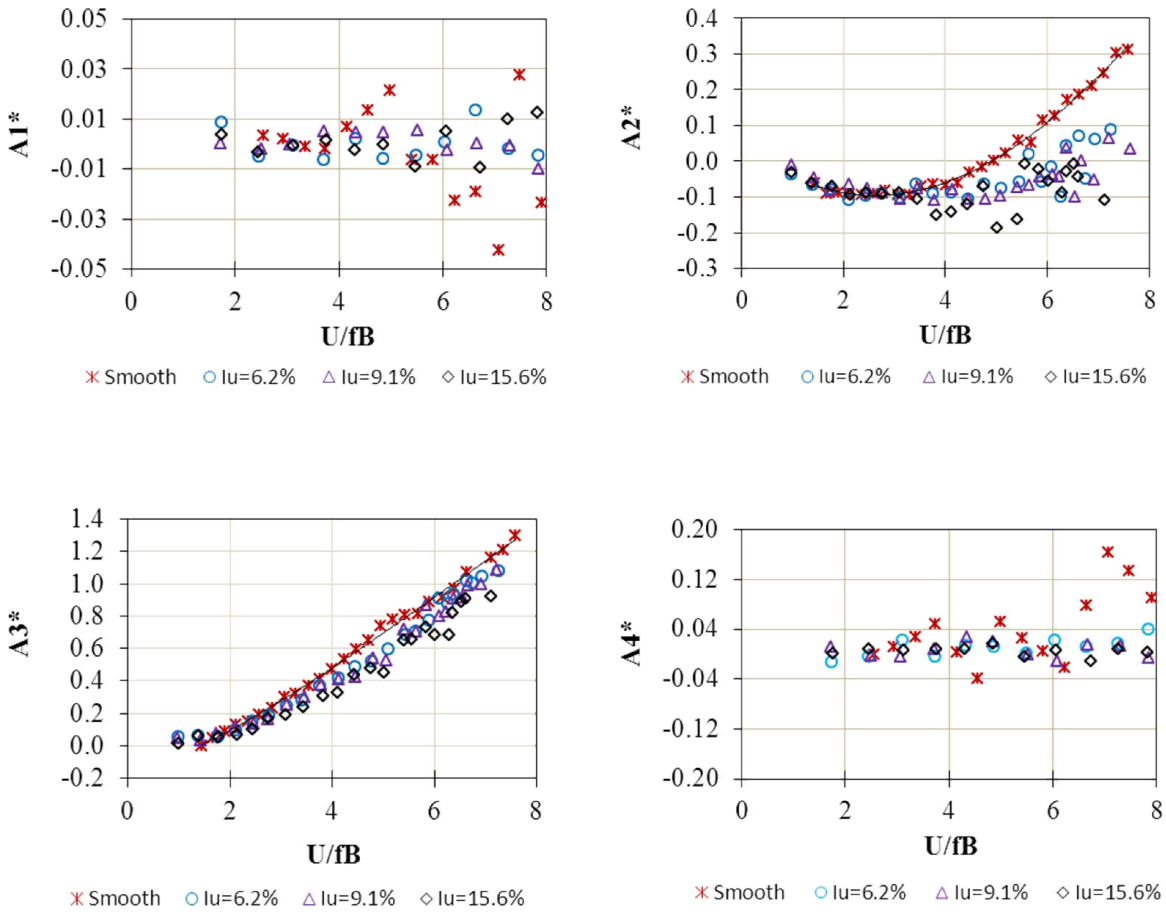

Figure 5.21 FDs (A_i) of the bridge section model under smooth and turbulent flows by free decay response (solid curve are fitted polynomial of smooth case)

From figures (5.18 & 5.20) it can be found that, in smooth flow the flutter derivative H_1^* increase faster than that extracted from turbulent flows. This equivalence that damping ratio of heaving mode under smooth flow is higher compared with in turbulent flow. Turbulence is very small effect on vertical and torsional frequency terms H_4^* and A_3^*, these values extracted from buffeting are somewhat less than in smooth flow.

As shown in figures (5.19 & 5.21), under smooth flow the positive value A_2^* at reduced wind speed (V_r = 5.2) coincides with the negative total torsional damping. The significant effects of turbulence flows on flutter derivatives are also illustrated particularly for aerodynamic torsional damping term A_2^*, the positive value correspond to the V_r around 6.5 to 7.8 under I_u = 6.2% and I_u = 9.1% respectively, whereas in case of I_u = 15.6% flutter does not occur up to V_r = 9. On the other hand, the effects of different turbulent intensities on FDs are fairly modest. This results is also suitable compared with model dynamic in previous section 4.5.

Slight difference can been seen that A_2^* tends to be lower in a high reduced velocity range as

turbulence intensity increases. The influence of turbulence on FDs will depend on the section. Sarkar (1994) found small effect for a streamlined section, while tests on a truss section showed appreciably effect which is shown clearly by torsional damping term A_2*.

The off diagonal terms H_2*, H_3*, A_1* and A_4* are fluctuated around zero value, which means that in this experiment, the coupled vibration is not appear at small wind velocity. The figures (5.22a & 5.22b) show the power spectrum density of free decaying responses at small wind velocity (5.6ms) and larger (8.8 m/s) in smooth case, which torsional frequency does not appear in vertical response and vertical frequency does not appear in torsional response. It may be sad that there is not coupling occured in smooth case.

In turbulent flows (figures (5.23-5.25)) at all a wind velocity, there is not vertical frequency appeared in torsional vibration. At small and medium wind velocity there is no torsional frequency appeared on vertical vibration. Therefore, in this experiment can be caculated flutter derivatives with separeted reduced frequency corresponding to heaving and torsional mode. On the other hand, the coupling flutter derivatives at very high wind speed should be calculated with a same reduced frequency of both heaving and torsional mode.

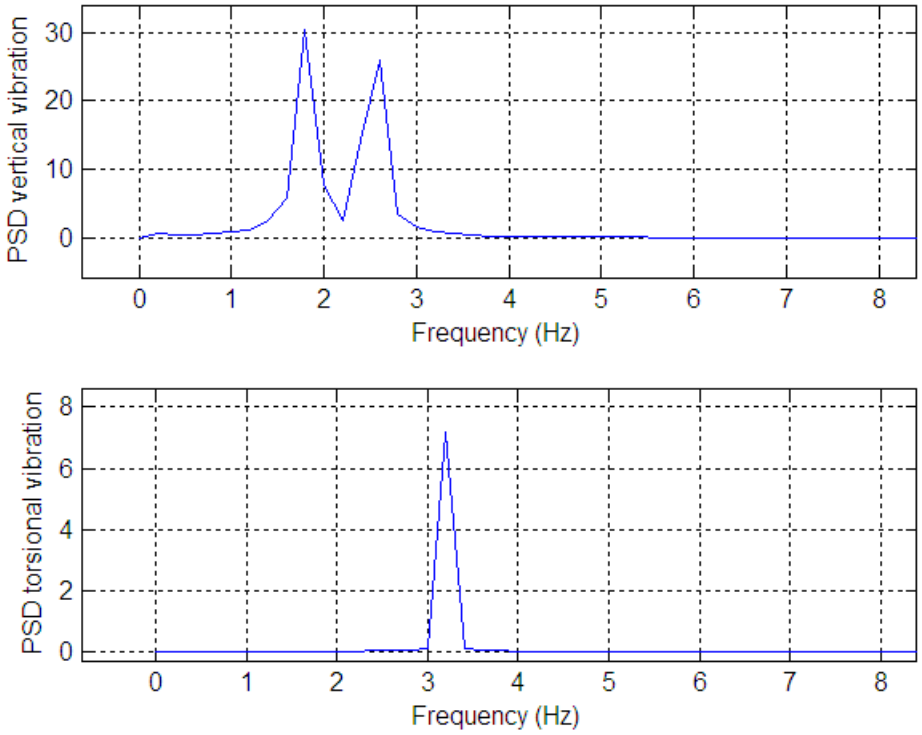

Figure 5.22a PSD of free decay response (smooth flow V=5.6 m/s)

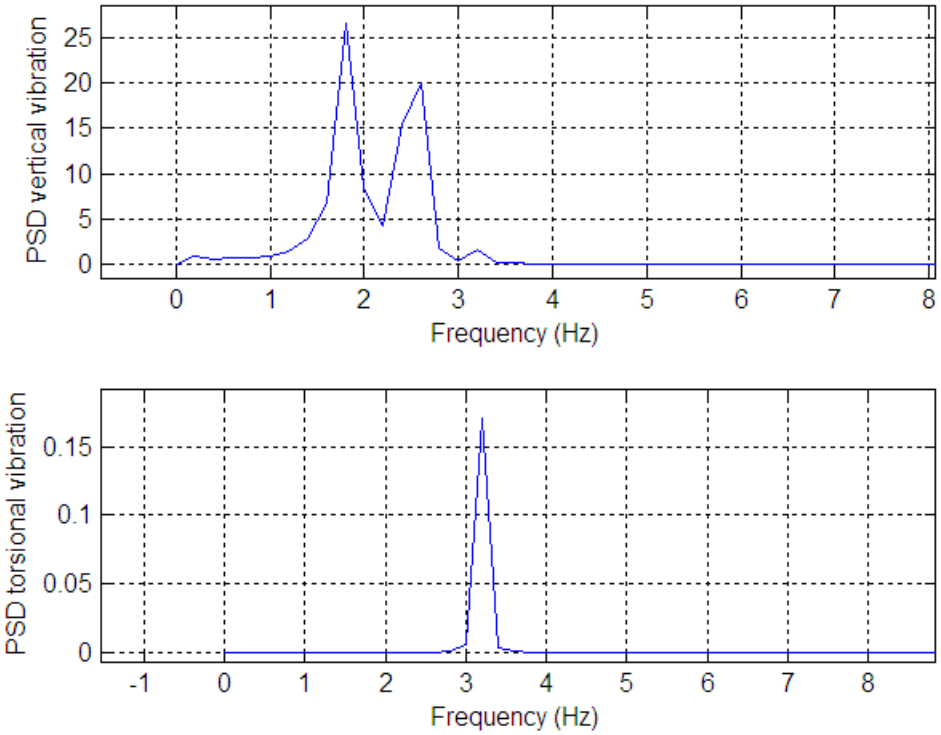

Figure 5.22b PSD of free decay response (smooth flow V=8.8 m/s)

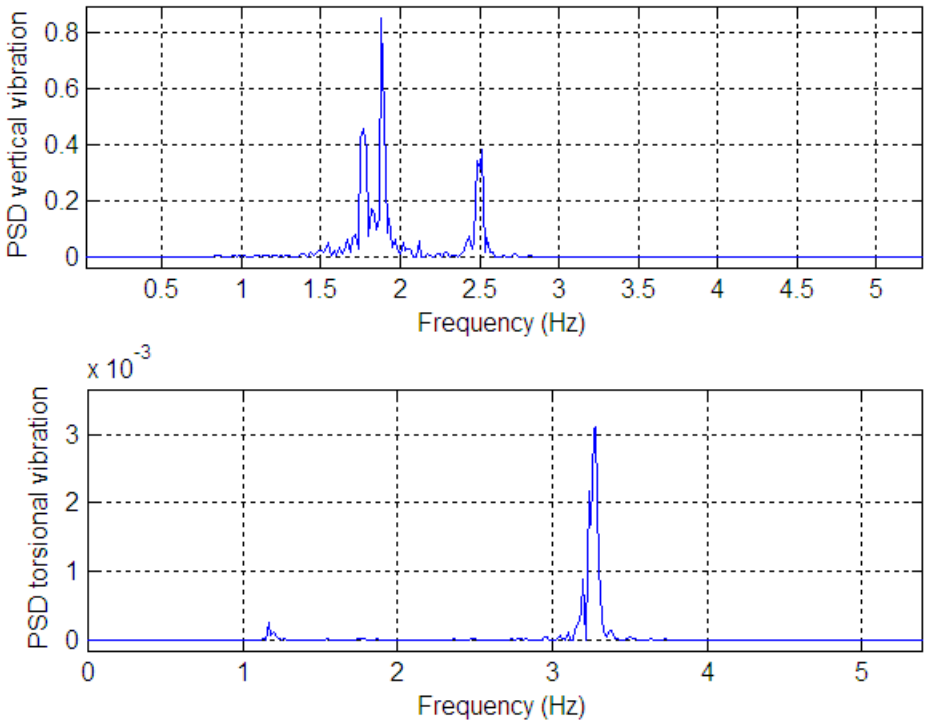

Figure 5.23a PSD of buffeting response (Iu=6.2%; V=2.9 m/s)

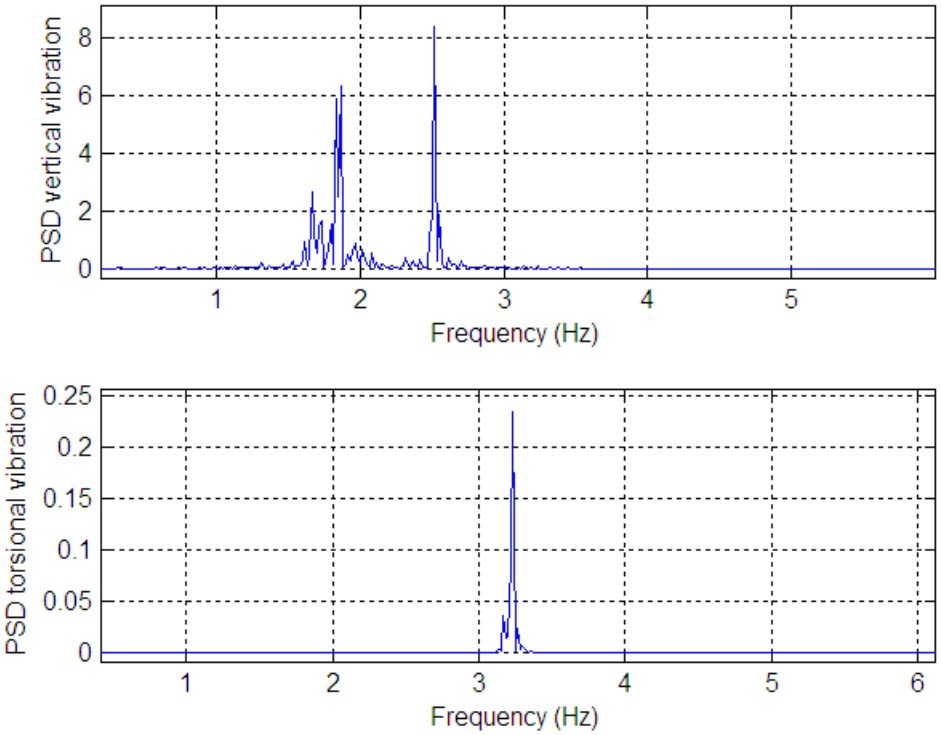

Figure 5.23b PSD of buffeting response (Iu=6.2%; V=6.1 m/s)

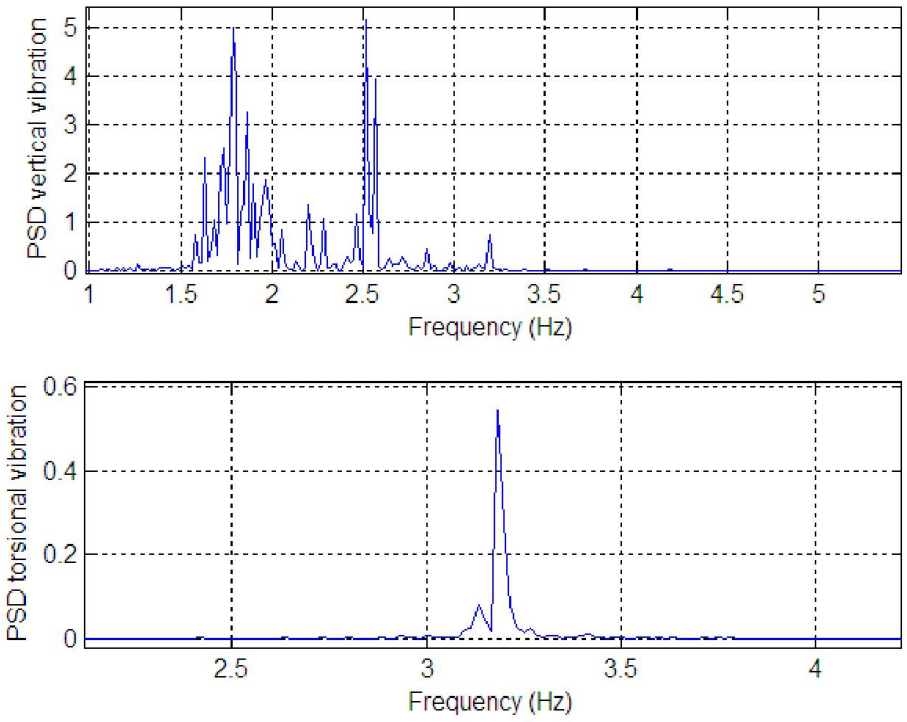

Figure 5.23c PSD of buffeting response (Iu=6.2%; V=8.05 m/s)

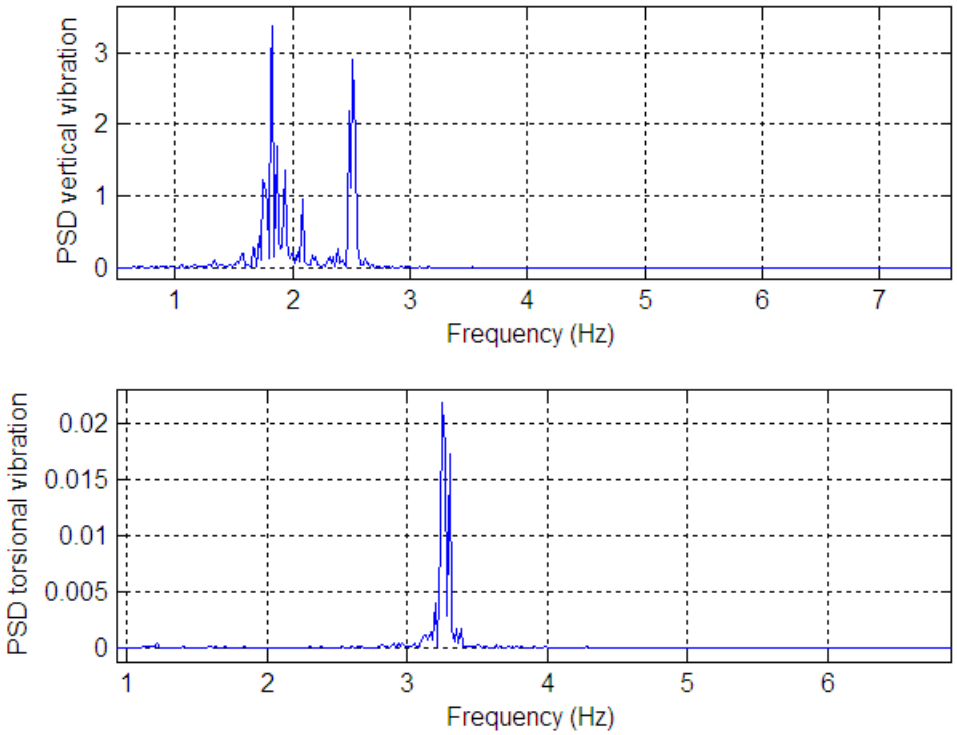

Figure 5.24a PSD of buffeting response (Iu=9.1%; V=4.1 m/s)

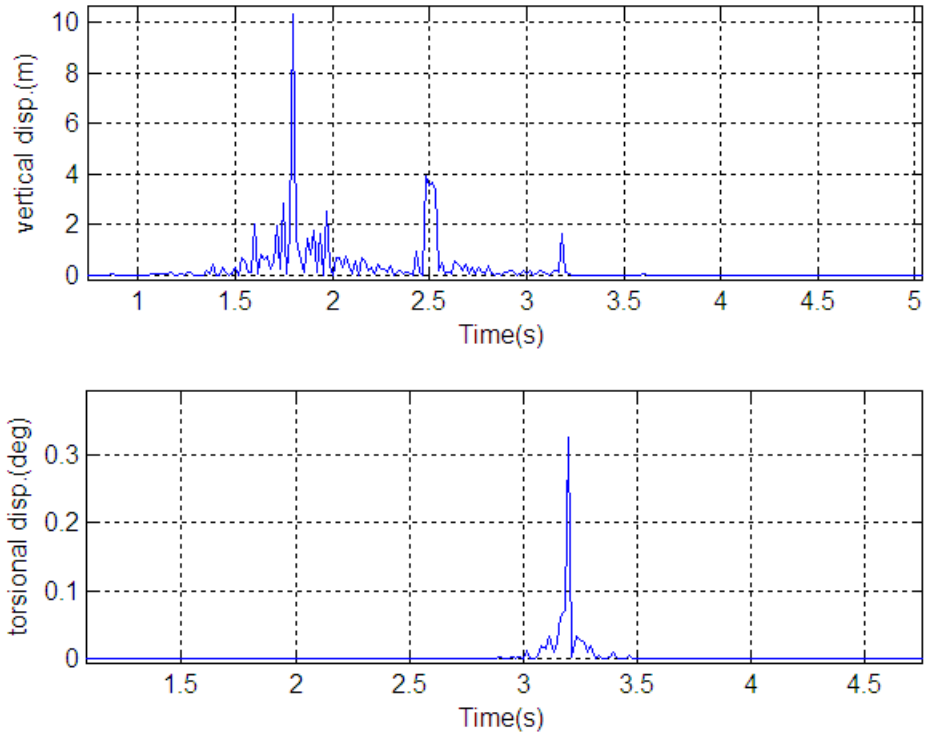

Figure 5.24b PSD of buffeting response (Iu=9.1%; V=8.45 m/s)

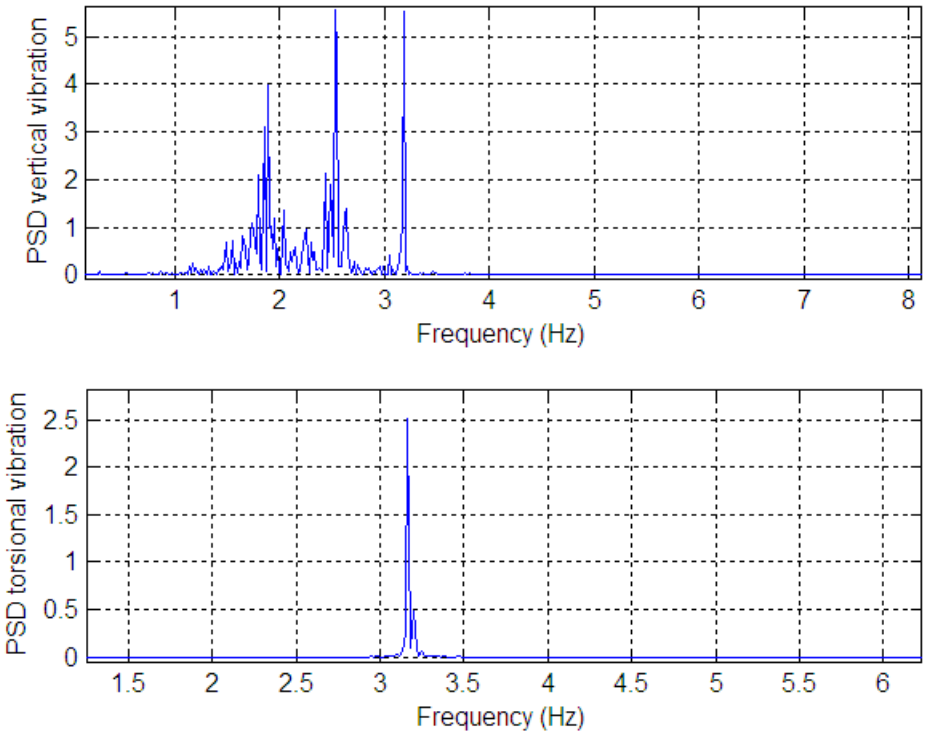

Figure 5.24b PSD of buffeting response (Iu=9.1%; V=9.14 m/s)

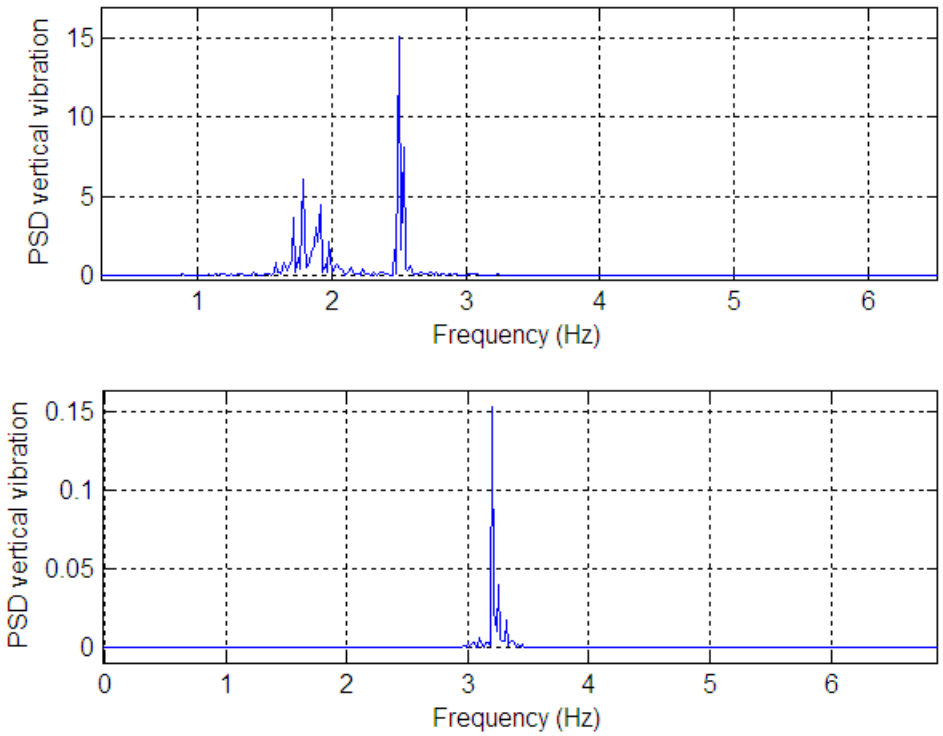

Figure 5.25a PSD of buffeting response (Iu=15.6%; V=6.06 m/s)

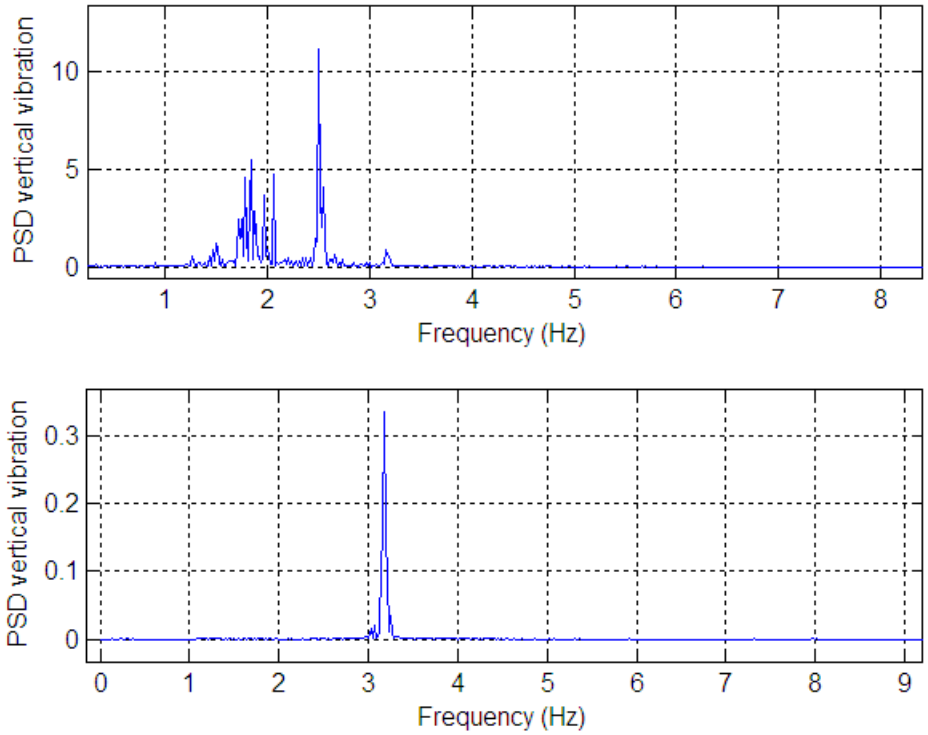

Figure 5.25b PSD of buffeting response (Iu=15.6%; V=9.03 m/s)

5.3.4 Estimation of variation in identification result

In order to estimate the variation in identification results, five data sets have been calculated with SSI_data which is same procedure aforementioned. The mean value, standard deviation and coefficient of variation of flutter derivatives at several certain reduced wind velocity show in tables (5.1-5.3) and display by figure 5.26.

Table 5.9a: Mean value and standard deviation of flutter derivatives in case I_u=6.2%

V_r	A_2^*			A_3^*		
	Mean value (μ)	Standard deviation (σ)	Coefficient of variation (C_v= σ/ μ)	Mean value (μ)	Standard deviation (σ)	Coefficient of variation (C_v= σ/ μ)
3.45	-0.029	0.026	0.896	0.3137	0.021	0.067
5.11	-0.0532	0.053	0.996	0.4827	0.032	0.066
6.73	0.0646	0.013	0.201	0.9594	0.036	0.038
7.28	0.0736	0.019	0.256	1.2614	0.113	0.0895

Table 5.9b: Mean value and standard deviation of flutter derivatives in case I_u=6.2%

V_r	H_1^*			H_4^*		
	Mean value	Standard deviation	Coefficient of variation (C_v= σ/ μ)	Mean value (μ)	Standard deviation (σ)	Coefficient of variation (C_v= σ/ μ)
4.30	-4.426	0.35	0.079	2.848	0.64	0.225
6.08	-2.95	0.43	0.146	-6.85	1.12	0.164
7.84	-7.34	0.97	0.13	0.072	0.032	0.45

Table 5.10a: Mean value and standard deviation of flutter derivatives in case I_u=9.1%

V_r	A_2^*			A_3^*		
	Mean value (μ)	Standard deviation (σ)	Coefficient of variation (C_v= σ/ μ)	Mean value (μ)	Standard deviation (σ)	Coefficient of variation (C_v= σ/ μ)
2.45	-0.105	0.028	-0.267	0.244	0.038	0.156
5.63	-0.175	0.031	0.177	0.864	0.026	0.03
6.72	0.0426	0.028	0.65	1.001	0.031	0.031
7.43	0.081	0.025	0.309	1.15	0.017	0.015

Table 5.10b: Mean value and standard deviation of flutter derivatives in case I_u=9.1%

V_r	H_1^*			H_4^*		
	Mean value	Standard deviation	Coefficient of variation (C_v= σ/ μ)	Mean value (μ)	Standard deviation (σ)	Coefficient of variation (C_v= σ/ μ)
4.32	-3.986	0.65	0.163	3.467	1.34	0.387
6.64	-2.339	0.244	0.104	-2.734	0.562	0.165
7.82	-3.544	0.788	0.222	-1.629	0.334	0.205

Table 5.11a: Mean value and standard deviation of flutter derivatives in case I_u=15.6%

V_r	A_2^*			A_3^*		
	Mean value (μ)	Standard deviation (σ)	Coefficient of variation (C_v= σ/ μ)	Mean value (μ)	Standard deviation (σ)	Coefficient of variation (C_v= σ/ μ)
3.4	-0.139	0.039	0.281	0.052	0.040	0.769
5.07	-0.138	0.043	0.312	0.65	0.022	0.034
6.51	-0.074	0.012	0.162	0.943	0.067	0.071
6.85	-0.015	0.038	2.53	0.937	0.020	0.02

Table 5.11b: Mean value and standard deviation of flutter derivatives in case I_u=15.6%

V_r	H_1^*			H_4^*		
	Mean value	Standard deviation	Coefficient of variation (C_v= σ/ μ)	Mean value (μ)	Standard deviation (σ)	Coefficient of variation (C_v= σ/ μ)
3.74	-2.676	0.71	0.265	0.522	0.138	0.264
6.0	-2.117	0.493	0.233	1.269	0.826	0.651
7.81	-2.159	0.148	0.068	-4.333	1.945	0.448

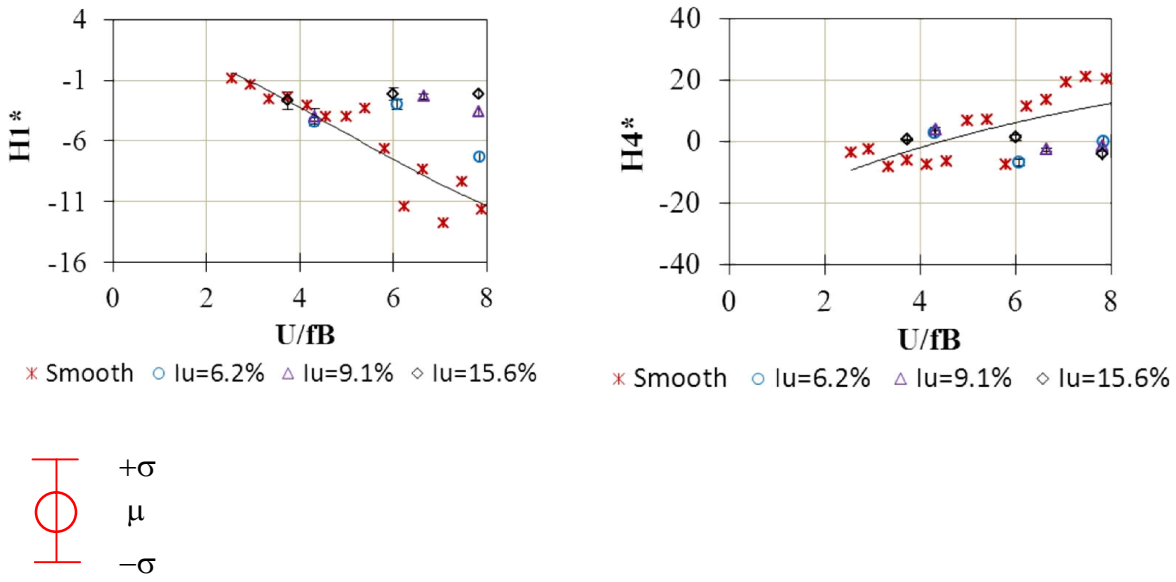

Figure 5.26 Variation of identification (cont.)

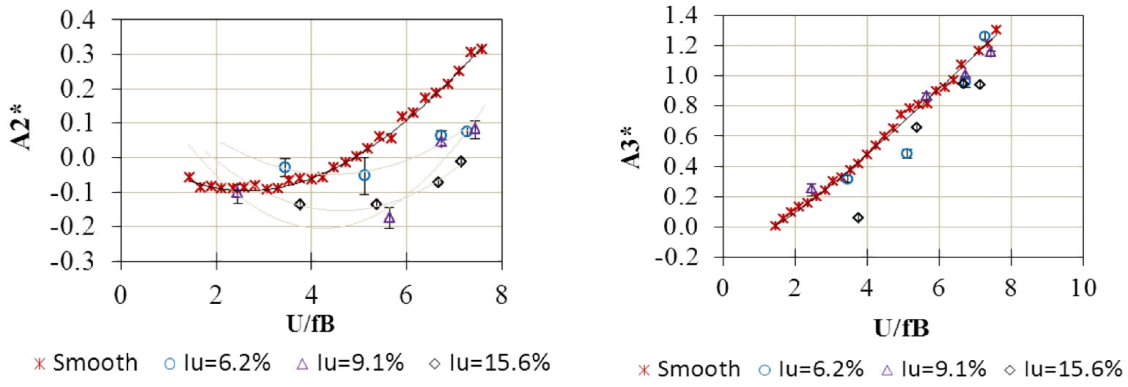

Figure 5.26 Variation of identification (cont.)

The flutter derivative A_3^* is more stable which is small coefficient of variation. The standard deviation and coefficient of variation of A_2^* decrease with increase reduced wind velocity. There are large scatter in A_2^*, however at large reduced wind velocity the standard deviation and coefficient of variation are small. Therefore, the A_2^* is reliability at high reduced wind speed (around onset flutter).

5.3.5 Flutter critical velocity

Equation of motion of long span suspension bridge to unsteady aerodynamic can be written as follows:

$$M\ddot{u} + C\dot{u} + Ku = F_A\ddot{u} + F_V\dot{u} + F_D u \tag{5.1}$$

Where: M is the mass matrix

C is the damping matrix

K is the stiffness matrix

u is the displacement vector

F_A, F_V and F_D are the motion-dependent unsteady aerodynamic force matrices associated with acceleration, velocity and displacement, respectively and are called flutter derivatives.

The flutter critical velocity can be found by solving the equation of motion with assumption dynamic response is harmonic vibration and undamped.

$$\begin{aligned} u &= \{\Phi\}\, e^{i\omega t} \\ u &= -\ddot{u} / \omega^2 \\ \dot{u} &= i\,\ddot{u} / \omega \end{aligned} \tag{5.2}$$

$$F\ddot{u} = F_A\ddot{u} + F_V\dot{u} + F_D u = \{F_A + \frac{i}{\omega^2}F_V - \frac{1}{\omega^2}F_D\}\ddot{u} \tag{5.3}$$

Inserting Eqs. 5.2 & 5.3 into Eq. 5.1, we have

$$[\mathrm{K}]^{-1}[\mathrm{M}-\mathrm{F}]\ddot{u} = \frac{1}{\omega^2}\ddot{u} \tag{5.4}$$

Apply Eigen-solution Eq.5.4 will be obtained complex eigenvalue and eigenvector

$$\begin{aligned} \omega &= \omega_R + \omega_I \\ \Phi &= \Phi_R + \Phi_I \end{aligned} \tag{5.5}$$

Damping ratio is

$$\xi = \frac{\omega_R}{\sqrt{\omega_R^2 + \omega_I^2}} \tag{5.5}$$

The flutter critical wind speed is defined as the cross point of torsional aerodynamic logarithmic decrement and torsional structural logarithmic decrement (δ=0.0263) (figures 5.27 to 5.30). The flutter critical velocity found from flutter derivatives are in good agreement compared with from model dynamic test, only case Iu=15.6% the flutter critical wind speed identified from flutter derivatives (Ucr=8.2) that is slightly smaller compared with from model dynamic test (Ucr=8.6).

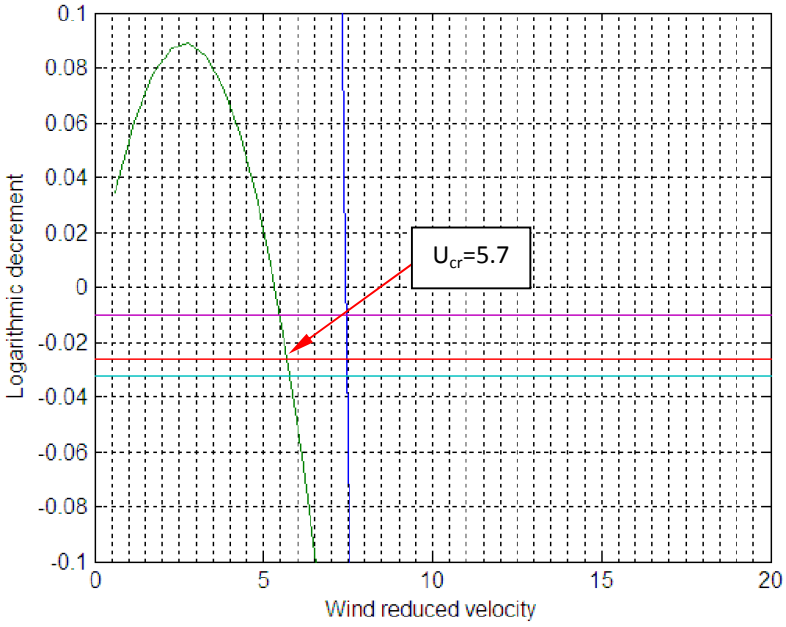

Figure 5.27 Logarithms decrement in smooth flow (Ucr=5.7)

(Modal dynamic experimental result Ucr=5.7)

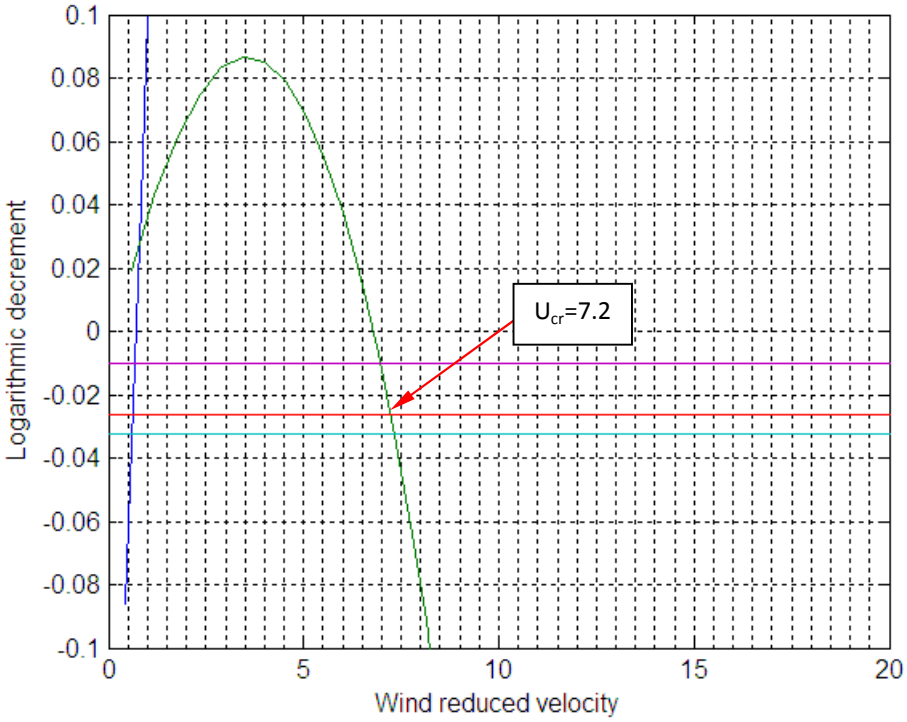

Figure 5.28 Logarithms decrement in turbulent flow Iu=6.2% (Ucr=7.2)

(Modal dynamic experimental result Ucr=7.2)

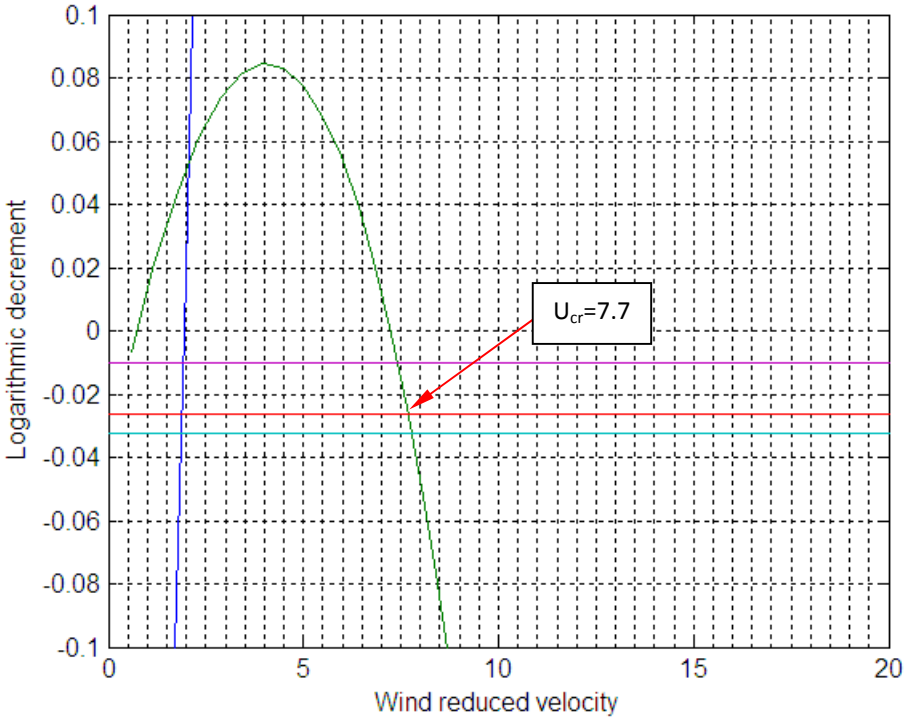

Figure 5.29 Logarithms decrement in turbulent flow Iu=9.1% (Ucr=7.7)

(Modal dynamic experimental result Ucr=7.7)

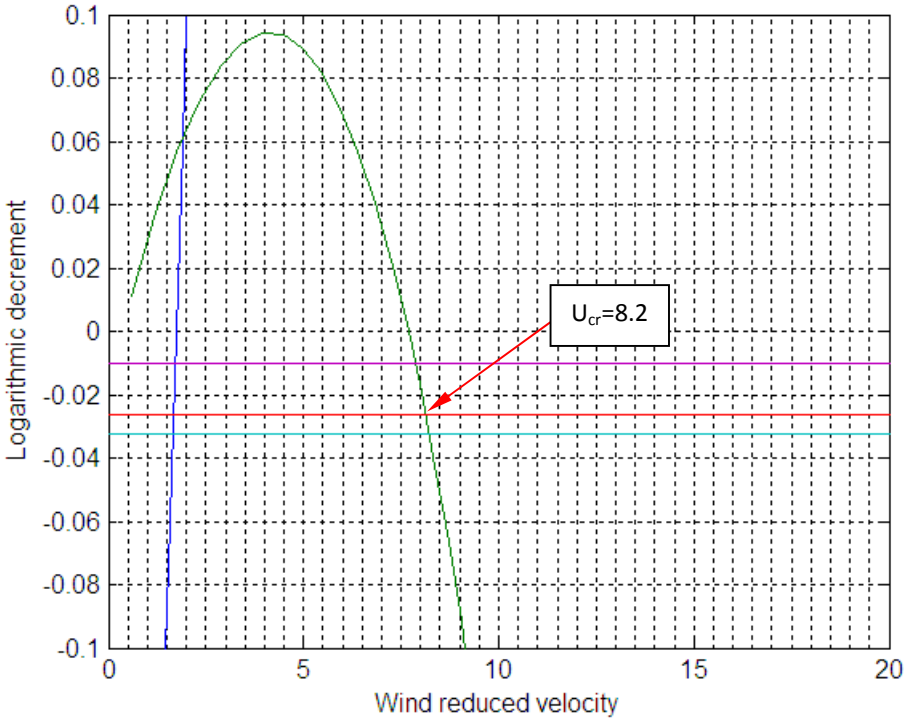

Figure 5.30 Logarithms decrement in turbulent flow Iu=15.6% (Ucr=8.2)

(Modal dynamic experimental result Ucr=8.6)

5.3.6 Stationarity tests of Gust response

Stationarity tests conducted with vertical gust response at wind velocity V=5.3m/s and torsional gust response at V=8.54 m/s in case of maximum turbulence intensity Iu=15.6% (figures 5.30 & 5.31). The 6000 data length with sample frequency 100Hz divided in to N = 20 data sets (1 data set is 3 second), then calculated standard deviation of each data set and plot in figures 5.32 & 5.33. The median are calculated also and plot in figure (horizontal line). By counting the number of group separated of median line and compared with table 5.12 (n=N/2=10), the number of groups are 8 and 7 correspond to vertical and torsional gust responses, these values fall inside of interval (6 and 15). Therefore, these gust responses are stationary.

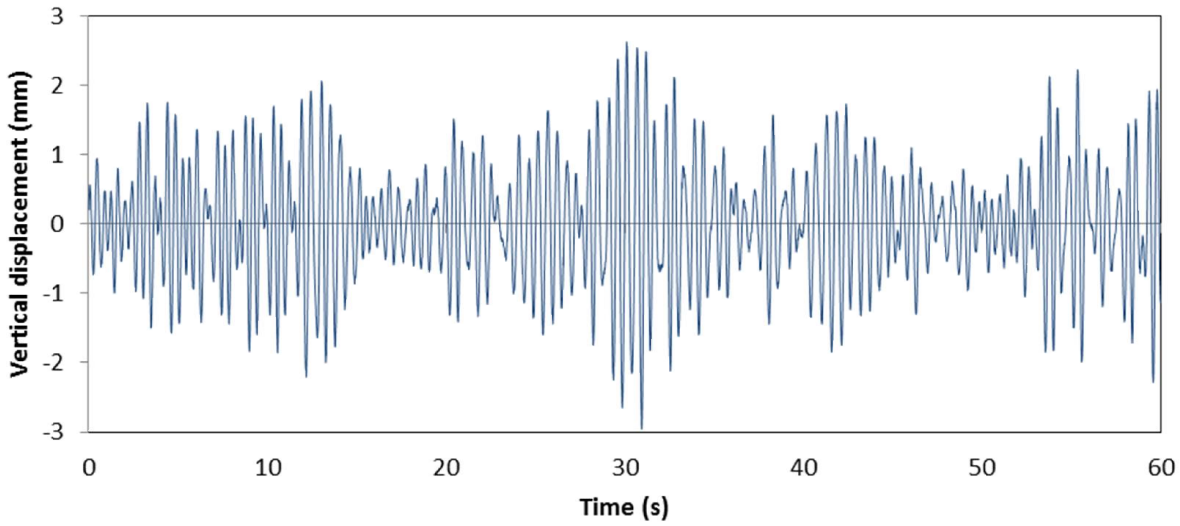

Figure 5.30 Vertical gust responses at V=5.3 (m/s), Iu=15.6%

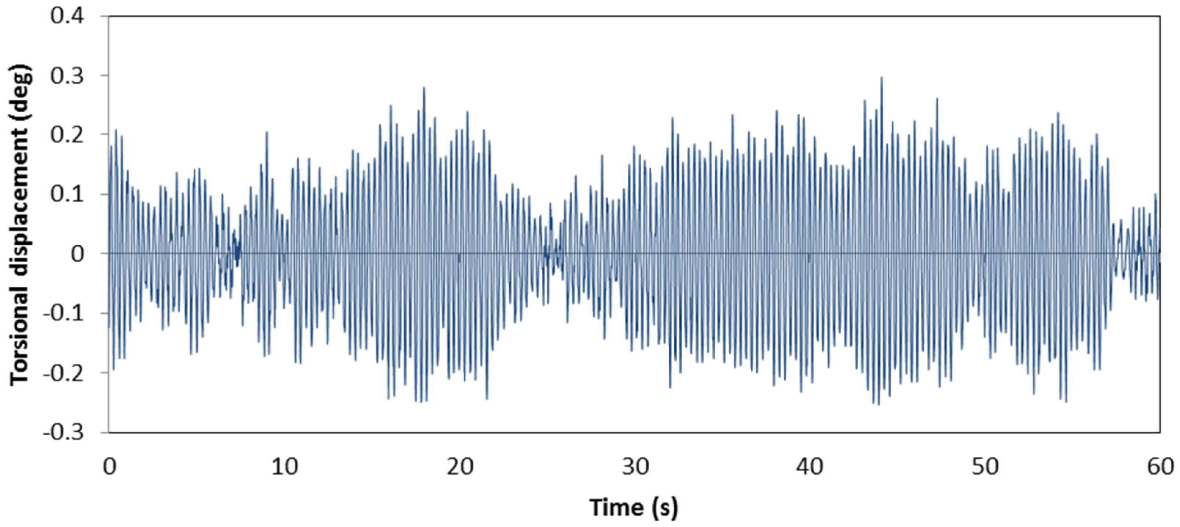

Figure 5.31 Torsional gust responses at V=8.54 (m/s), Iu=15.6%

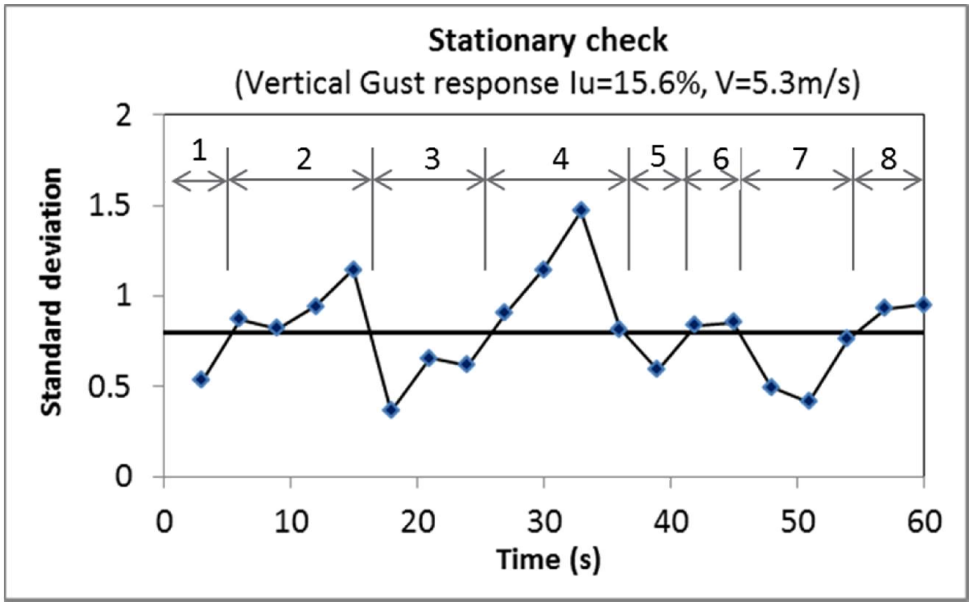

Figure 5.30 Standard deviation and median (horizontal line) vs. time of vertical gust response

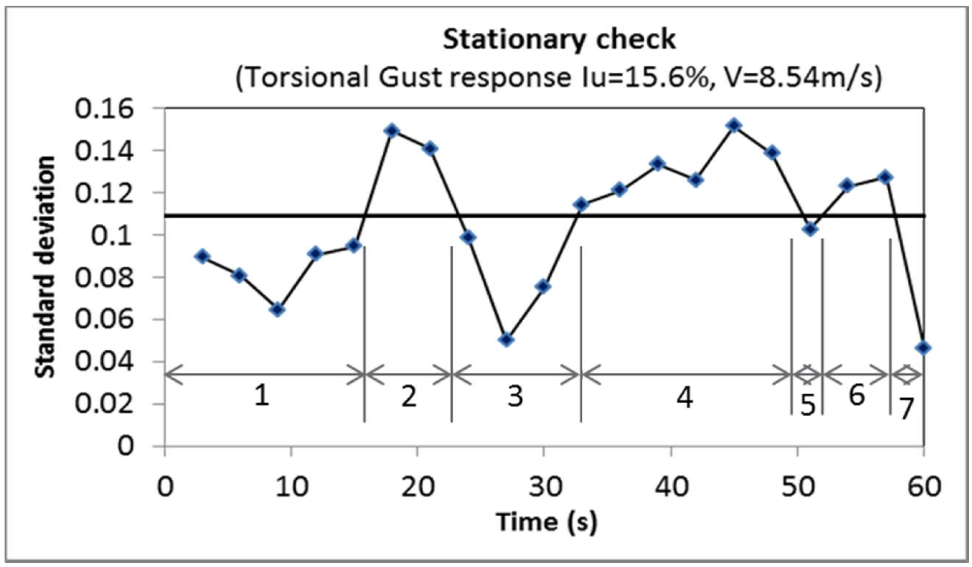

Figure 5.31 Standard deviation and median (horizontal line) vs. time of torsional gust response

Table 5.12: Stationarity with exceeding range probability

表 A.6　連の分布表

Prob$[r_n > r_{n;\alpha}] = \alpha$ となる $r_{n;\alpha}$ の値，ただし $n = N_1 = N_2 = N/2$

	α					
$n = N/2$	0.99	0.975	0.95	0.05	0.025	0.01
5	2	2	3	8	9	9
6	2	3	3	10	10	11
7	3	3	4	11	12	12
8	4	4	5	12	13	13
9	4	5	6	13	14	15
10	5	6	6	15	15	16
11	6	7	7	16	16	17
12	7	7	8	17	18	18
13	7	8	9	18	19	20
14	8	9	10	19	20	21
15	9	10	11	20	21	22
16	10	11	11	22	22	23
18	11	12	13	24	25	26
20	13	14	15	26	27	28
25	17	18	19	32	33	34
30	21	22	24	37	39	40
35	25	27	28	43	44	46
40	30	31	33	48	50	51
45	34	36	37	54	55	57
50	38	40	42	59	61	63
55	43	45	46	65	66	68
60	47	49	51	70	72	74
65	52	54	56	75	77	79
70	56	58	60	81	83	85
75	61	63	65	86	88	90
80	65	68	70	91	93	96
85	70	72	74	97	99	101
90	74	77	79	102	104	107
95	79	82	84	107	109	112
100	84	86	88	113	115	117

CHAPTER 6

CONCLUSION

Flutter derivatives are utmost important parameters in the estimation of the flutter instability and responses of long-span bridges. These parameters can be identified under wind tunnel test by a section model. Normally wind tunnel test is conducted with free vibration method in smooth flow condition. However, the free vibration method holds a shortcoming which at high wind velocity the extraction of FDs may not be obtained accurately because the aerodynamic damping of vertical mode is too high and vertical free-vibration data is too short for the analysis. Furthermore, the wind in the atmospheric boundary layer is always turbulence. Therefore any research of wind-induced vibration problems must consider this issue. Not many researchers study the effect of turbulence on self-excited via flutter derivatives. A past study only dealt with quire small range of turbulence intensity, such as Sarkar (1994) with I_{max}=3.42%. However long-span cable supported bridges are often subject to the turbulence intensity up to 20% such as Akashi Kaikyo bridge of I = (4%-15%) during typhoon number 7 in 1998 and I = (4%-22%) during typhoon number 18 in 1999 (Miyata 2002).

The objective of study is identification of flutter derivatives of trussed bridge deck by gust response. The aim is to clarify the effects of oncoming turbulence on the self-excited force of a cable-supported long span bridge deck by using a section model. Moreover, it is aimed at developing a mathematic algorithm as namely stochastic system identification method for extraction flutter derivatives, which is not only from buffeting response but also from free vibration response. The gust responses obtained from wind tunnel test by bilinear wooden grid and numerical simulation with turbulence intensity from 6.2% to 15.6%. The flutter derivatives were extracted from gust responses by using output only state space stochastic system identification technique.

Both SSI_cov and SSI_data methods show good results even under turbulence flows because an advantage of those methods are considered buffeting force and response as inputs instead of noises. Both subspace methods identify state-space models from output data by applying robust numerical techniques such as QR factorization, SVD and least squares. The SSI_data is considerably faster than SSI_cov.

FDs are reasonable comparison between both free decay and buffeting response of 1DOF and 2DOF systems. The A_2^* related to torsional damping extracted from buffeting is slightly

scatter than from free decay response but the trend line seem to be similar.

An identification of flutter derivatives from buffeting responses is plausible. The advantage of this technique is easier to obtain buffeting response under turbulent flows. This is less time consuming than free decay test. Especially at high wind velocity it can be avoided that the vertical free decay data is too short causing less accuracy. In addition, mechanism of free vibration method is far from real bridges behavior in wind field. On the other hand, the extraction of FDs from buffeting response more closely reflects a real bridge behavior under turbulent wind field. The bridge deck section model will vibrate under the excitation of turbulent flow even at small wind velocity. The method is simpler than free vibration technique which is corrupted by exciting the section-model. It is reasonable to extract FDs from buffeting response. The flutter derivative H_1^*, H_4^* and A_3^* are more stable which are small coefficient of variations. The standard deviation and coefficient of variation of A_2^* decrease with increase reduced wind velocity. At large reduced wind velocity range the A_2^* is reliability because the standard deviation and coefficient of variation are small.

Turbulent flows significantly affect dynamic responses and flutter derivatives of the truss bridge deck section. Buffeting raises the response amplitude level progressively in proportion to the reduced wind speed and turbulent intensity. Specifically, turbulence induces buffeting response but increase flutter critical velocity, as shown in aerodynamic torsional damping term A_2^*. The flutter derivative H_1^* extracted from buffeting response decrease with the increase of reduced velocity, but decrease a little in turbulence compared with that from smooth flow. H_4^* found under turbulent flow slightly changes compared with that under smooth flow. The direct FD A_3^*seems to be same trend in both cases.

REFERENCES

1) Matsumoto, M., Matsumiya, H., Fujiwara, S., Ito, Y., (2008), "New consideration on Flutter properties basing on SBS-Fundamental flutter mode, similar Selberg's formula, torsional divergence instability and new coupled flutter phenomena affected by structural coupling.", *BBAA VI international colloquium on: Bluff bodies aerodynamics and applications*.
2) Matsumoto, M., Matsumiya, H., Fujiwara, S., Ito, Y., (2010), "New consideration on flutter properties based on step-by-step analysis.", *J. Wind Eng. Ind. Aerodyn*, 98, 429-437.
3) Matsumoto, M., Nihara, Y., Kobayashi, Y., Sato, H., Hamasaki, H., (1995) "Flutter mechanism and its stabilization of bluff bodies.", *Proceedings of 9th ICWE*, 827–838.
4) Matsumoto, M., Kobayashi, Y., Shirato, H., (1996), "The influence of aerodynamic derivatives on flutter.", *J. Wind Eng. Ind. Aerodyn*, 60, 227-239.
5) Matsumoto, M., Tamwaki, Y. and Shijo, R., (2001), "Frequency characteristics in various flutter instabilities of bridge girders.", *J. Wind Eng. Ind. Aerodyn*, 89, 385-408.
6) Matsumoto, M., Shiraishi, N. and Shirato, H., (1992), "Rain-wind induced vibration of cables of cabled-stay bridge.", *J. Wind Eng. Ind. Aerodyn*, 41-44, 2011-2022.
7) Scanlan, R. H., and Tomko, J. I. (1971). "Airfoil and bridge deck flutter derivatives." *J. Eng. Mech., ASCE,* 97(6), 1717-1737.
8) Scanlan, R. H., and Jones, N. P. (1990). "Aeroelastic analysis of cable-stay bridges." *J. Struct. Engrg., ASCE,* 116, 279-297.
9) Jain, A., Jones, N. P., and Scanlan, R. H. (1996). ''Coupled flutter and buffeting analysis of long-span bridges.'' *J. Struct. Engrg., ASCE,* 122, 716–725
10) Katsuchi, H., Jones, N. P., and Scanlan, R. H., (1999). ''Multimode coupled flutter and buffeting analysis of the Akashi-Kaikyo Bridge.'' *J. Struct. Engrg., ASCE*, 125, 60-70.
11) Chen, X., Kareem, A, Matsumoto, M., (2001), "Multimode coupled flutter and buffeting analysis of long span bridges.", *J. Wind Eng. Ind. Aerodyn*, 89, 649-664.
12) Scanlan, R.H. and Lin, W.H. (1978), "Effects of turbulence on bridge flutter derivatives", *J. Engrg. Mech. Div.*, 104, 719-733.
13) Scanlan, R.H. (1997), "Amplitude and turbulence effects on bridge flutter derivatives", *J. Struct. Eng.*, 123, 232-236.
14) Huston, D.R. (1986), The Effects of upstream gusting on the aeroelastic behavior of long Suspended-Span Bridges, Ph.D. Dissertation, Princeton University.

15) Falco, M., Curami, A., Zasso, A., (1992), "Nonlinear effect in sectional model aerodynamic parameters identification.", *J. Wind Eng. Ind. Aerodyn*, 41-44, 1321-1332.
16) Sarkar, P.P., Jones, N.P, Scanlan, R.H., (1994), "Identification of aeroelastic parameters of flexible bridges.", *J. Engrg. Mech., ASCE,* 120, 1718-1742.
17) Sarkar, P.P., Jones, N.P, Scanlan, R.H, (1992), "System identification for estimation of flutter derivatives.", *J. Wind Eng. Ind. Aerodyn*, 42, 1243-1254.
18) Sarkar, P.P., Caracoglia, L. Haan Jr.F.L, Sato, H., Murakoshi, J. (2009), "Comparative and sensitivity study of flutter derivatives of selected bridge deck sections, Part 1: Analysis of inter-laboratory experimental data.", J. Eng. Struct., 31, 158-169.
19) Caracoglia, L., Sarkar, P.P., Haan Jr.F.L, Sato, H., Murakoshi, J. (2009), "Comparative and sensitivity study of flutter derivatives of selected bridge deck sections, Part 2: Implications on the aerodynamic stability of long-span bridges.", J. Eng. Struct., 31, 2194-2202.
20) Yamada, H., Miyata, T. and Ichikawa, H., (1992), "Measurement of aerodynamic coefficients by system identification method", J. Wind Eng. Ind. Aerodyn, 42, 1255-1263.
21) Chiang D.Y. and Lin C.S., (2010), "Identification of modal parameters from ambient vibration data using eigensystem realization algorithm with correlation technique", J. Mechanical Science and Technology, 24 (12), 2377-2382.
22) Gu, M., Zhang, R.X., Xiang, H., (2000), "Identification of flutter derivatives of bridge decks", *J. Wind Eng. Ind. Aerodyn*, 84, 151–162.
23) Haan, F.L. (2000), "The effects of turbulence on the aerodynamics of long-span bridges", Ph.D. Dissertation; University of Notre Dame, US.
24) Gan Chowdhury, A., Sarkar, P.P., (2003), "A new technique for identification of eighteen flutter derivatives using a three-degree-of-freedom section model", *J. Wind Eng. Ind. Aerodyn*, 42, 1255-1263.
25) Jakobsen, J.B, Hjorth-Hansen, E., (1995), "Determination of the aerodynamic derivatives by a system identification method", *J. Wind Eng. Ind. Aerodyn*, 57, 295-305.
26) Nikitas, N., Macdonald, J.H.G. and Jakobsen, J.B., (2011), "Identification of flutter derivatives from full-scale ambient vibration measurements of the Clifton suspension bridge", *J. Wind and Struct.*, 14, 221-238.
27) Zhang, X., Brownjohn, J.M.W., (2004), "Effect of relative amplitude on bridge deck flutter", *J. Wind and Struct.*, 92, 493-508.
28) Juang, J.N., and Pappa, R.S., (1985), "An eigensystem realization algorithm (ERA) for modal parameter identification and model reduction", *J. Guid. Contr. Dyn*., 299-318.

29) Zhang, X., Brownjohn, J.M.W., (2004), “Effect of relative amplitude on bridge deck flutter”, *J. Wind Eng. Ind. Aerodyn*, 92, 493-508.

30) Kirkegaar, P.H. and Andersen, P., (1997), “State space identification of civil engineering structures from output measurement”, *Proc. of the 15th International Modal Analysis Conference*, Orlando, Florida, USA.

31) Scanlan, R.H. and Tomko, J.J, (1971), “Airfoil and bridges deck flutter derivative”, *EM6, J. Engrg. Mech., ASCE*, 1717-1733.

32) Iwamoto, M. and Fujino, Y., (1995), “Identification of flutter derivatives of bridge deck from free vibration data”, *J. Wind Eng. Ind. Aerodyn*, 54/55, 55-63.

33) Boonyapinyo, V., Janesupasaeree, T. (2010), “Data-driven stochastic subspace identification of flutter derivatives of bridge decks”, *J. Wind Eng. Ind. Aerodyn*, 98, 784-799.

34) Simiu, E. and Scanlan, R.H., “Wind Effects on Structures”, 3rd edition, John Wiley & Sons, New York, 1996.

35) Peeters B. and Roeck G. D., (1999), “Reference-based stochastic subspace identification for output-only modal analysis”, *Mechanical Systems and Signal Processing*, 13(6), 855-878.

36) Overchee, P. V. and De-Moor, B. (1996). Subspace Identification for Linear Systems: *Theory, Implementation and Applications*, volume 1. Kluwer Academic Publishers, Katholieke Universiteit Leuven, Belgium

37) Reynders, E., Pintelon, R. and Roeck, G. D. (2008), “Uncertainty bounds on modal parameters obtained from stochastic subspace identification” *Mechanical Systems and Signal Processing,* 22 (4), 948–969.

38) Peeters, B., (2000), “System identification and damage detection in civil engineering”, Ph.D. Dissertation; Katholieke Universiteit Leuven, Belgium.

39) Nakamura, Y. and Ozono S. (1987), “The effects of turbulence on a separated and reattaching flow”, *J. Fluid Mech*., (178), 477-490.

40) Fujino, Y., Kimura, K., Tanaka, H. (2012): Wind Resistant Design of Bridges in Japan, Springer Tokyo.

41) Siringoringo, D.M. and Fujino, Y. (2008), “System identification of suspension bridge from ambient vibration response”, *J. Eng. Struct*., (30), 462-477.

42) Diana G., Bruni S., Cigada A., Collina A., (1993), “Turbulence effect on flutter velocity in long span suspended bridges.”, *J. Wind Eng. Ind. Aerodyn*, 48, pp.329-342.

43) Miyata, T.,Yamada, H., Katsuchi, H., Kitagawa M. (2002), “Full-scale measurement of Akashi-Kaikyo Bridge during typhoon.”, *J. Wind Eng. Ind. Aerodyn*, 90, pp.1517-1527.
44) Emil Simiu and Robert H. Scanlan, (1996): *Wind Effects on Structures*, Third Edition, John Wiley & Sons, New York.
45) Claes Dyrbye and Svend O. Hansen, (1997): *Wind Loads on Structures*, John Wiley & Sons, New York.